Supporting Information for

Nuclearity growth of new Pd^{II} complexes induced by the electronic effect of selenium-containing ligands

Camila N. Cechin[a], Bruno N. Cabral[a], Fabrício Bublitz[a], Tanize Bortolotto[a], Géssica D. da Silveira[b], Leandro M. de Carvalho[c], Roberta Cargnelutti[a], Ulrich Abram[d], Shirley Nakagaki[e], Ernesto S. Lang[a], Bárbara Tirloni[a].*

[a]Laboratório de Materiais Inorgânicos, Departamento de Química – Universidade Federal de Santa Maria, 97105-900 - Santa Maria, RS, Brazil.

[b]Instituto de Química, Universidade Estadual de Campinas, Rua Josué de Castro 126 Cidade Universitária, Campinas, SP 13081361, Brazil

[c]Laboratório de Análises Químicas – LACHEM, Departamento de Química – Universidade Federal de Santa Maria, Santa Maria, RS 97110970, Brazil

[d]Freie Universität Berlin, Institute of Chemistry and Biochemistry, Fabeckstr. 34-36, D-14195 Berlin, Germany.

[e]Laboratório de Bioinorgânica e Catálise, Departamento de Química – Universidade Federal do Paraná, 81531-990 - Curitiba, PR, Brazil.

[*]Corresponding author

E-mail address: barbara.tirloni@ufsm.br

Experimental section…… **3-8**
Synthetic procedures…… **3-6**
Materials and methods…… **6-8**
Supplemental crystallographic data **9-14**
Table of crystallographic and structure refinement data **9**
Table of selected bond lengths (Å) and angles (°) **10-11**
ORTEP Figures **12-14**
Supplemental FT-IR spectra for compounds 1 – 5 ..... **14-16**
Supplemental NMR spectra **16-38**
NMR spectra for compound **1** **16-19**
NMR spectra for compound **2** **20-24**
NMR spectra for compound **3** **25-31**
^{31}P and ^{19}F NMR spectra of the followed reaction to obtain **3** **31-32**
NMR spectra for compound **4** **33-36**
NMR spectra for $(ArSe)_2$ starting materials **37-38**
Supplemental mass spectra for compounds 1 – 5 ..... **39-52**
Supplemental electrochemical voltammograms for compounds 3 and 5 ..... **52-53**
Supplemental solid-state UV-Visible spectroscopy for compounds 1 – 5 ..... **53-56**
References…….. **57**

Experimental section

Synthetic procedures

Preparation of the diaryldiselenides, $(ArSe)_2$, Ar = Ph, Mes, *p*-ClC_6H_4, *p*-FC_6H_4,[1] palladium selenolate polymers, $\{Pd(SePh)_2\}_n$, $\{Pd(SeC_6H_4Cl\text{-}p)_2\}_n$,[2] and the complex $[Pd(bipy)(py)_2](PF_6)_2$,[3,4] followed procedures reported in the literature. During the synthesis of the diaryldiselenide $(p\text{-}FC_6H_4Se)_2$, the formation of an impurity of ca. 25% of the diarylselenide $(p\text{-}FC_6H_4)_2Se$ was observed by ^{19}F and ^{77}Se NMR spectroscopy. Syntheses of compounds **1** – **5** were carried out using standard vacuum-line and Schlenk techniques under argon atmosphere. The resulting air-stable crystals were washed with diethyl ether and dried in vacuum before analyzed. Elemental analysis (CHN) was performed in a Vario EL III CHN elemental analyzer (Elementar Analysensysteme GmbH). IR-Spectra (Figures S6 – S10) were obtained using a FT-IR spectrometer (Nicolet iS10, Thermo Scientific). Absorption bands are classified as ν_s = symmetric stretching; ν_{as} = asymmetric stretching; *Arom* = aromatic; *Aliph* = aliphatic; δ_{ip} = in-plane deformation; δ_{op} = out-of-plane deformation.

$[Pd_2(\mu\text{-}SePh)_2(bipy)_2](PF_6)_2$ (1). To prepare compound **1,** a $\{Pd(SePh)_2\}_n$ suspension (0.1 mmol; 42 mg) in acetonitrile (MeCN - 4 mL), $[Pd(bipy)(py)_2][(PF_6)_2]$ (0.1 mmol; 71 mg) and bipy (0.1 mmol; 16 mg) were added and stirred under reflux for 16 hours. To the resulting clear, orange-red solution, methanol (MeOH - 2 mL) was added for crystallization. Yield: 77 mg (69%) of orange-red crystals based on $\{Pd(SePh)_2\}_n$. Elemental analysis for $C_{32}H_{26}F_{12}N_4P_2Pd_2Se_2$ (1127.23 g.mol^{-1}): Calcd. C 34.10%, H 2.32%, N = 4.97%; Found C 34.02%, H 2.36%, N 4.99 %. FT-IR (cm^{-1}): $\nu_{s(C\text{-}H)Arom}$ = 3116; $\nu_{as(C\text{-}H)Arom}$ = 3054; $\nu_{(C=C/C\text{-}N)}$ = 1574; 1474; 1447; $\delta_{ip(C=C\text{-}H)}$= 1073; $\delta_{op(C=C\text{-}H)}$ = 763; $\nu_{(P\text{-}F)}$ = 819. ESI$^+$ (*m/z*): 418.9306 $[M - 2(PF_6)]^{2+}$ (calcd. 418.9283); 982.8243 $[M - PF_6]^+$ (calcd. 982.8216); 1400.6411 $[M - PF_6 + Pd + 2(SePh)]^+$ (calcd. 1400.6370); 836.7475 $[M - 2(PF_6) + 2Pd + 4(SePh)]^{2+}$ (calcd. 836.7472); 261.9731 $[Pd(bipy)]^+$ (calcd. 261.9722); 157.0764 $[bipy + H]^+$ (calcd. 157.0767). ^1H NMR (600 MHz, CD_3CN, ppm): species **1** in equilibrium: 8.79 – 8.78 (m, 4H); 8.25 – 8.25 (m, 4H); 8.24 – 8.23 (m, 4H); 7.92 – 7.91 (m, 4H); 7.67 – 7.65 (m, 4H); 7.25 – 7.22 (m, 2H); 7.00 – 6.98 (m, 4H)); species **1'** in equilibrium: 8.62 – 8.61 (m, 4H); 8.41 – 8.39 (m, 4H); 8.35 – 8.34 (m, 4H); 8.27 – 8.26 (m, 4H); 7.63 – 7.61 (m, 4H); 7.46 – 7.44 (m, 2H); 7.32 – 7.30 (m, 4H). $^{13}C\{^1H\}$ NMR (151 MHz, CD_3CN, ppm): species **1** in equilibrium: 156.8; 151.0; 143.2; 136.4; 130.9; 130.3; 129.7; 126.4; 125.5; species **1'** in equilibrium: 157.0; 151.4; 142.9; 136.9; 131.2; 130.9; 129.1; 126.8; 125.2. ^{77}Se

NMR (114 MHz, CD_3CN, ppm): species **1** and **1'** in equilibrium: 78.4; 42.1. ^{19}F NMR (565 MHz, CD_3CN, ppm): –72.18; –73.43 for $(PF_6)^-$.

[Pd$_2$(μ-SeC$_6$H$_4$Cl-*p*)$_2$(bipy)$_2$](PF$_6$)$_2$ (2). Compound **2** was obtained and crystallized by the same procedure adopted to obtain **1**, using $\{Pd(SeC_6H_4Cl\text{-}p)_2\}_n$ (0.1 mmol; 45 mg) as reactant. Yield: 87 mg (73%) of orange-red crystals based on $\{Pd(SeC_6H_4Cl\text{-}p)_2\}_n$. Elemental analysis for $C_{32}H_{25}F_{12}N_4Cl_2P_2Pd_2Se_2$ (1197.12 g.mol^{-1}): Calcd. C 32.11%, H 2.10%, N 4.68%; Found C 32.52%, H 2.10%, N 4.81%. FT-IR (cm^{-1}): $\nu_{as(C\text{-}H)Arom}$ = 3088; $\nu_{(C=C/C\text{-}N)}$ = 1568; 1472; 1447; $\delta_{ip(C=C\text{-}H)}$ = 1072; $\delta_{op(C=C\text{-}H)}$ = 766; $\nu_{(P\text{-}F)}$ = 828. ESI$^+$ (*m/z*): 452.8924 [M – 2(PF$_6$)]$^{2+}$ (calcd. 452.8895); 1050.7469 [M – PF$_6$]$^+$ (calcd. 1050.7437); 1538.4853 [M + Pd + 2(SeAr) – PF$_6$]$^+$ (calcd. 1538.4800); 940.6309 [M + 2Pd + 4(SeAr) – 2(PF$_6$)]$^{2+}$ (calcd. 940.6275); 261.9742 [Pd(bipy)]$^+$ (calcd. 261.9722); 157.0775 [bipy + H]$^+$ (calcd. 157.0767). ^1H NMR (600 MHz, CD_3CN, ppm): species **2** in equilibrium: 8.98 (m, 4H); 8.42 – 8.40 (m, 4H); 8.35 – 8.33 (m, 4H); 7.79 – 7.77 (m, 4H); 7.73 – 7.71 (m, 4H); 6.95 – 6.93 (m, 4H); species **2'** in equilibrium: 8.61 – 8.60 (m, 4H); 8.39 – 8.37 (m, 4H); 8.35 – 8.33 (m, 4H); 8.28 – 8.25 (m, 4H); 7.67 – 7.64 (m, 4H); 7.33 – 7.32 (m, 4H). $^{13}C\{^1H\}$ NMR (151 MHz, CD_3CN, ppm): species **2** in equilibrium: 157.4; 151.6; 143.3; 137.9; 136.1; 130.6; 129.8; 125.7; 125.0; species **2'** in equilibrium: 157.2; 151.6; 143.1; 138.4; 137.3; 131.0; 129.3; 125.5; 125.3. ^{77}Se NMR (114 MHz, CD_3CN, ppm): species **2** and **2'** in equilibrium: 71.8; 64.8. ^{19}F NMR (565 MHz, CD_3CN, ppm): –72.24; –73.49 for $(PF_6)^-$.

[Pd$_2$(μ-SeC$_6$H$_4$F-*p*)$_2$(bipy)$_2$](PF$_6$)$_2$ (3). (*p*-FC$_6$H$_4$Se)$_2$ (0.1 mmol; 35 mg) and PPh$_3$ (0.1 mmol; 24 mg) were dissolved in MeCN (0.5 mL). [Pd(bipy)(py)$_2$](PF$_6$)$_2$ (0.15 mmol; 140 mg) dissolved in MeCN (4 mL) was added to the first solution and kept under stirring for 4 hours. To the resulting clear orange-red solution, dichloromethane (DCM – 2 mL) was added for crystallization. Yield: 53 mg (46%) of orange crystals based on [Pd(bipy)(py)$_2$](PF$_6$)$_2$. Elemental analysis for $C_{32}H_{24}F_{14}N_4P_2Pd_2Se_2$ (1163.21 g.mol^{-1}): Calcd. C 33.04%, H 2.08%, N 4.82%; Found C 31.66%, H 2.16%, N 5.79%. FT-IR (cm^{-1}): $\nu_{as(C\text{-}H)Arom}$ = 3082; $\nu_{(C=C/C\text{-}N)}$ = 1545; 1482; 1462; $\delta_{ip(C=C\text{-}H)}$ = 1078; $\delta_{op(C=C\text{-}H)}$ = 739; $\nu_{(P\text{-}F)}$ = 821. ESI$^+$ (*m/z*): 436.9217 [M – 2(PF$_6$)]$^{2+}$ (calcd. 436.9190); 1018.8064 [M – PF$_6$]$^+$ (calcd. 1018.8028); 663.8217 [M + Pd + 2(SeAr) – 2(PF$_6$)]$^{2+}$ (calcd. 663.8185); 1472.6033 [M + Pd + 2(SeAr) – PF$_6$]$^+$ (calcd. 1472.5988); 890.7199 [M + 2Pd + 4(SeAr) – 2(PF$_6$)]$^{2+}$ (calcd. 890.7180); 157.0768 [bipy + H]$^+$ (calcd. 157.0767). ^1H NMR (600 MHz, CD_3CN, ppm):

species **3** in equilibrium: 9.00 – 8.99 (m, 4H); 8.42 – 8.40 (m, 4H); 8.20 – 8.19 (m, 4H); 8.16 – 8.14 (m, 4H); 7.67 – 7.63 (m, 4H); 7.09 – 7.06 (m, 4H); species **3'** in equilibrium: 8.69 – 8.66 (m, 4H); 8.31 – 8.30 (m, 4H); 8.28 – 8.25 (m, 4H); 7.91 – 7.91 (m, 4H); 7.67 – 7.63 (m, 4H); 6.79 – 6.76 (m, 4H). $^{13}C\{^{1}H\}$ NMR (151 MHz, CD_3CN, ppm): species **3** in equilibrium: 164.8 (d, *J* = 250 Hz); 156.5; 153.1; 141.6; 139.0 (d, *J* = 8.6 Hz); 128.9; 124.7; 121.5 (d, *J* = 3.3 Hz); 117.8 (d, *J* = 22.4 Hz); species **3'** in equilibrium: 164.2 (d, *J* = 250 Hz); 156.9; 151.2; 143.1; 138.6 (d, *J* = 8.6 Hz); 129.6; 125.5; 121.6 (d, *J* = 3.3 Hz); 118.0 (d, *J* = 22.4 Hz); ^{77}Se NMR (114 MHz, CD_3CN, ppm): species **3** and **3'** in equilibrium: 67.1; 51.3. ^{19}F NMR (565 MHz, CD_3CN, ppm): –72.19; –73.44 for $(PF_6)^-$ and –111.37; –112.76 for species **3** and **3'** in equilibrium, respectively.

$[Pd_3(\mu_3\text{-}Se)_2(bipy)_3](PF_6)_2\cdot 5THF$ (4). To a solution containing $(p\text{-}FC_6H_4Se)_2$ (0.1 mmol; 35 mg) dissolved in MeCN (4 mL), $[Pd(bipy)(py)_2](PF_6)_2$ (0.2 mmol; 140 mg) was added and the solution kept stirring under reflux for 16 hours. To the resulting clear red solution, tetrahydrofuran (THF - 2 mL) was added for crystallization. Yield: 40 mg (49%) of orange-red crystals based on $[Pd(bipy)(py)_2](PF_6)_2$. Elemental analysis for $C_{30}H_{24}F_{12}N_6P_2Pd_3Se_2$ (1235.61 g.mol^{-1}): Calcd. C 29.16%, H 1.96%, N 6.80%; Found C 29.26%, H 2.07%, N 6.81%. FT-IR (cm^{-1}): $\nu_{as(C\text{-}H)Arom}$ = 3080; $\nu_{(C=C/C\text{-}N)}$ = 1564; 1470; 1446; $\delta_{ip(C=C\text{-}H)}$ = 1070; $\delta_{op(C=C\text{-}H)}$ = 758; $\nu_{(P\text{-}F)}$ = 827. ESI$^+$ (*m/z*): 472.8806 $[M – 2(PF_6)]^{2+}$ (calcd. 472.8754); 1090.7215 $[M – PF_6]^+$ (calcd. 1090.7156); 394.8453 $[M – bipy – 2(PF_6)]^{2+}$ (calcd. 394.8411); 239.9678 $[M – 3bipy – 2(PF_6)]^{2+}$ (calcd. 239.7719); 261.9741 $[Pd(bipy)]^+$ (calcd. 261.9722); 157.0770 $[bipy + H]^+$ (calcd. 157.0767). ^1H NMR (600 MHz, (CD_3CN, ppm): 8.96 – 8.95 (m, 6H); 8.32 – 8.30 (m, 6H); 8.24 – 8.21 (m, 6H); 7.70 – 7.68 (m, 6H). $^{13}C\{^{1}H\}$ NMR (151 MHz, (CD_3CN, ppm): 156.7; 153.1; 141.6; 128.8; 124.8. ^{77}Se NMR (114 MHz, (CD_3CN, ppm): 2.2. ^{19}F NMR (565 MHz, (CD_3CN, ppm): –72.15; –73.40 for $(PF_6)^-$.

$[Pd_3(\mu\text{-}SeMes)_4(bipy)_2](PF_6)_2\cdot 2MeCN$ (5). Compound **5** was prepared by the same procedure used to prepare compound **4**, using $(MesSe)_2$ (0.1 mmol; 38mg). To the resulting clear orange-red solution, diethyl ether (Et_2O - 2 mL) was added for crystallization. Yield: 29 mg (32%) of orange-red crystals based on $[Pd(bipy)(py)_2](PF_6)_2$. Elemental analysis for $C_{60}H_{66}F_{12}N_6P_2Pd_3Se_4$ (1796.16 g.mol^{-1}): Calcd. C 40.12%, H 3.70%, N 4.68%; Found C 39.38%, H 3.65%, N 3.90%. FT-IR (cm^{-1}): $\nu_{as(C\text{-}H)Arom}$ = 3083; $\nu_{s(C\text{-}H)Arom}$ = 3055; $\nu_{as(C\text{-}H)Aliph}$ = 2961; $\nu_{s(C\text{-}H)Aliph}$ = 2921; $\nu_{(C=C/C\text{-}N)}$ = 1565; 1471; 1437; $\delta_{ip(C=C\text{-}H)}$ = 1074; $\delta_{op(C=C\text{-}H)}$ = 771; $\nu_{(P\text{-}F)}$ =

833. ESI$^+$ (*m/z*): 711.9362 [M – 2(PF_6)]$^{2+}$ (calcd. 711.9300); 460.9779 [M – Pd - 2(SeMes) – 2(PF_6)]$^{2+}$ (calcd. 460.9754); 157.0777 [bipy + H]$^+$ (calcd. 157.0767).

Materials and methods

Single-crystal X-ray Diffraction

Single-crystal data were collected with a Bruker D8 Venture diffractometer operating with an Incoatec X-ray source with Montel two-dimensional optics, Mo-Kα radiation (λ = 0.71073 Å) and a Photon 100 detector. The structures were solved by dual space methods using the XT/SHELXT-2015 program.[5] The refinements were performed using the XL/SHELXL-2015 program[6] with full matrix/least squares method of structural factors, F^2, and anisotropic thermal displacement parameters for all non-hydrogen atoms. Hydrogen atoms were calculated in the idealized positions. The graphical representations for the structures, in ellipsoid mode, were obtained using the DIAMOND program.[7] More detailed information about the crystal data for **1** − **5** are given in Table S1. Positional disorder was detected for the aromatic ring, *p*-Cl-C_6H_4, of compound **2** (Figure S2). Two positions of *p*-Cl-C_6H_4 were localized and the disorder resolution was carried out using the occupational factor of the atoms as a free variable, through the commands PART1 and PART2 of the XL/SHELXL-2015 program.[6] The positions of C27A, C28A, C29A, C30A, C31A, C32A, Cl1A and C27B, C28B, C29B, C30B, C31B, C32B, Cl1B show occupational probabilities of 51% and 49%, respectively. CCDC numbers 2044736, 2044722, 2045039, 2044723 and 2044733 (see Supporting Information) include the supplementary crystallographic data for **1** – **5,** respectively, which can be obtained free of charge from The Cambridge Crystallographic Data Centre via www.ccdc.cam.ac.uk/data_request/cif, or by emailing data_request@ccdc.cam.ac.uk, or by contacting The Cambridge Crystallographic Data Centre, 12 Union Road, Cambridge CB2 1EZ, UK; fax: +44 1223 336033.

NMR Spectroscopy

^{1}H, ^{13}C, ^{77}Se, ^{19}F, COSY, HSQC and HMBC NMR spectra in solution were recorded for the crystalline compounds **1** – **4** besides the ^{77}Se NMR spectra in solution for $(ArSe)_2$ on Bruker Advance III HD 600 or JEOL 400 MHz ECS-400 spectrometers at 25 ºC. The low solubility of compound **5** prevented the acquisition of the NMR spectra of sufficient quality. Chemical shifts (δ) are given relative to the signals of internal

standards (tetramethylsilane for ^{1}H and ^{13}C) and external standards ($ClCF_3$ for ^{19}F, 85% phosphoric acid for ^{31}P and dimethylselenide for ^{77}Se).

Mass Spectrometry

Electrospray ionization mass spectrometry (ESI MS) was carried out for compounds **1** – **5** using an Agilent 6210 TOF LC/MS system, in ESI^+ mode (cationic fragment detection) and the samples were prepared in MeCN.

Solid-state electrochemistry

Solid-state electrochemical behavior for compounds **1** – **5** was evaluated through Voltammetry of Immobilized microparticles (VIMP) using a Potentiostat PGSTAT302 N (Metrohm Autolab, Netherlands) equipped with a VA Stand 694 (Metrohm Autolab, Netherlands) and controlled by Nova 2.1.4 software (Eco Chemie). A three-electrode electrochemical cell was used: a graphite bar (5 mm diameter cylindrical rods, HB from Faber-Castell, composition graphite and ceramic material) as working electrode, an Ag/AgCl (KCl 3 mol L^{-1}) as reference electrode and platinum wire as auxiliary electrode. VIMP was performed by immobilizing the individual solid compounds (few μg) directly on the surface of the graphite rod through an abrasive impregnation. The graphite bar was carefully placed into the voltammetric cell (0.01 mol L^{-1} H_2SO_4 as supporting electrolyte) to produce a meniscus between the electrode surface and the electrolyte. Between each measurement, the working electrode was polished into a 2000 grit sandpaper, then in a craft paper sheet and finally washed with water and ethanol to remove any residual sample. Cyclic voltammetry (CV) and square wave voltammetry (SWV) were used as detection mode in VIMP analysis. When CV measurements were not sensitive enough to clearly detect any electrochemical behavior for the compounds, SWV was also performed. The CV parameters used were scan rate 50 mV s^{-1}, E_{step} 2 mV and scan range from -0.5 to +1.5 V with start potential at 0V. SWV parameters used were scan range -0.6 to +1.5 V, frequency 5 Hz, E_{step} 5 mV and E_{amp} 25 mV. Electrolysis was performed previously to some specific measurements and it consisted in the application of the constant potential -0.6 V during 300 s, afterwards the scans were performed.

Solid-state UV-Visible Spectroscopy

Diffuse reflectance spectra for compounds **1** – **5** were performed using a UV-Vis 2600-PC Shimadzu spectrometer fitted with a diffuse reflectance accessory over the UV-Vis wavelength range of 200 to 800 nm to evaluate the optical band gap energy (E_g). The values were estimated following the methodology described in the literature, the Kubelka-Munk model.[8–10]

Table S1. Crystallographic and structure refinement data for compounds **1** – **5**.

Compound	**1**	**2**	**3**	**4**	**5**
Formula	$C_{32}H_{26}F_{12}N_4P_2Pd_2Se_2$	$C_{32}H_{24}Cl_2F_{12}N_4P_2Pd_2Se_2$	$C_{32}H_{24}F_{14}N_4P_2Pd_2Se_2$	$C_{30}H_{24}F_{12}N_6P_2Pd_3Se_2$	$C_{60}H_{66}F_{12}N_6P_2Pd_3Se_4$
F.W. (g.mol^{-1})	1127.23	1196.11	1163.21	1235.61	1796.16
Crystal system	Monoclinic	Triclinic	Monoclinic	Triclinic	Monoclinic
Space group	$P2_1/c$	P-1	$P2_1/c$	P-1	$P2_1/n$
a (Å)	15.7921(11)	8.2149(5)	16.4295(8)	12.8829(13)	12.4503(7)
b (Å)	46.834(4)	15.0033(10)	14.9858(8)	14.2924(15)	15.3071(10)
c (Å)	16.0606(11)	16.3008(10)	16.3738(10)	16.5898(17)	34.150(2)
α (°)	90	107.372(2)	90	72.297(4)	90
β (°)	116.209(2)	92.431(2)	118.122(2)	70.672(3)	90.411(2)
γ (°)	90	105.091(2)	90	67.031(4)	90
T (K)	100	145	100	100	103
V (Å^3)	10657.3(13)	1835.5(2)	3555.5(3)	2599.6(5)	6508,1(7)
Z	12	2	4	2	4
$\rho_{calc.}$ (g.cm^{-3})	2.108	2.164	2.173	1.579	1.833
μ (mm^{-1})	3.247	3.290	3.256	2.555	3.184
F(000)	6528	1152	2240	1180	3520
Collected reflections	115285	31789	51136	45149	70138
Independent reflections [R_{int}]	23554 [0.0628]	7546 [0.0891]	7874 [0.0382]	11557 [0.0534]	11119 [0.1155]
R_1 *[I > 2σ(I)]*	R_1 = 0.0532	R_1 = 0.0416	R_1 = 0.0252	R_1 = 0.0341	R_1 = 0.0451
wR_2 [I > 2σ(I)]	wR_2 = 0.0762	wR_2 = 0.0649	wR_2 = 0.0545	wR_2 = 0.0734	wR_2 = 0.0720
R_1 (all data)[a]	R_1 = 0.0802	R_1 = 0.0751	R_1 = 0.0314	R_1 = 0.0521	R_1 = 0.0825
wR_2 (all data)[b]	wR_2 = 0.0821	wR_2 = 0.0732	wR_2 = 0.0569	wR_2 = 0.0811	wR_2 = 0.0816
GOOF on F^2	1.106	1.014	1.042	1.031	1.035
Largest diff. peak and hole (e.Å^{-3})	1.086 and -2.668	2.021 and -1.329	1.169 and -1.893	1.072 and -1.299	1.343 and -1.224

[a]$R_1 = \sum||F_o|-|F_c||/\sum|F_o|$; [b]$wR_2 = \{\sum w(F_o^2-F_c^2)^2/\sum w(F_o^2)^2\}^{1/2}$

Table S2. Selected bond lengths (Å) and angles (°) for compounds **1** − **5**.

Bond lengths (Å)		**Bond angles (°)**	
1			
Pd1–Se1	2.4125(7)	N2–Pd1–N1	80.05(17)
Pd1–Se2	2.3798(7)	N1–Pd1–Se2	97.93(12)
Pd2–Se1	2.4082(7)	N1–Pd1–Se1	179.30(12)
Pd2–Se2	2.3926(7)	N2–Pd1–Se2	177.00(12)
Pd1–N1	2.065(4)	N2–Pd1–Se1	100.63(12)
Pd1–N2	2.062(4)	Se2–Pd1–Se1	81.40(2)
Pd2–N3	2.066(4)	N4–Pd2–Se2	98.87(12)
Pd2–N4	2.061(4)	N4–Pd2–Se1	176.83(12)
Pd1···Pd2	3.5751(2)	N4–Pd2–N3	79.74(17)
		N3–Pd2–Se2	176.75(12)
		N3–Pd2–Se1	100.32(12)
		N4–Pd2–Se1	176.83(12)
		Se2–Pd2–Se1	81.23(2)
		Pd1–Se1–Pd2	95.74(2)
		Pd1–Se2–Pd2	97.03(2)
		Pd1–Se1–C27	101.11(15)
		Pd1–Se2–C21	103.76(15)
		Pd2–Se1–C27	101.70(16)
		Pd2–Se2–C21	95.74(2)
2			
Pd1–Se1	2.3965(7)	N2–Pd1–N1	80.32(17)
Pd1–Se2	2.3953(6)	N1–Pd1–Se2	98.49(12)
Pd2–Se1	2.4093(7)	N1–Pd1–Se1	177.41(11)
Pd2–Se2	2.3986(6)	N2–Pd1–Se2	178.31(13)
Pd1–N1	2.048(4)	N2–Pd1–Se1	99.31(13)
Pd1–N2	2.053(4)	Se2–Pd1–Se1	81.83(2)
Pd2–N3	2.059(4)	N4–Pd2–Se2	99.08(11)
Pd2–N4	2.064(4)	N4–Pd2–Se1	177.94(11)
Pd1···Pd2	3.5541(2)	N4–Pd2–N3	79.83(17)
		N3–Pd2–Se2	178.62(12)
		N3–Pd2–Se1	99.57(13)
		N4–Pd2–Se1	177.94(11)
		Se2–Pd2–Se1	81.50(2)
		Pd1–Se1–Pd2	95.38(2)
		Pd1–Se2–Pd2	95.69(2)
		Pd1–Se2–C21	102.60(18)
		Pd2–Se2–C21	99.79(18)
		Pd1–Se1–C27A	99.1(4)
		Pd1–Se1–C27B	106.7(4)
		Pd2–Se1–C27A	104.9(4)
		Pd2–Se1–C27B	97.2(4)
3			
Pd1–Se1	2.3955(5)	N2–Pd1–N1	79.75(9)
Pd1–Se2	2.3935(3)	N1–Pd1–Se2	97.81(6)
Pd2–Se1	2.3935(3)	N1–Pd1–Se1	177.33(6)
Pd2–Se2	2.3884(3)	N2–Pd1–Se2	175.21(6)
Pd1–N1	2.070(2)	N2–Pd1–Se1	101.80(6)
Pd1–N2	2.079(2)	Se2–Pd1–Se1	80.802(10)

Pd2–N3	2.067(2)	N4–Pd2–Se2	80.802(10)
Pd2–N4	2.068(2)	N4–Pd2–Se1	177.17(6)
Pd1···Pd2	3.6088(2)	N4–Pd2–N3	80.16(8)
		N3–Pd2–Se2	176.83(6)
		N3–Pd2–Se1	100.91(6)
		N4–Pd2–Se1	177.17(6)
		Se2–Pd2–Se1	80.973(10)
		Pd1–Se1–Pd2	96.116(11)
		Pd1–Se2–Pd2	97.993(11)
		Pd1–Se1–C1	101.72(8)
		Pd1–Se2–C9	98.47(8)
		Pd2–Se1–C1	96.48(7)
		Pd2–Se2–C9	104.01(8)
4			
Pd1–Se1	2.3955(5)	N2–Pd1–N1	79.96(11)
Pd1–Se2	2.3942(5)	N1–Pd1–Se2	176.95(8)
Pd2–Se1	2.3963(5)	N1–Pd1–Se1	101.83(8)
Pd2–Se2	2.3924(5)	N2–Pd1–Se2	101.45(8)
Pd3–Se1	2.3928(5)	N2–Pd1–Se1	178.18(8)
Pd3–Se2	2.4014(5)	Se2–Pd1–Se1	76.743(16)
Pd1–N1	2.069(3)	N4–Pd2–Se2	177.70(8)
Pd1–N2	2.067(3)	N4–Pd2–Se1	101.58(8)
Pd2–N3	2.074(3)	N4–Pd2–N3	79.60(12)
Pd2–N4	2.065(3)	N3–Pd2–Se2	102.05(9)
Pd3–N5	2.062(4)	N3–Pd2–Se1	178.77(9)
Pd3–N6	2.080(4)	N4–Pd2–Se1	101.58(8)
Pd1···Pd2	3.2919(3)	Se2–Pd2–Se1	76.761(16)
Pd2···Pd3	3.2290(3)	N5–Pd3–N6	79.27(16)
Pd1···Pd3	3.2360(3)	N5–Pd3–Se1	79.27(16)
		N6–Pd3–Se1	101.82(11)
		N5–Pd3–Se2	102.27(12)
		N6–Pd3–Se2	178.46(11)
5			
Pd1–Se1	2.4290(7)	N2–Pd1–N1	79.46(18)
Pd1–Se2	2.4246(7)	N1–Pd1–Se2	177.53(13)
Pd2–Se1	2.4376(7)	N1–Pd1–Se1	101.09(13)
Pd2–Se2	2.4222(7)	N2–Pd1–Se2	100.84(13)
Pd2–Se3	2.4236(7)	N2–Pd1–Se1	178.02(13)
Pd2–Se4	2.4394(7)	Se2–Pd1–Se1	78.53(2)
Pd3–Se3	2.4157(7)	N4–Pd3–N3	79.32(19)
Pd3–Se4	2.4294(7)	N3–Pd3–Se3	102.53(13)
Pd1–N1	2.090(5)	N3–Pd3–Se4	178.97(14)
Pd1–N2	2.081(5)	N4–Pd3–Se3	176.57(13)
Pd3–N3	2.102(5)	N4–Pd3–Se4	99.67(13)
Pd3–N4	2.081(5)	Se2–Pd2–Se1	78.41(2)
		Se2–Pd2–Se4	178.88(3)
		Se1–Pd2–Se4	100.86(3)
		Se2–Pd2–Se3	102.68(3)
		Se3–Pd2–Se1	174.01(3)
		Se3–Pd2–Se4	78.14(2)

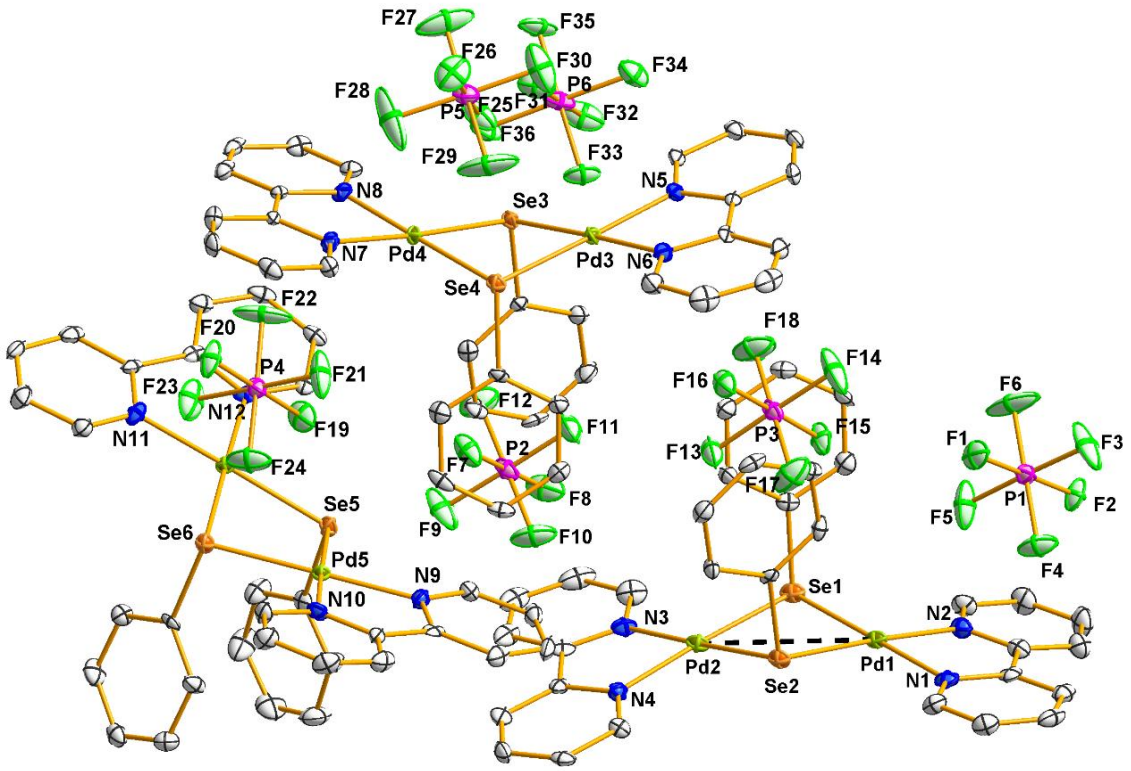

Figure S1. ORTEP representation of the molecular structure of compound $[Pd_2(\mu\text{-}SePh)_2(bipy)_2](PF_6)_2$ (**1**). Ellipsoids are depicted with 50% of probability. Hydrogen atoms are omitted for clarity.

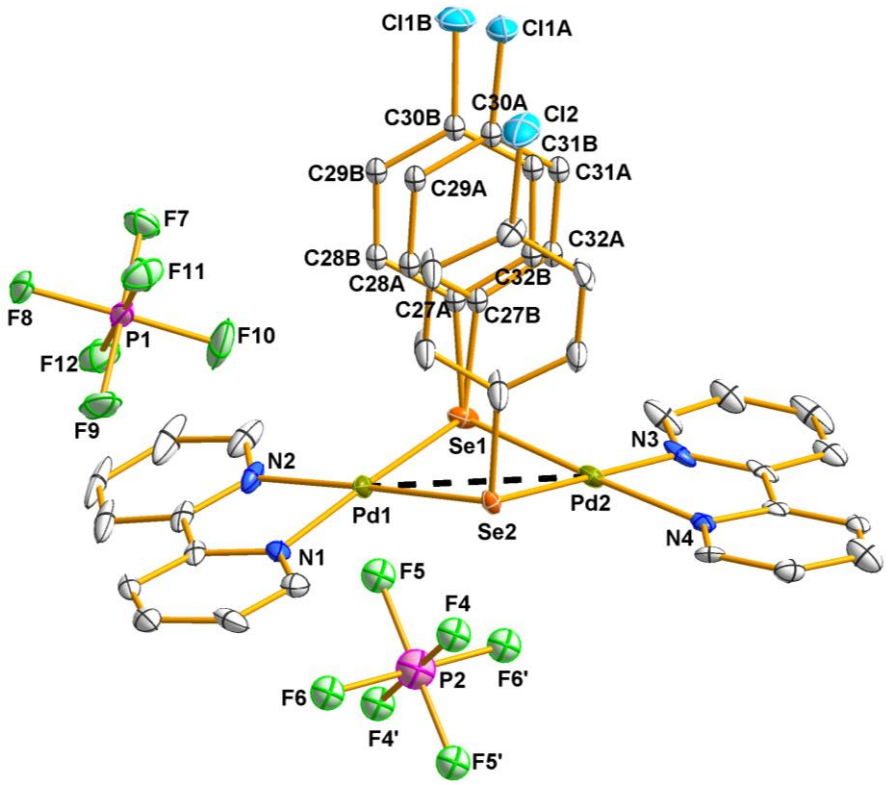

Figure S2. ORTEP representation of the molecular structure of compound $[Pd_2(\mu\text{-}SeC_6H_4Cl\text{-}p)_2(bipy)_2](PF_6)_2$ (**2**). Ellipsoids are depicted with 50% of probability. Hydrogen atoms are omitted for clarity. Symmetry code: (') 2-x, 1-y, -z.

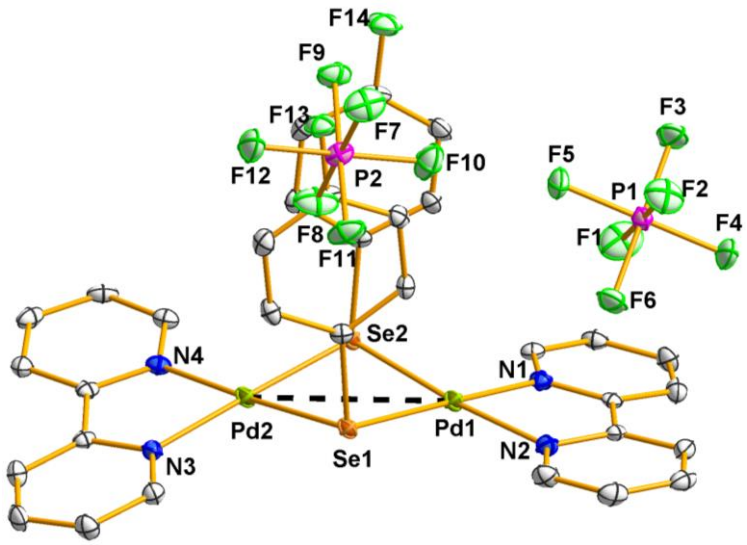

Figure S3. ORTEP representation of the molecular structure of compound $[Pd_2(\mu\text{-}SeC_6H_4F\text{-}p)_2(bipy)_2](PF_6)_2$ (**3**). Ellipsoids are depicted with 50% of probability. Hydrogen atoms are omitted for clarity.

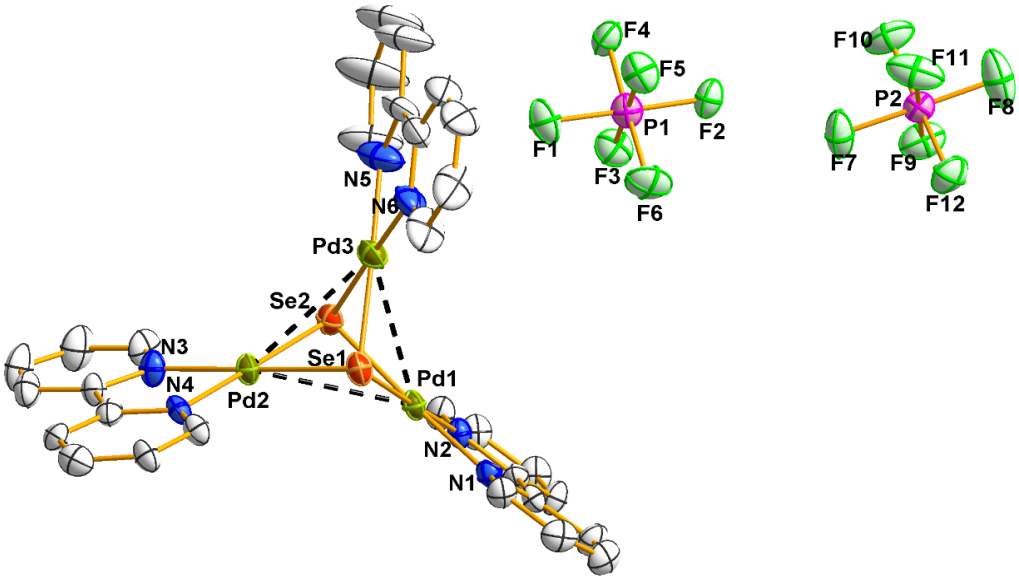

Figure S4. ORTEP representation of the molecular structure of compound $[Pd_3(\mu_3\text{-}Se)_2(bipy)_3](PF_6)_2\cdot 5THF$ (**4**). Ellipsoids are depicted with 50% of probability. Hydrogen atoms are omitted for clarity. Diffuse solvent molecules have been removed by SQUEEZE.

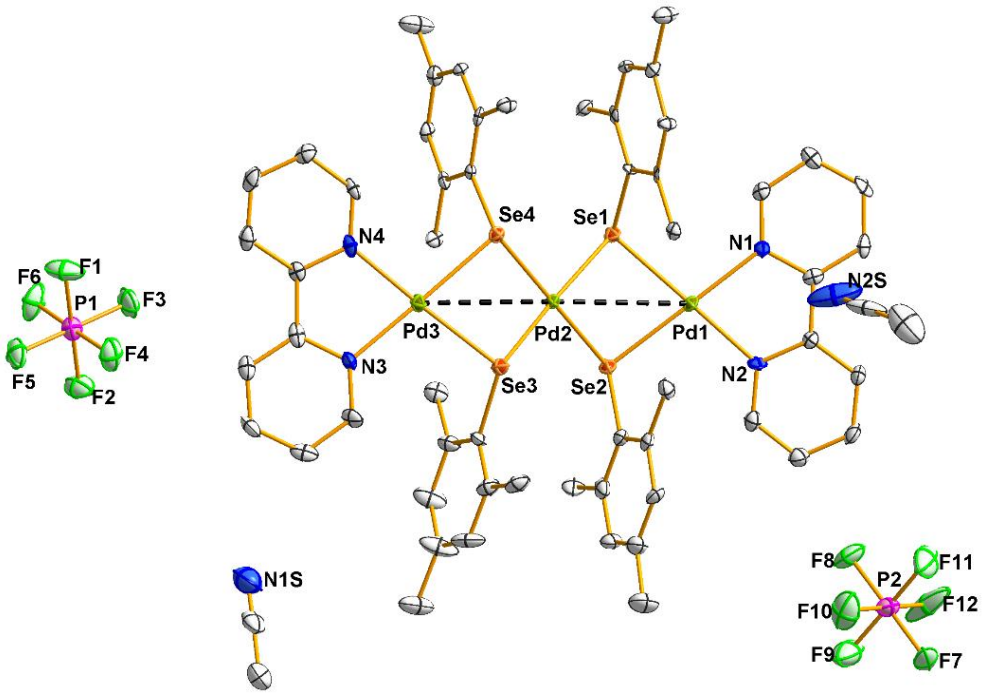

Figure S5. ORTEP representation of the molecular structure of compound $[Pd_3(\mu\text{-}SeMes)_4(bipy)_2](PF_6)_2{\cdot}2MeCN$ (**5**). Ellipsoids are depicted with 50% of probability. Hydrogen atoms are omitted for clarity.

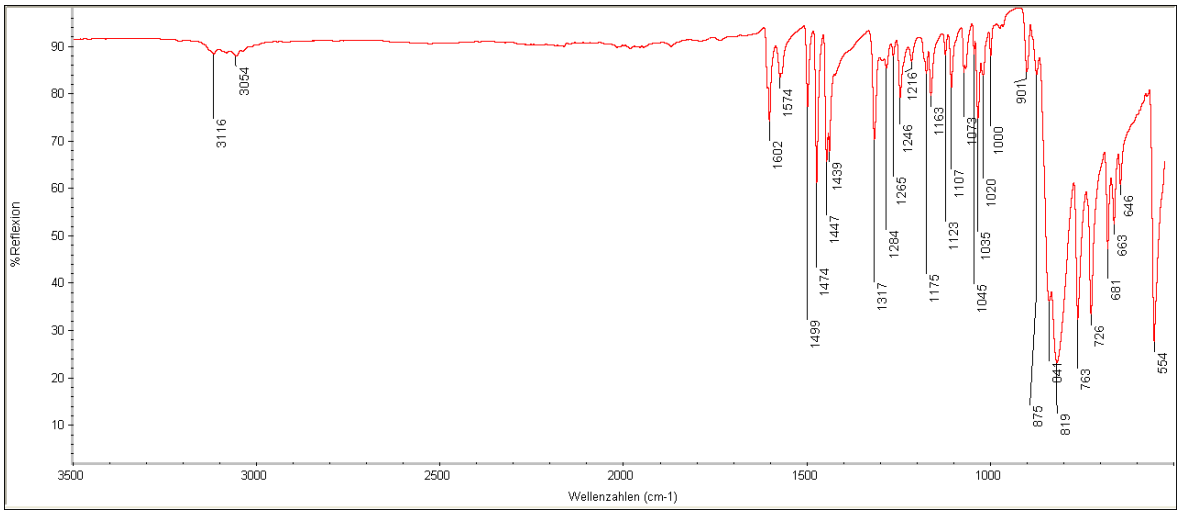

Figure S6. FT-IR spectrum for compound $[Pd_2(\mu\text{-}SePh)_2(bipy)_2](PF_6)_2$ (**1**).

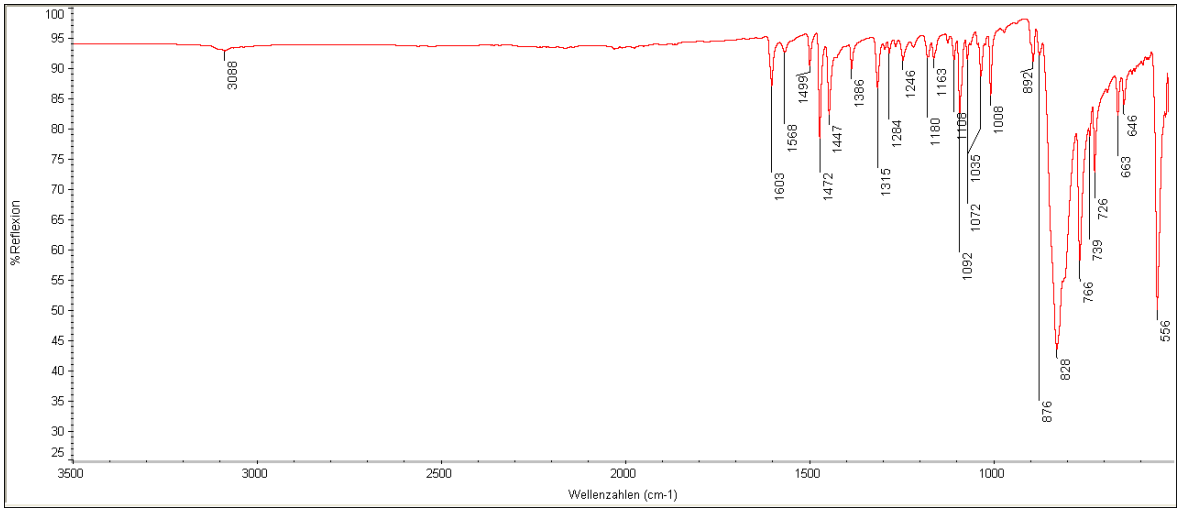

Figure S7. FT-IR spectrum for compound $[Pd_2(\mu\text{-}SeC_6H_4Cl\text{-}p)_2(bipy)_2](PF_6)_2$ (**2**).

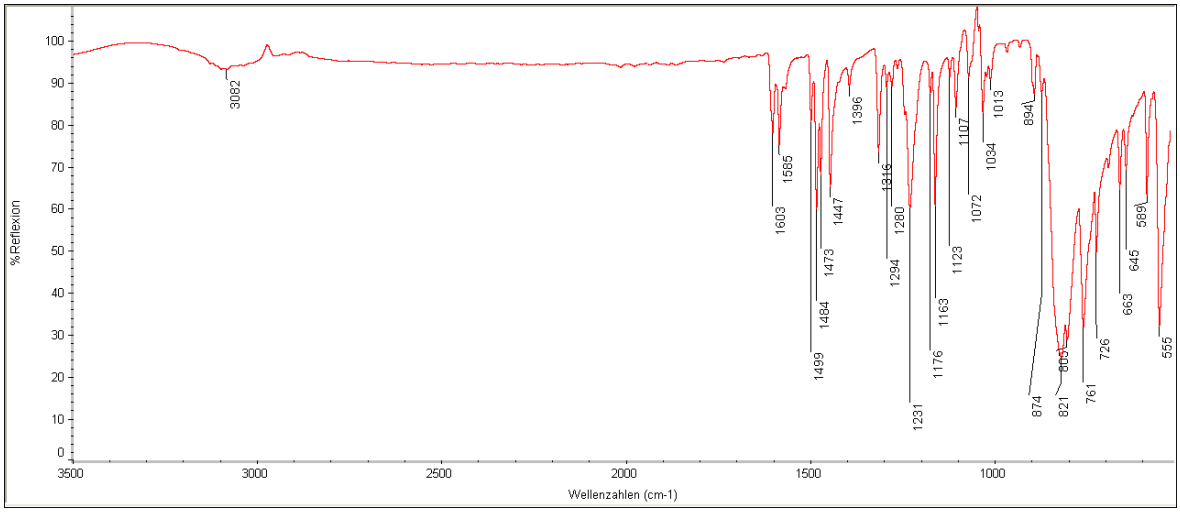

Figure S8. FT-IR spectrum for compound $[Pd_2(\mu\text{-}SeC_6H_4F\text{-}p)_2(bipy)_2](PF_6)_2$ (**3**).

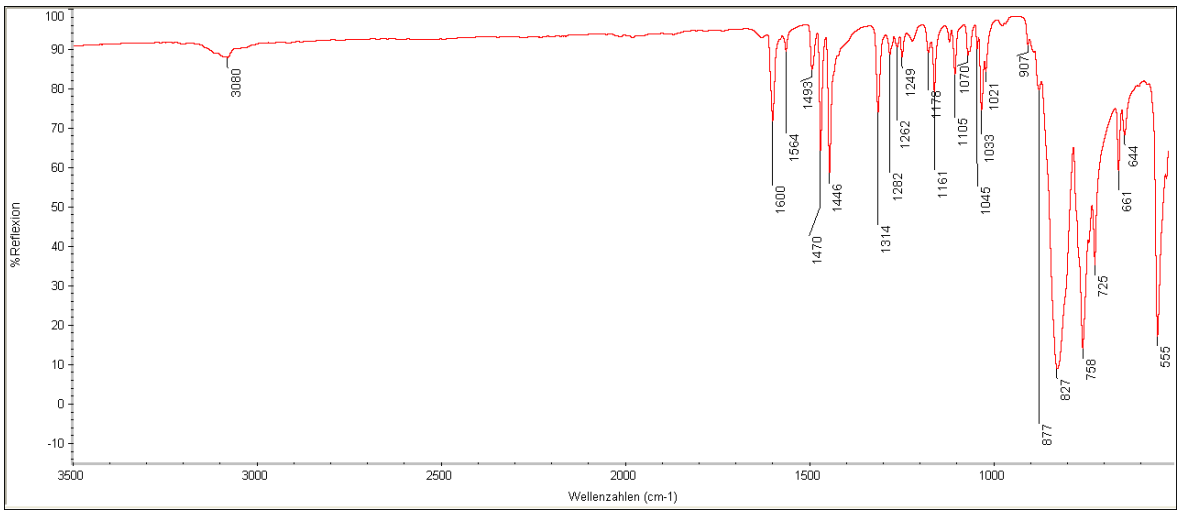

Figure S9. FT-IR spectrum for compound $[Pd_3(\mu_3\text{-}Se)_2(bipy)_3](PF_6)_2\cdot 5THF$ (**4**).

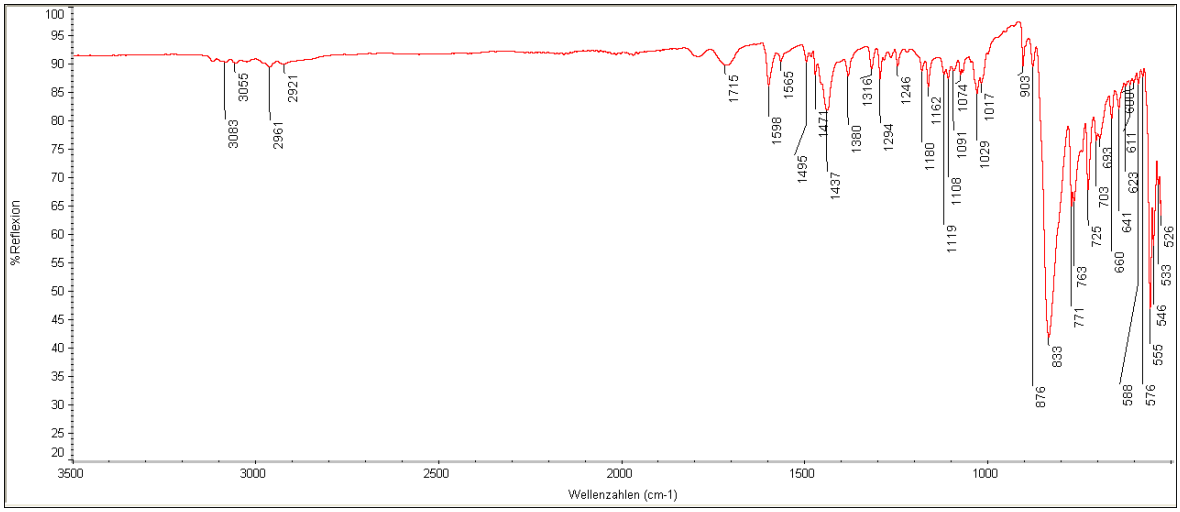

Figure S10. FT-IR spectrum for compound $[Pd_3(\mu\text{-SeMes})_4(bipy)_2](PF_6)_2\cdot 2MeCN$ (**5**).

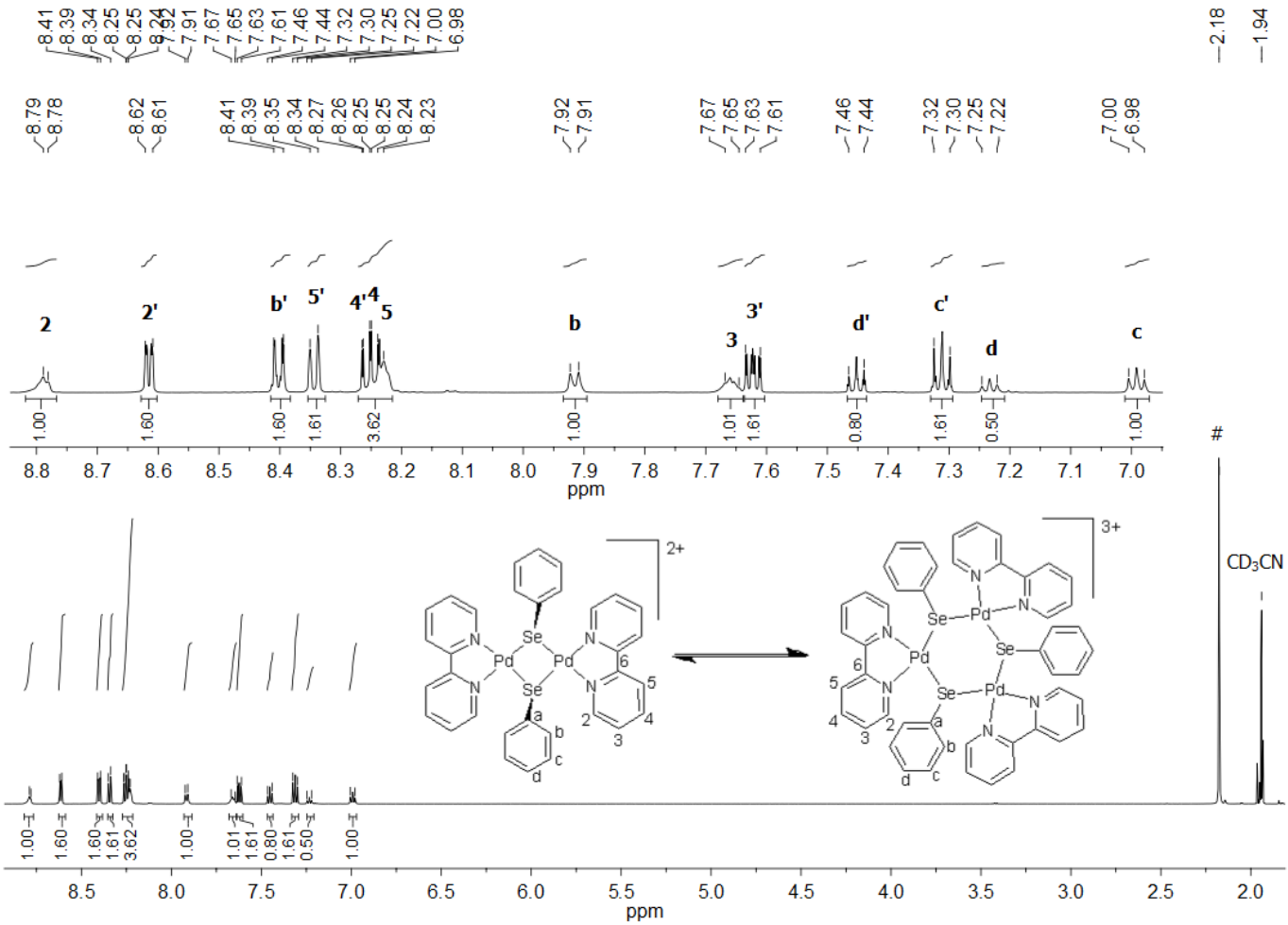

Figure S11. 600 MHz ^{1}H NMR spectrum of $[Pd_2(\mu\text{-SePh})_2(bipy)_2](PF_6)_2$ (**1**) in CD_3CN at 25 ºC. # = water from the solvent.

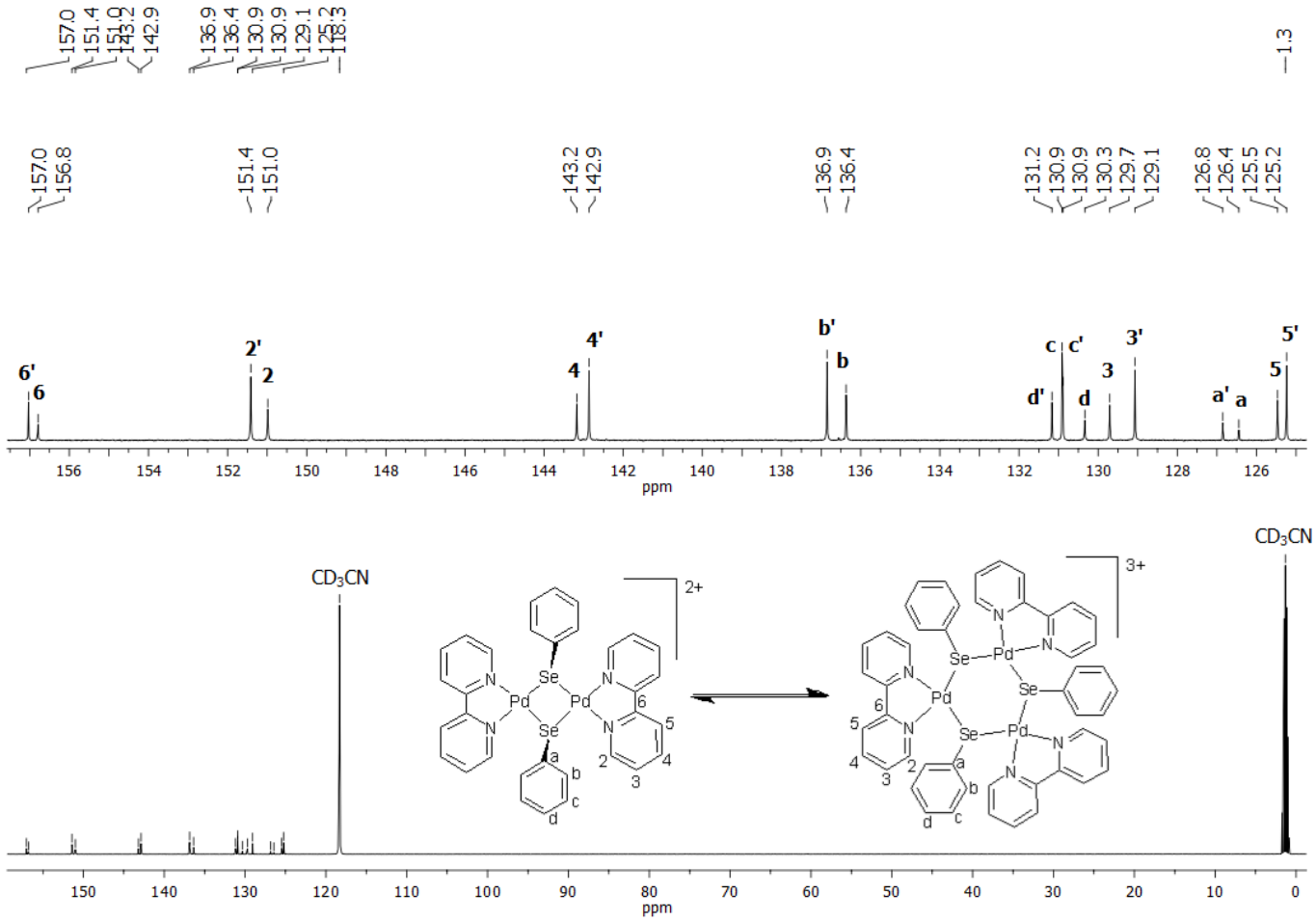

Figure S12. 151 MHz $^{13}C\{^{1}H\}$ NMR spectrum of $[Pd_2(\mu\text{-SePh})_2(bipy)_2](PF_6)_2$ (**1**) in CD_3CN at 25 ºC.

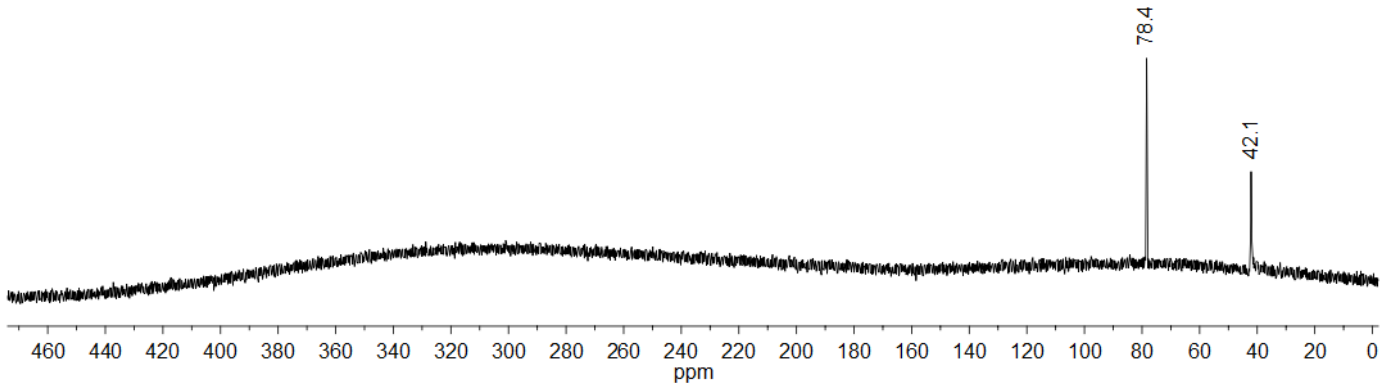

Figure S13. 114 MHz ^{77}Se NMR spectrum of $[Pd_2(\mu\text{-SePh})_2(bipy)_2](PF_6)_2$ (**1**) in CD_3CN at 25 ºC.

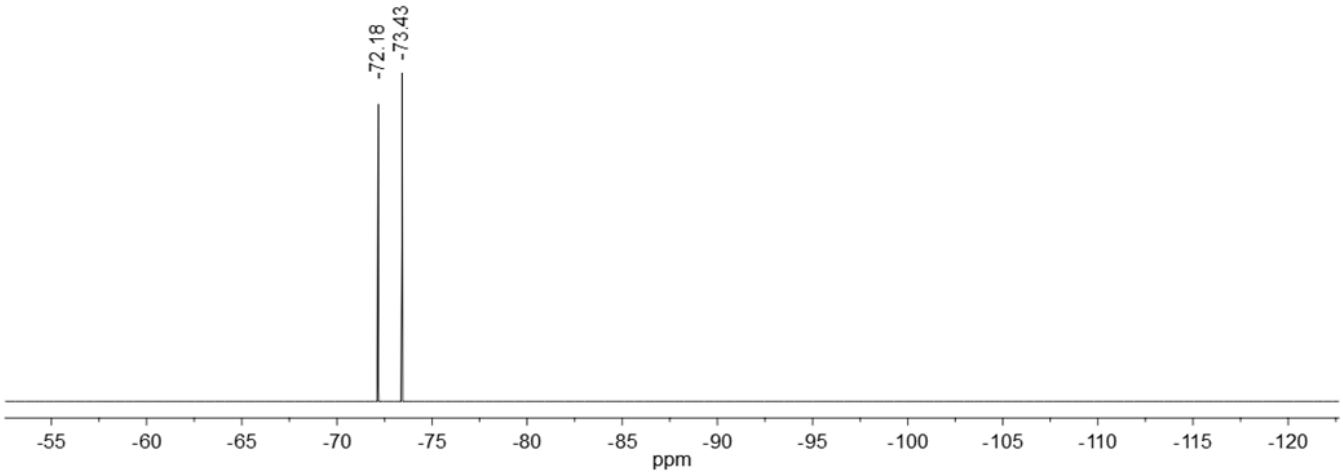

Figure S14. 565 MHz ^{19}F NMR spectrum of $[Pd_2(\mu\text{-SePh})_2(bipy)_2](PF_6)_2$ (**1**) in CD_3CN at 25 ºC.

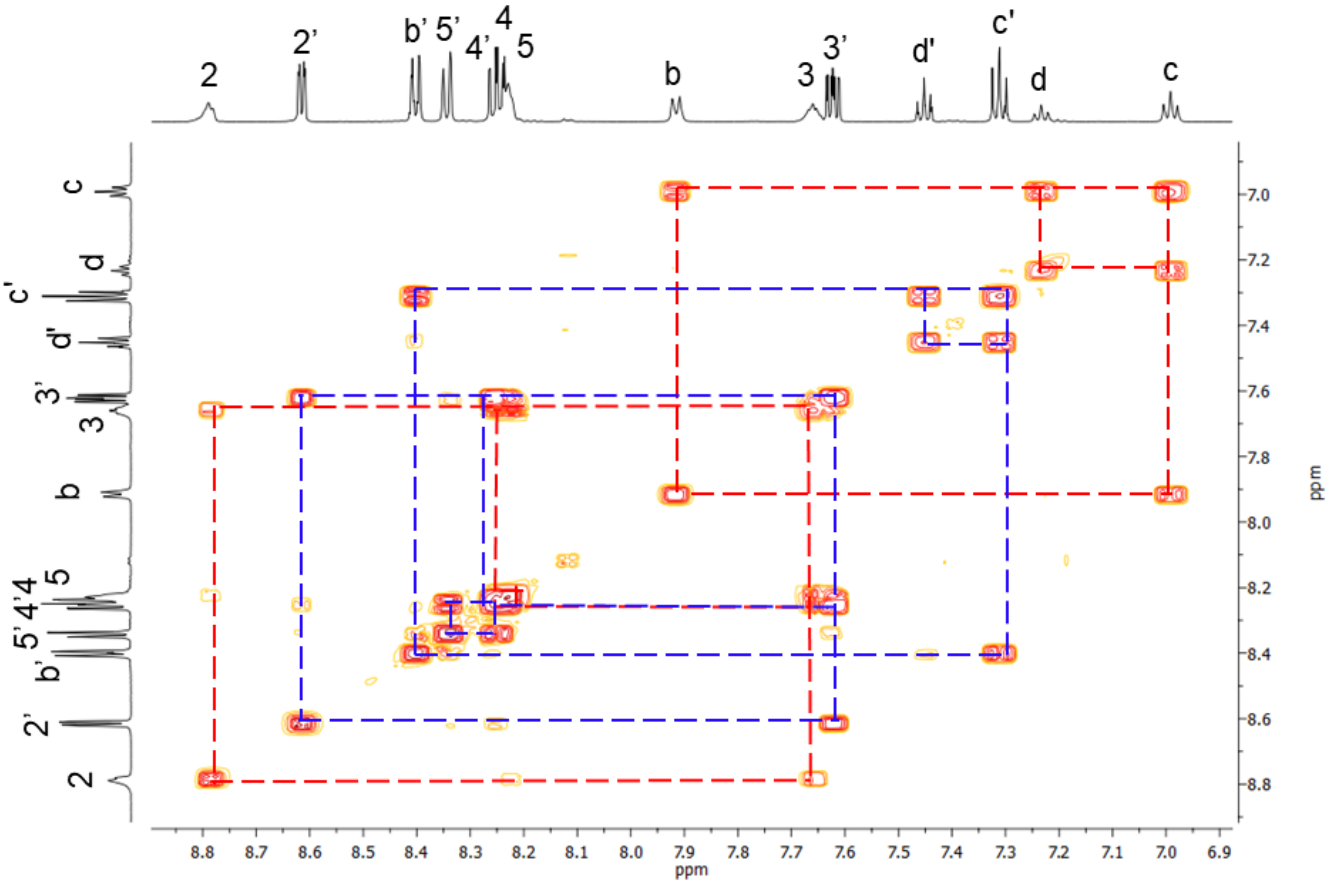

Figure S15. 2D COSY NMR spectrum of $[Pd_2(\mu\text{-SePh})_2(bipy)_2](PF_6)_2$ (**1**).

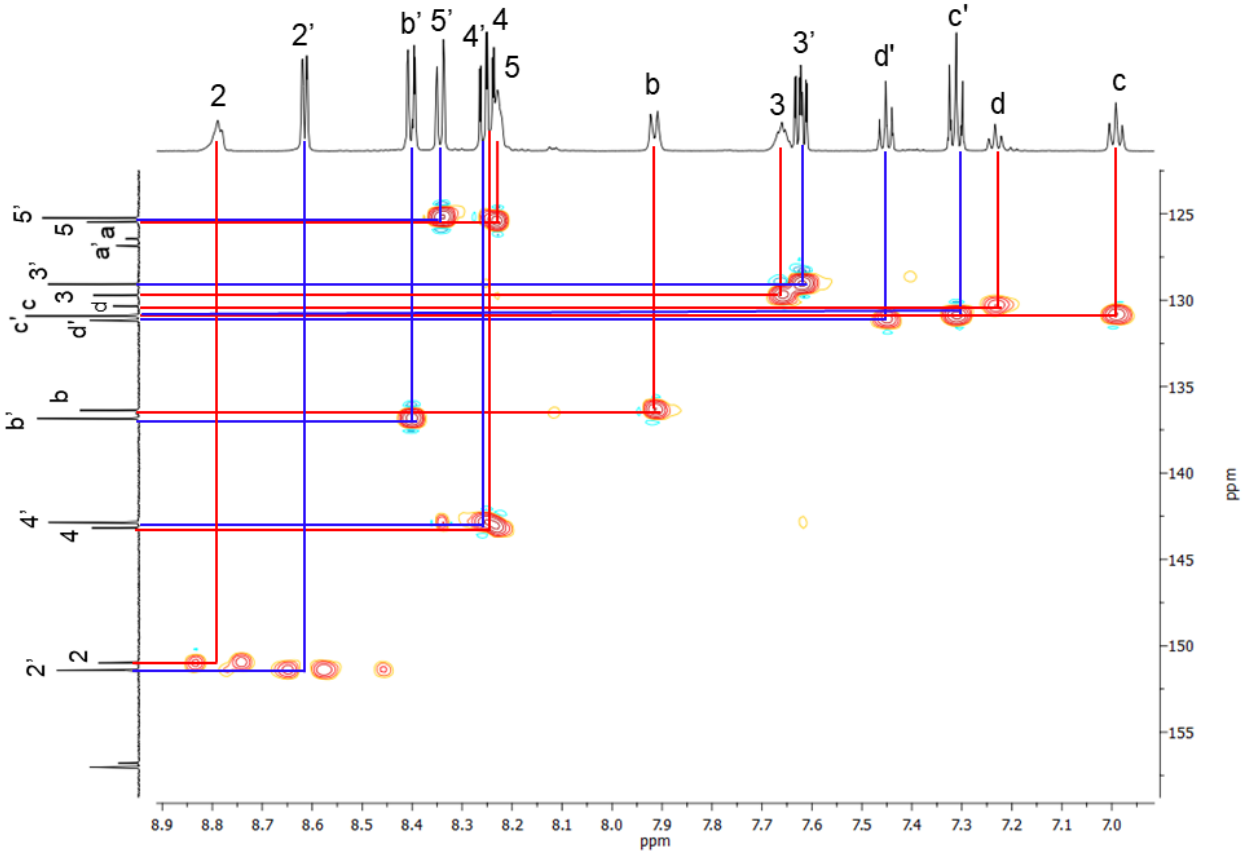

Figure S16. 2D HSQC NMR spectrum of $[Pd_2(\mu\text{-SePh})_2(bipy)_2](PF_6)_2$ (**1**).

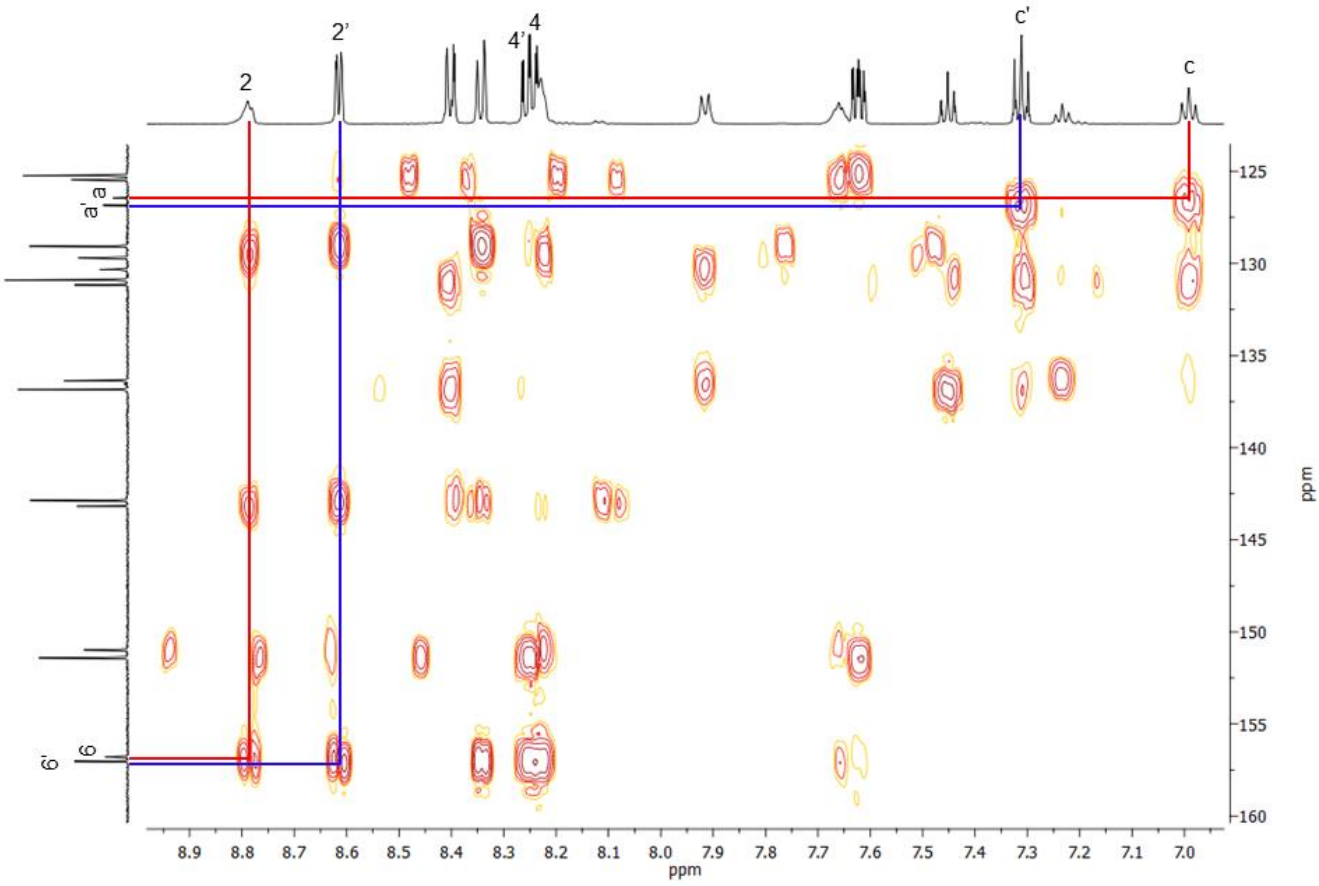

Figure S17. 2D HMBC NMR spectrum of $[Pd_2(\mu\text{-SePh})_2(bipy)_2](PF_6)_2$ (**1**).

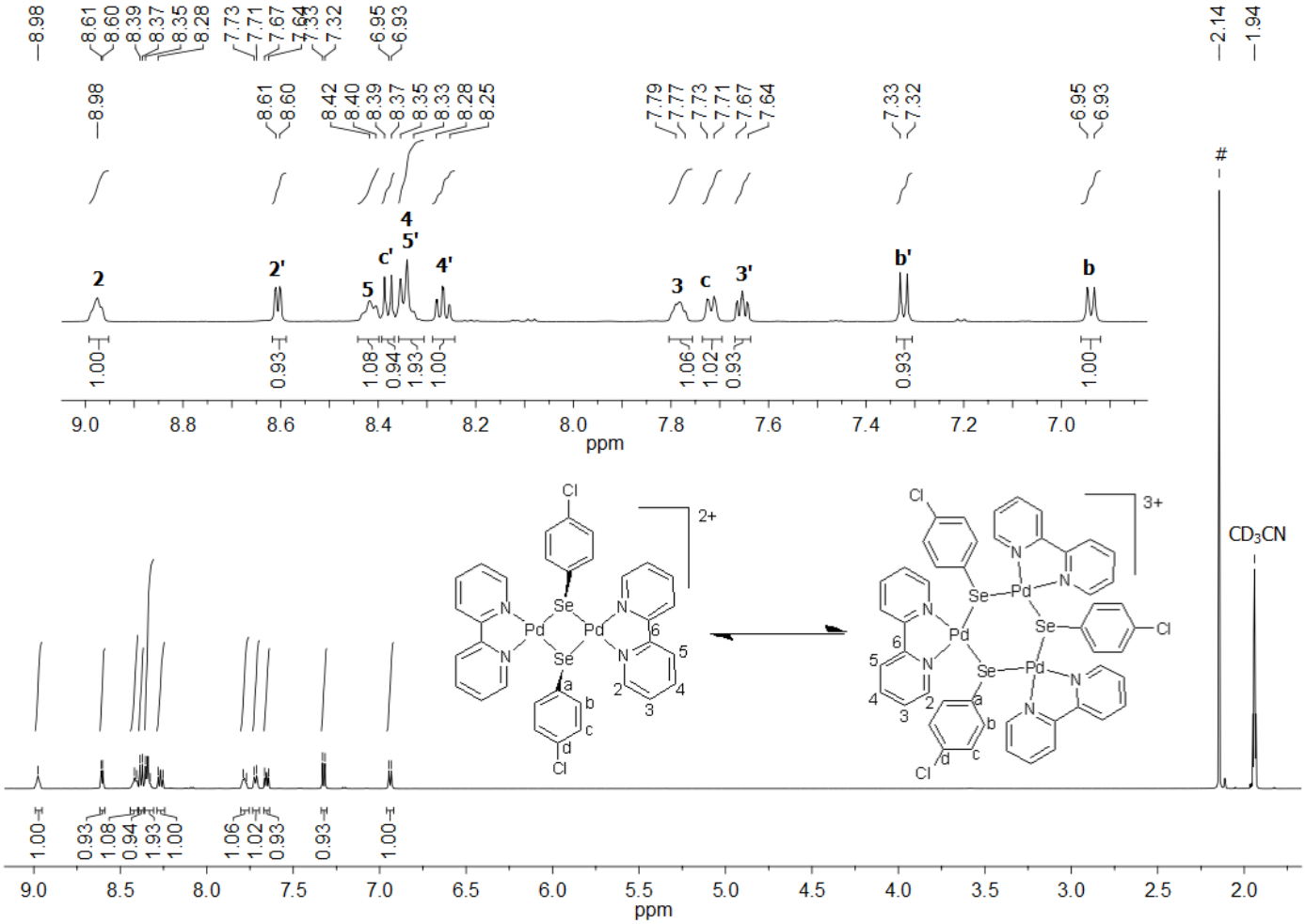

Figure S18. 600 MHz ^{1}H NMR spectrum of $[Pd_2(\mu\text{-}SeC_6H_4Cl\text{-}p)_2(bipy)_2](PF_6)_2$ (**2**) in CD_3CN at 25 ºC. # = water from the solvent.

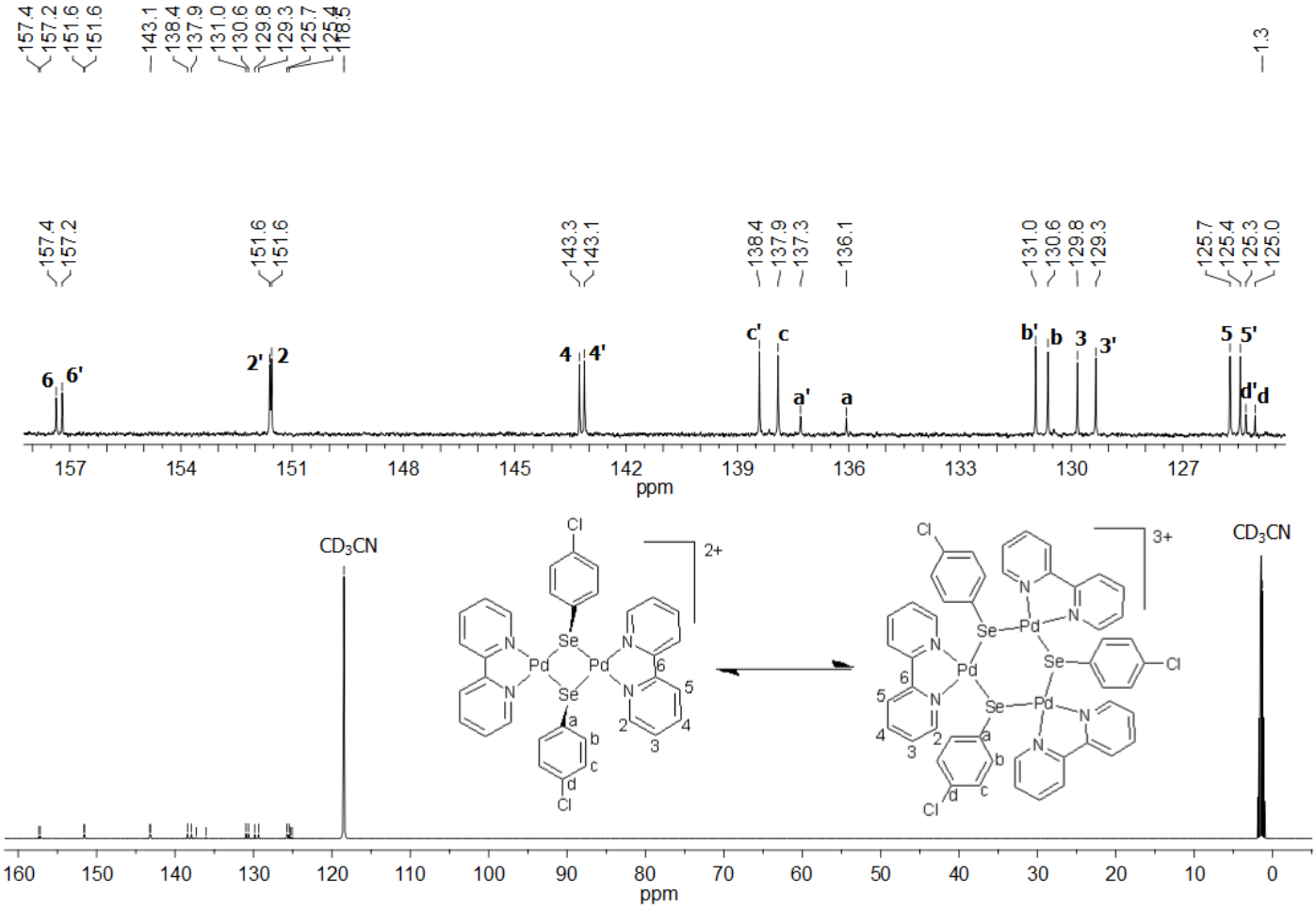

Figure S19. 151 MHz $^{13}C\{^{1}H\}$ NMR spectrum of $[Pd_2(\mu\text{-}SeC_6H_4Cl\text{-}p)_2(bipy)_2](PF_6)_2$ (**2**) in CD_3CN at 25 ºC.

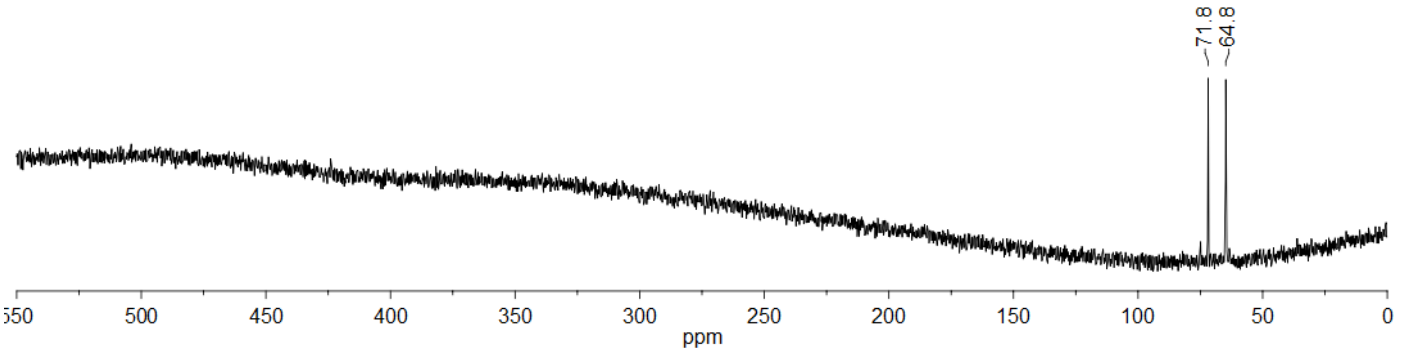

Figure S20. 114 MHz ^{77}Se NMR spectrum of $[Pd_2(\mu\text{-}SeC_6H_4Cl\text{-}p)_2(bipy)_2](PF_6)_2$ (**2**) in CD_3CN at 25 ºC.

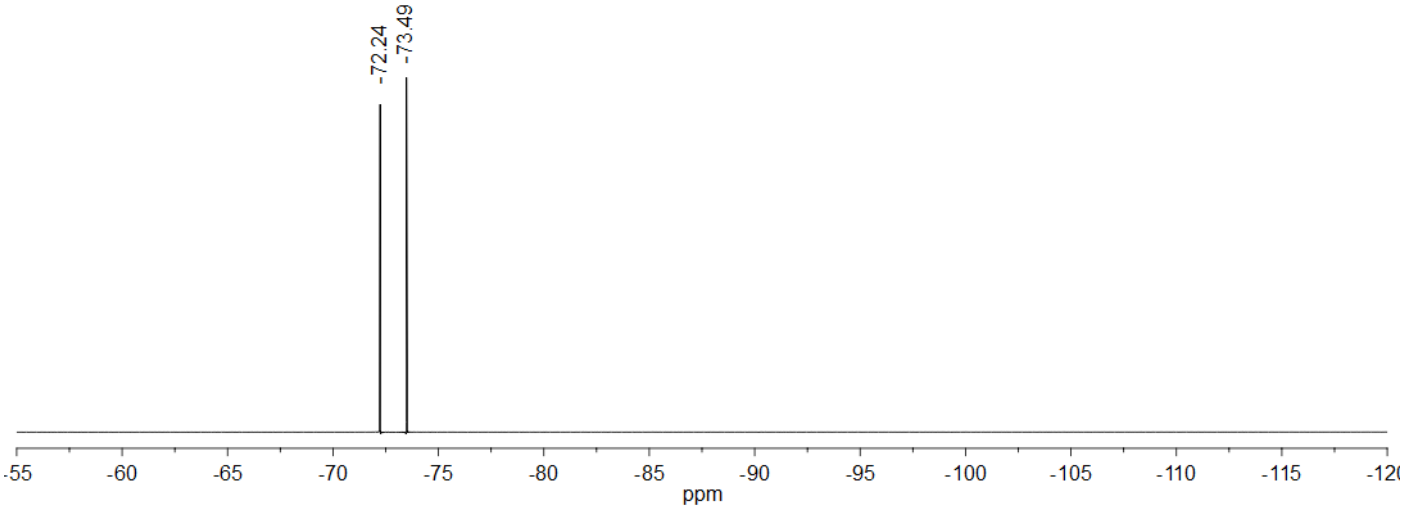

Figure S21. 565 MHz ^{19}F NMR spectrum of $[Pd_2(\mu\text{-}SeC_6H_4Cl\text{-}p)_2(bipy)_2](PF_6)_2$ (**2**) in CD_3CN at 25 ºC.

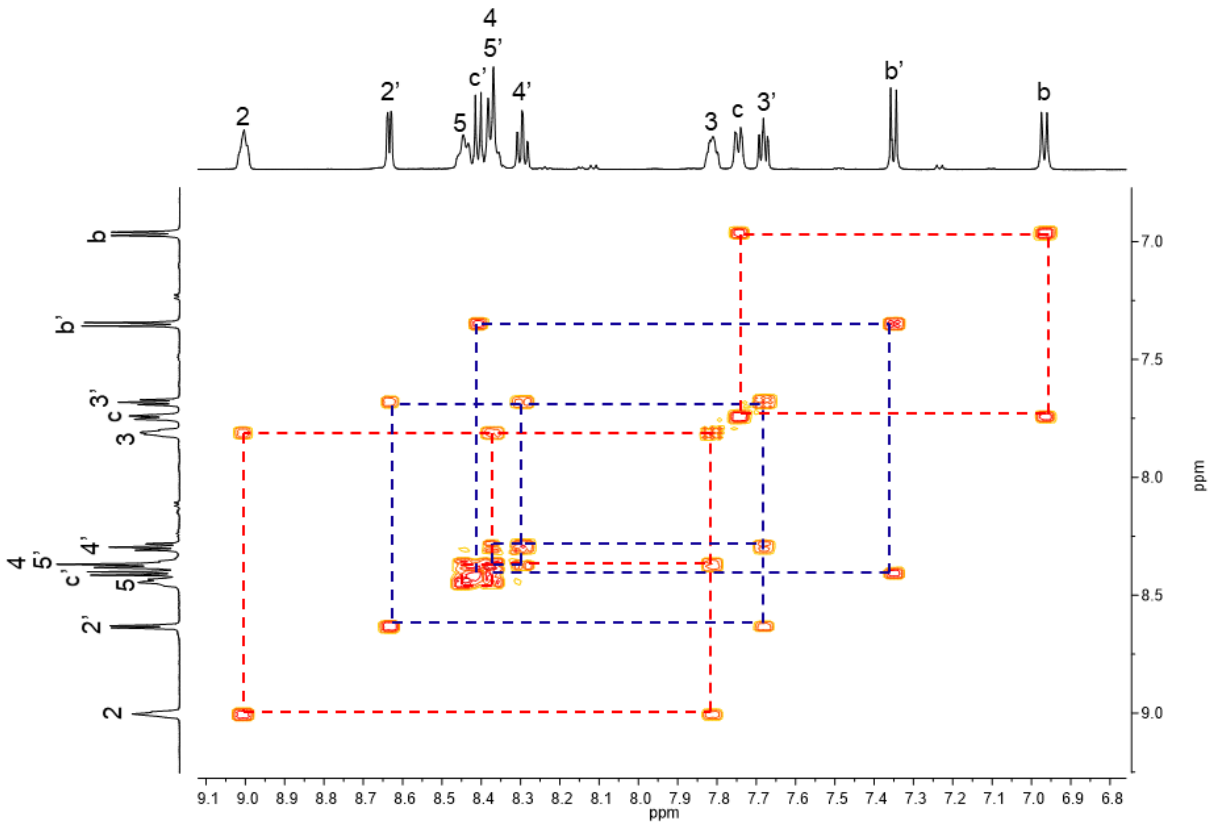

Figure S22. 2D COSY NMR spectrum of $[Pd_2(\mu\text{-}SeC_6H_4Cl\text{-}p)_2(bipy)_2](PF_6)_2$ (**2**).

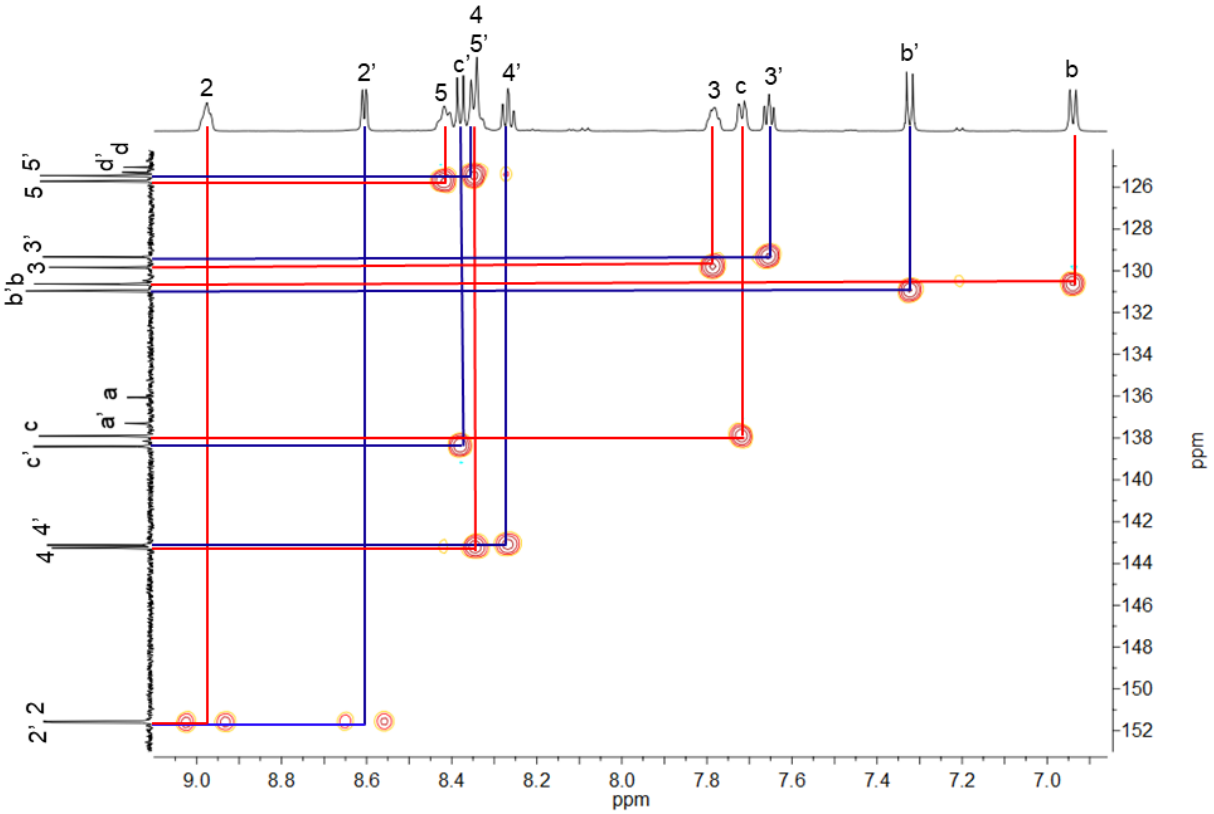

Figure S23. 2D HSQC NMR spectrum of $[Pd_2(\mu\text{-}SeC_6H_4Cl\text{-}p)_2(bipy)_2](PF_6)_2$ (**2**).

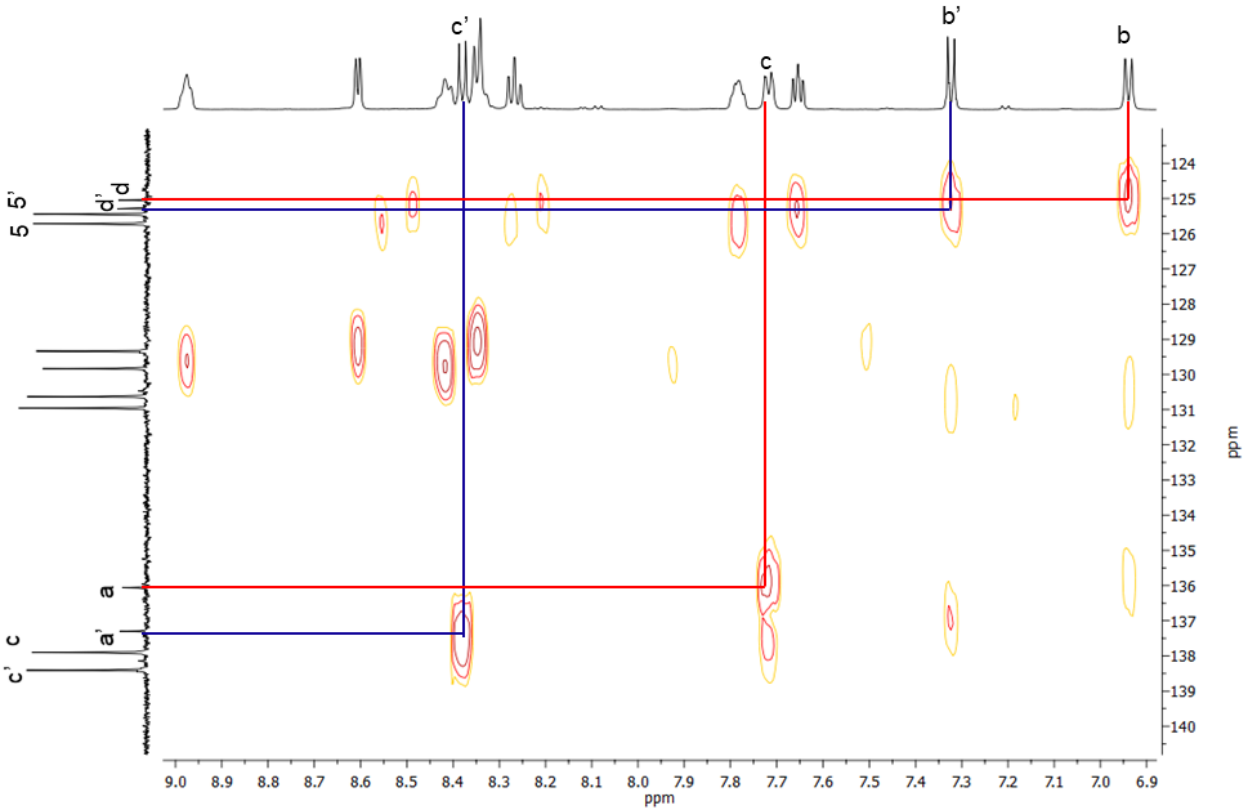

Figure S24. 2D HMBC NMR spectrum of $[Pd_2(\mu\text{-}SeC_6H_4Cl\text{-}p)_2(bipy)_2](PF_6)_2$ (**2**) zoomed in.

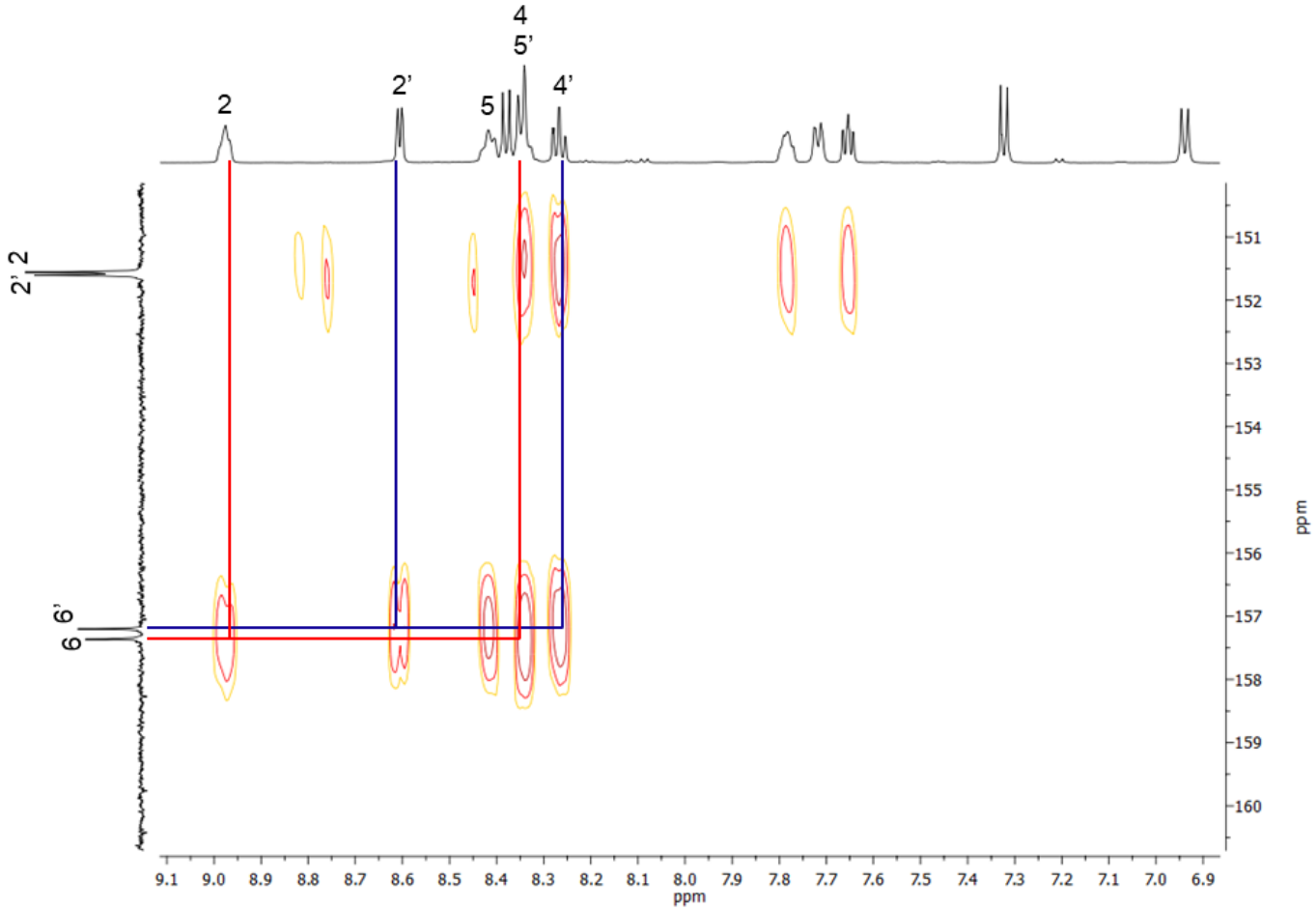

Figure S25. 2D HMBC NMR spectrum of $[Pd_2(\mu\text{-}SeC_6H_4Cl\text{-}p)_2(bipy)_2](PF_6)_2$ (**2**) zoomed in.

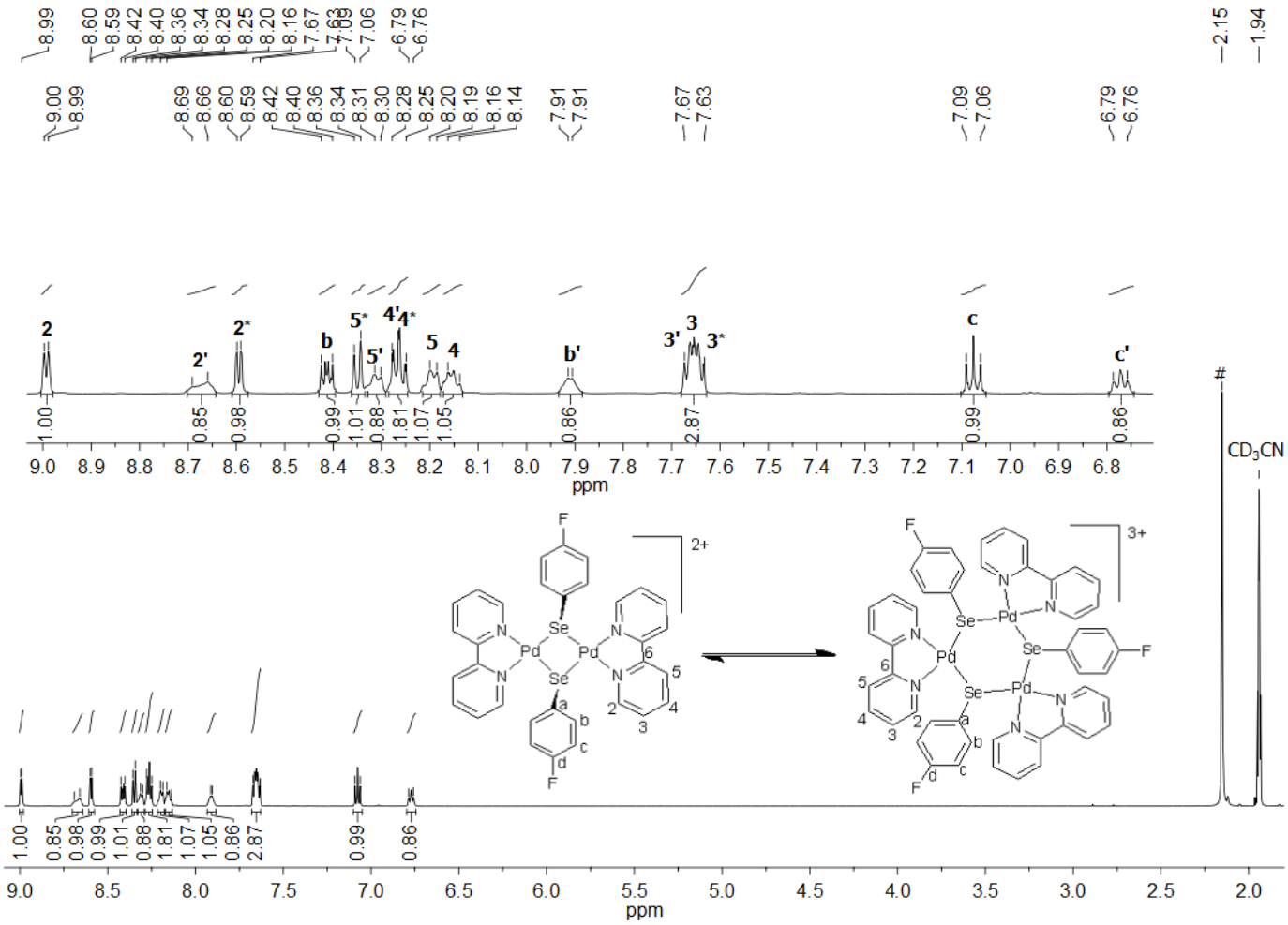

Figure S26. 600 MHz ^{1}H NMR spectrum of $[Pd_2(\mu\text{-}SeC_6H_4F\text{-}p)_2(bipy)_2](PF_6)_2$ (**3**) in CD_3CN at 25 ºC. # = water from the solvent; number* = residual bipy.

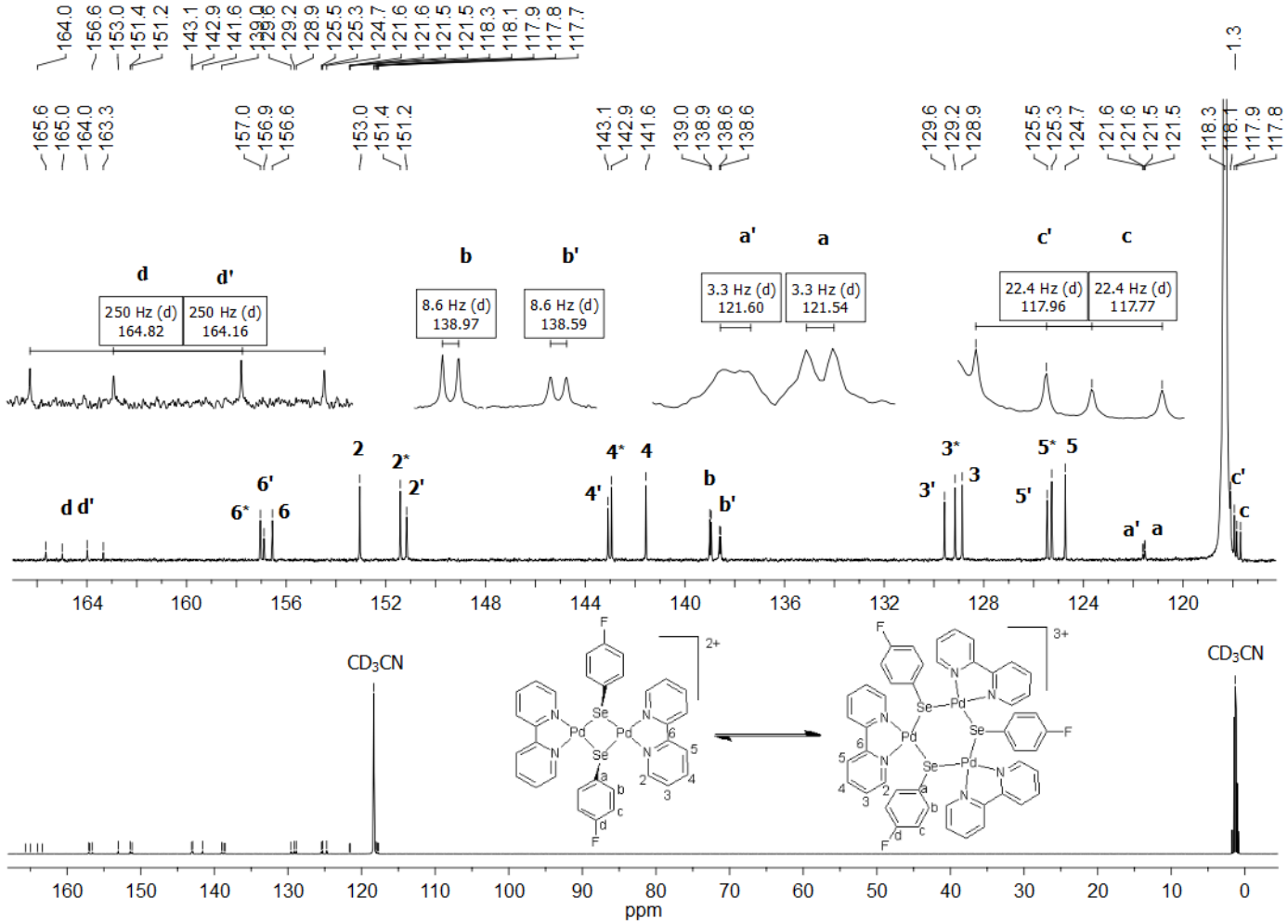

Figure S27. 151 MHz $^{13}C\{^{1}H\}$ NMR spectrum of $[Pd_2(\mu\text{-}SeC_6H_4F\text{-}p)_2(bipy)_2](PF_6)_2$ (**3**) in CD_3CN at 25 ºC. Number* = residual bipy.

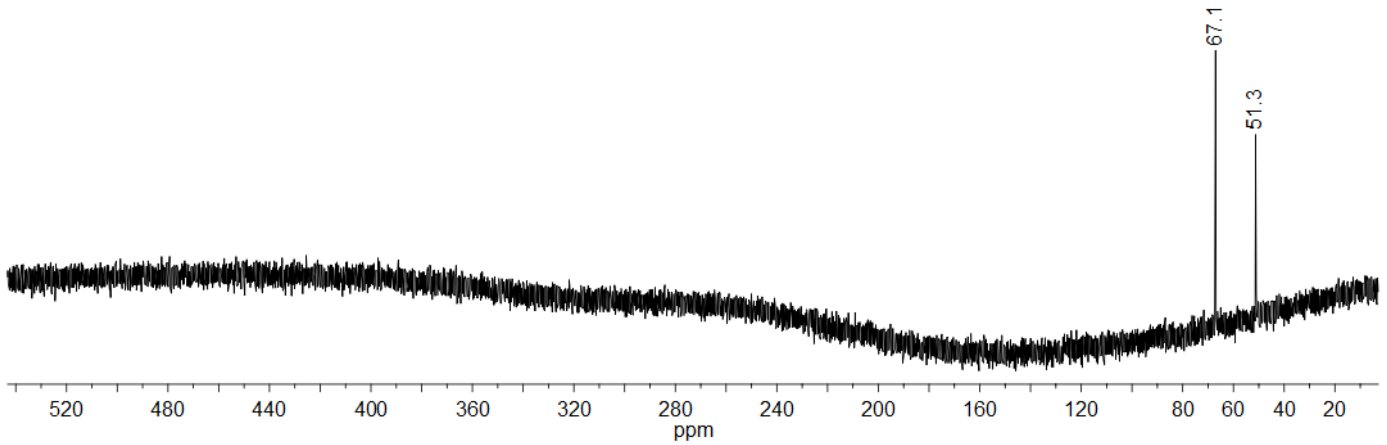

Figure S28. 114 MHz ^{77}Se NMR spectrum of $[Pd_2(\mu\text{-}SeC_6H_4F\text{-}p)_2(bipy)_2](PF_6)_2$ (**3**) in CD_3CN at 25 ºC.

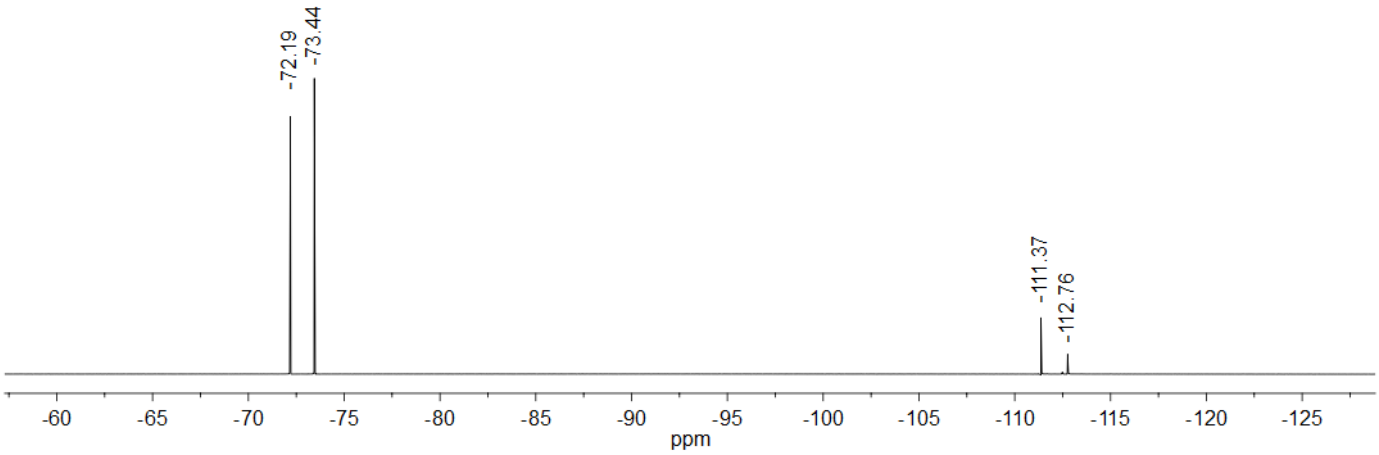

Figure S29. 565 MHz ^{19}F NMR spectrum of $[Pd_2(\mu\text{-}SeC_6H_4F\text{-}p)_2(bipy)_2](PF_6)_2$ (**3**) in CD_3CN at 25 ºC.

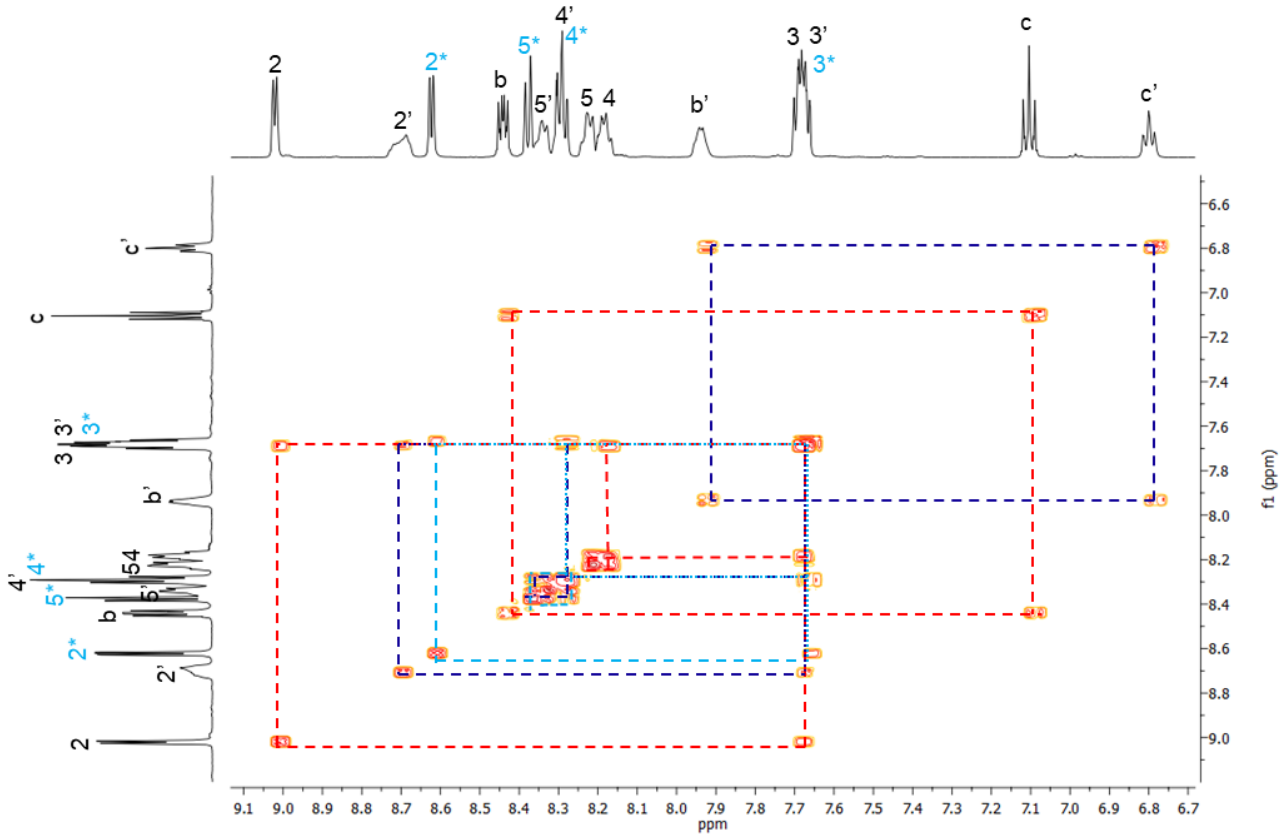

Figure S30. 2D COSY NMR spectrum of $[Pd_2(\mu\text{-}SeC_6H_4F\text{-}p)_2(bipy)_2](PF_6)_2$ (**3**). number* = residual bipy.

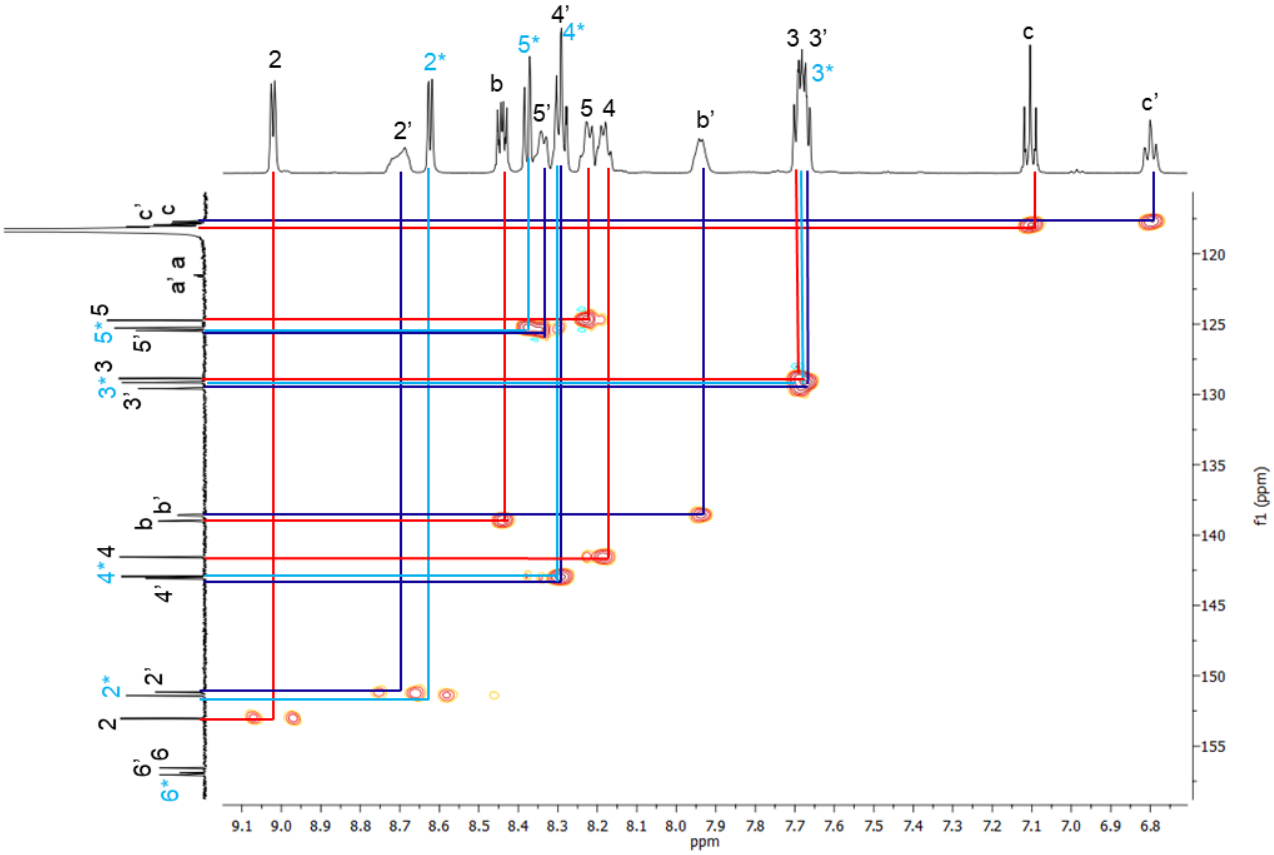

Figure S31. 2D HSQC NMR spectrum of $[Pd_2(\mu\text{-}SeC_6H_4F\text{-}p)_2(bipy)_2](PF_6)_2$ (**3**) zoomed in. number* = residual bipy.

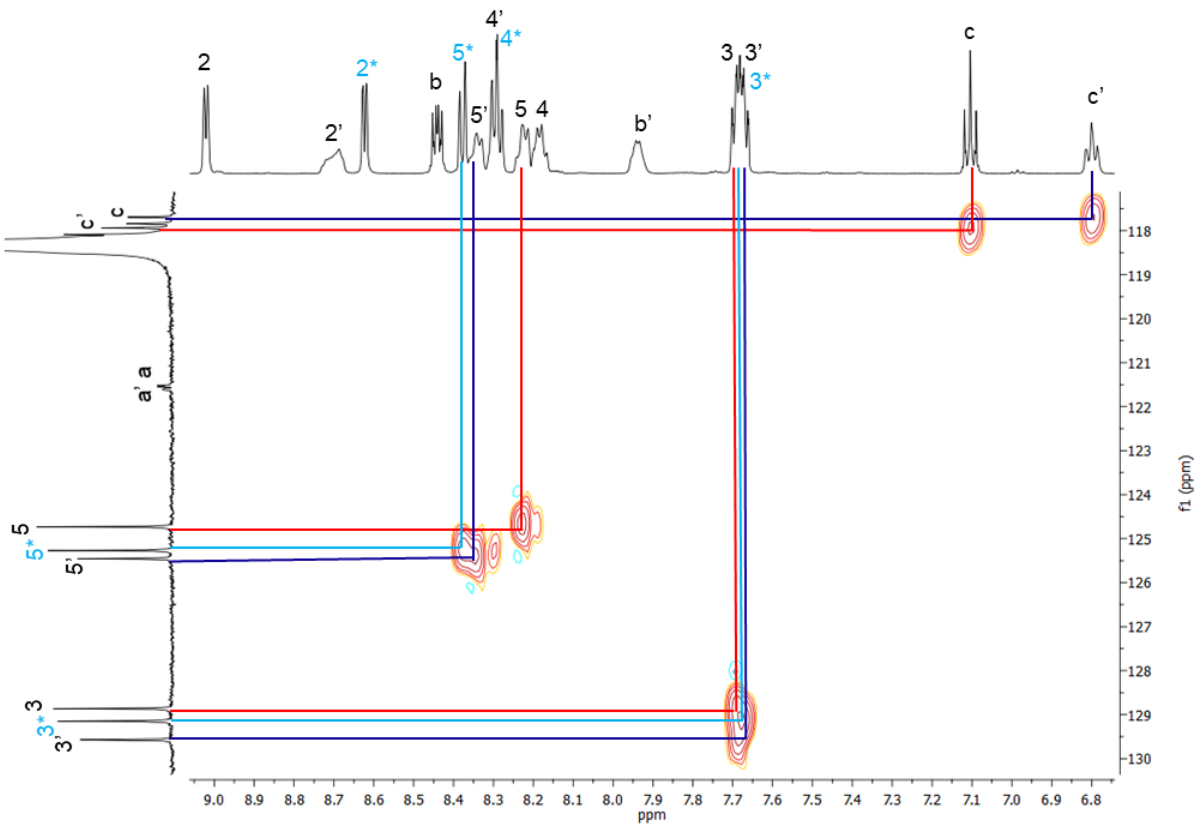

Figure S32. 2D HSQC NMR spectrum of $[Pd_2(\mu\text{-}SeC_6H_4F\text{-}p)_2(bipy)_2](PF_6)_2$ (**3**) zoomed in. number* = residual bipy.

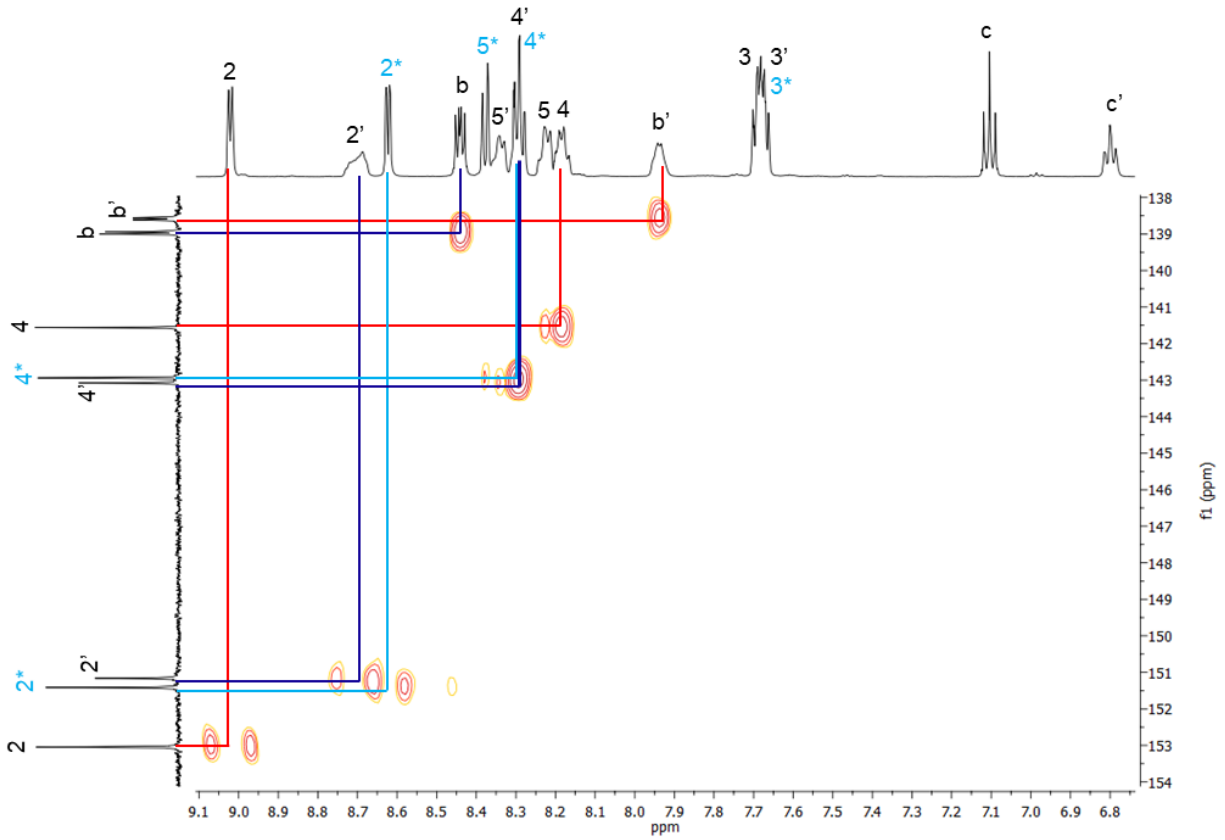

Figure S33. 2D HSQC NMR spectrum of $[Pd_2(\mu\text{-}SeC_6H_4F\text{-}p)_2(bipy)_2](PF_6)_2$ (**3**) zoomed in. number* = residual bipy.

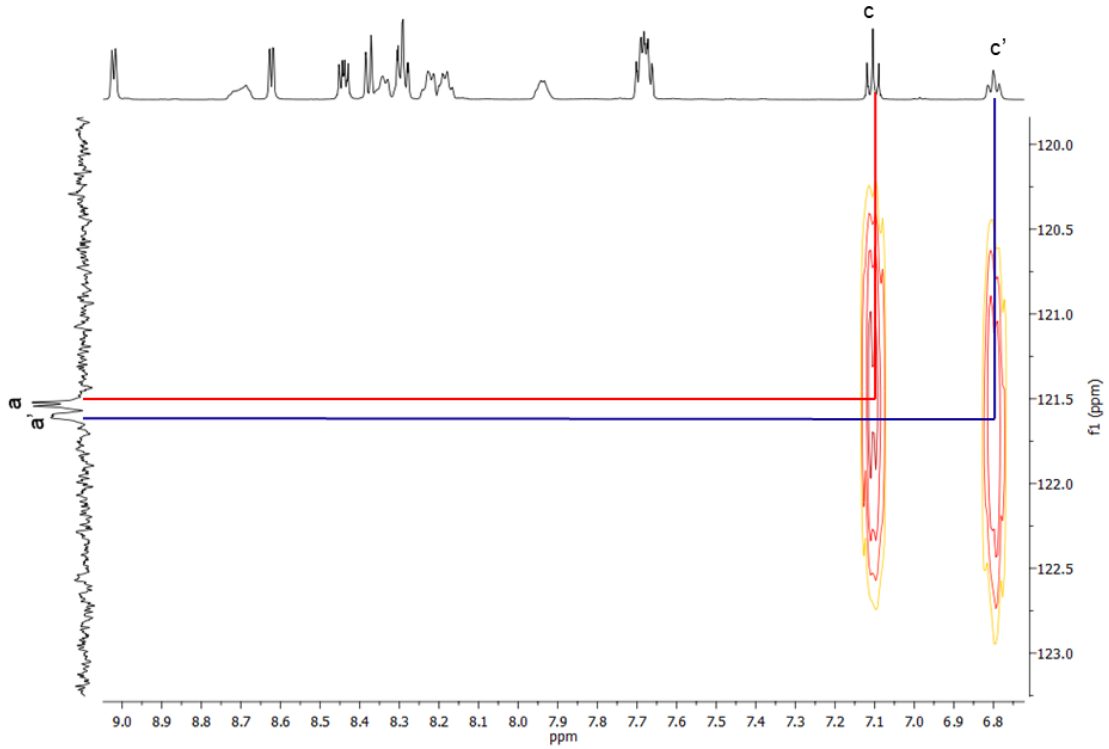

Figure S34. 2D HMBC NMR spectrum of $[Pd_2(\mu\text{-}SeC_6H_4F\text{-}p)_2(bipy)_2](PF_6)_2$ (**3**) zoomed in. number* = residual bipy.

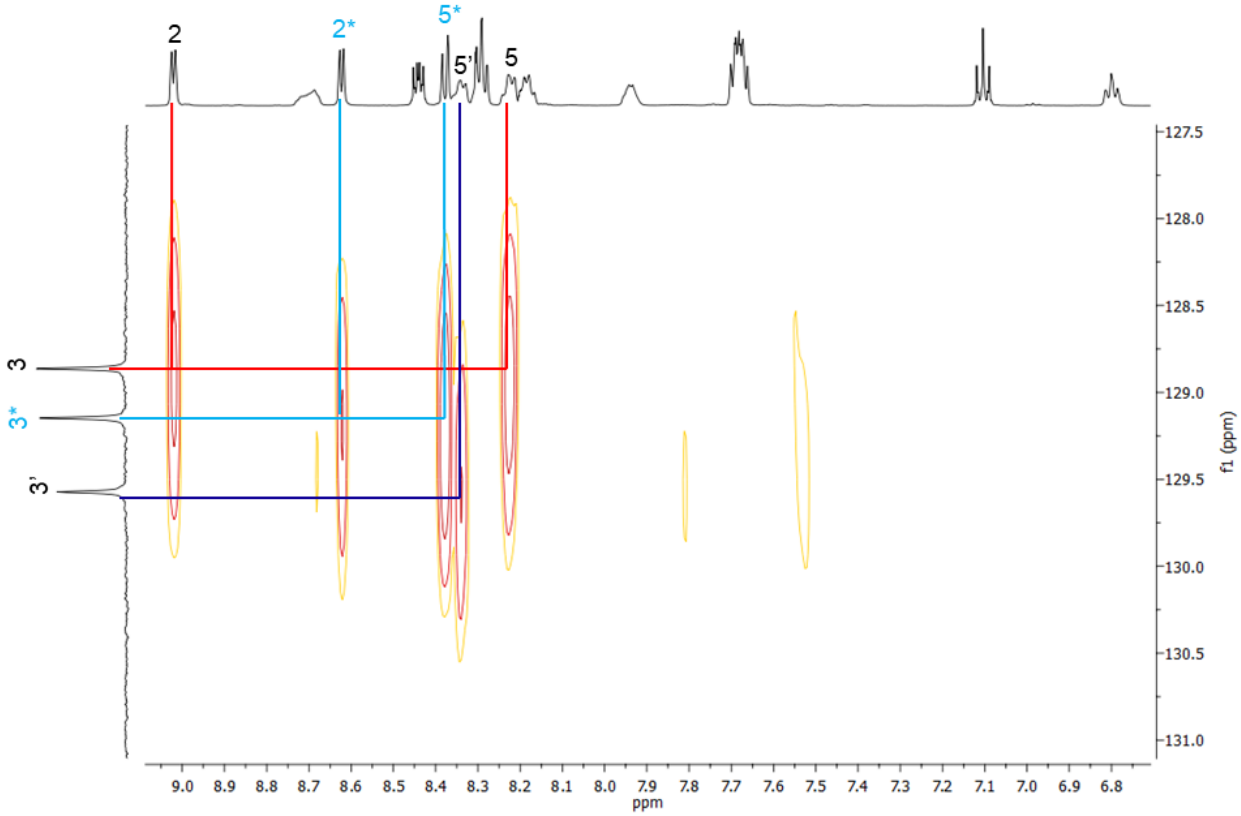

Figure S35. 2D HMBC NMR spectrum of $[Pd_2(\mu\text{-}SeC_6H_4F\text{-}p)_2(bipy)_2](PF_6)_2$ (**3**) zoomed in. number* = residual bipy.

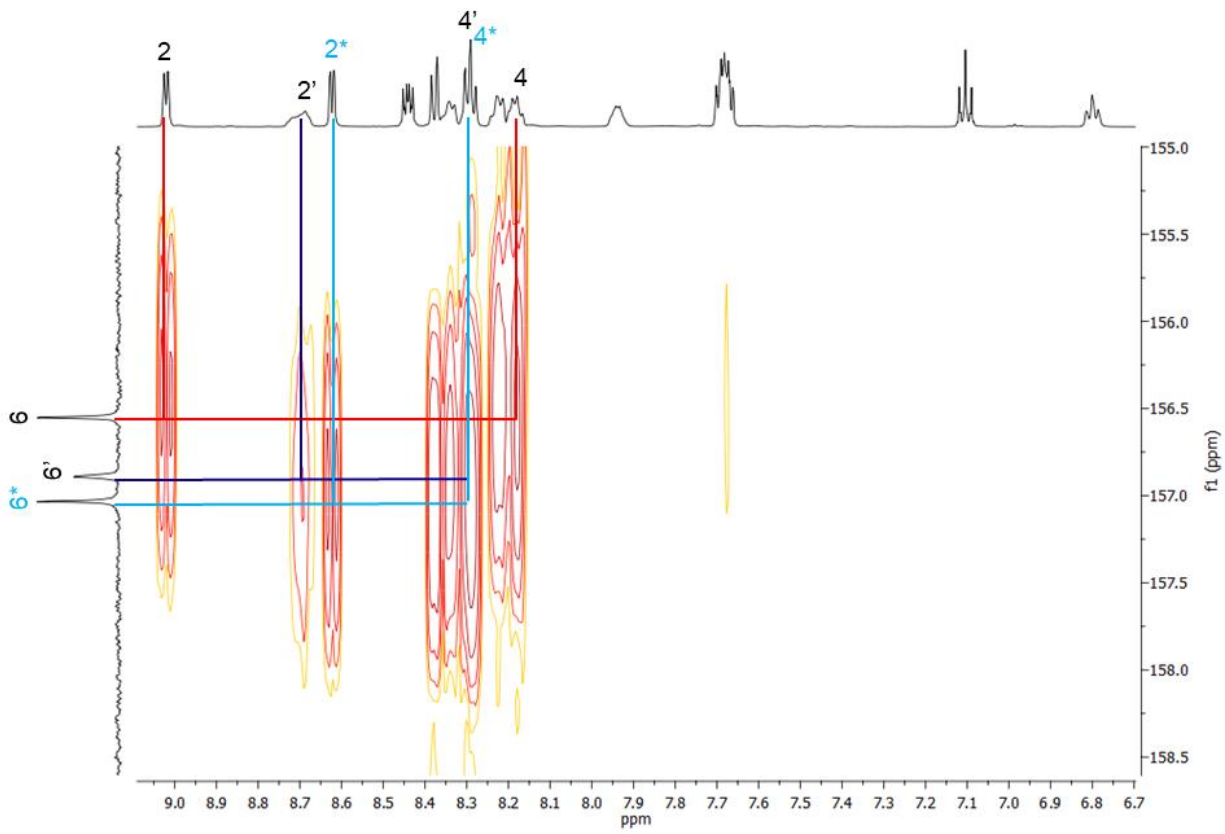

Figure S36. 2D HMBC NMR spectrum of $[Pd_2(\mu\text{-}SeC_6H_4F\text{-}p)_2(bipy)_2](PF_6)_2$ (**3**) zoomed in. number* = residual bipy.

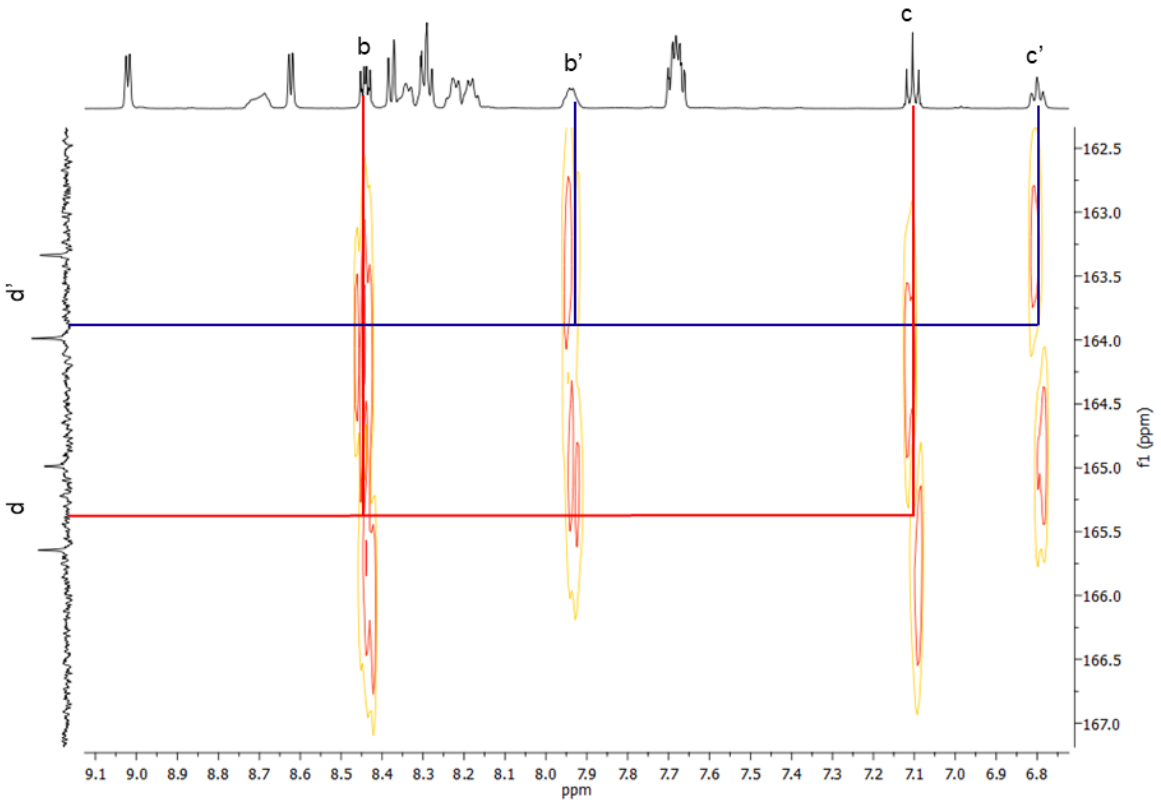

Figure S37. 2D HMBC NMR spectrum of $[Pd_2(\mu\text{-}SeC_6H_4F\text{-}p)_2(bipy)_2](PF_6)_2$ (**3**) zoomed in. number* = residual bipy.

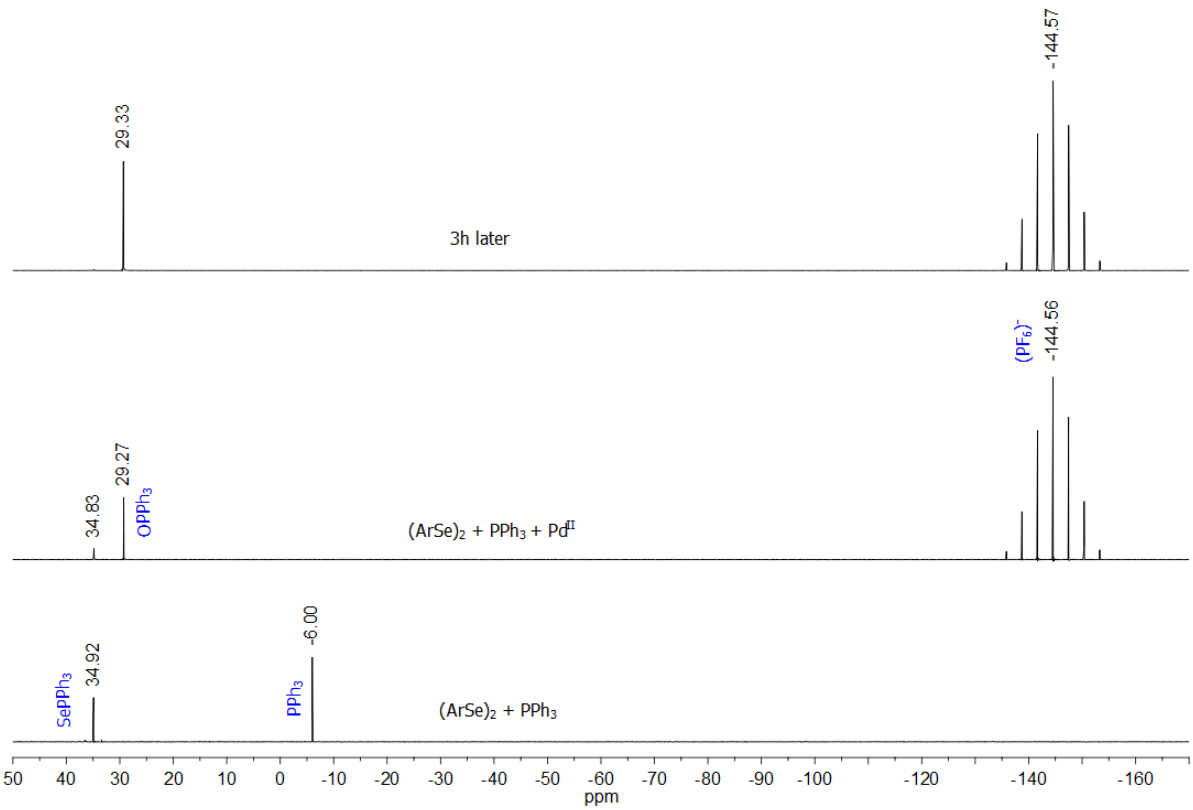

Figure S38. ^{31}P NMR spectra of the followed reaction to obtain $[Pd_2(\mu\text{-}SeC_6H_4F\text{-}p)_2(bipy)_2](PF_6)_2$ (**3**).

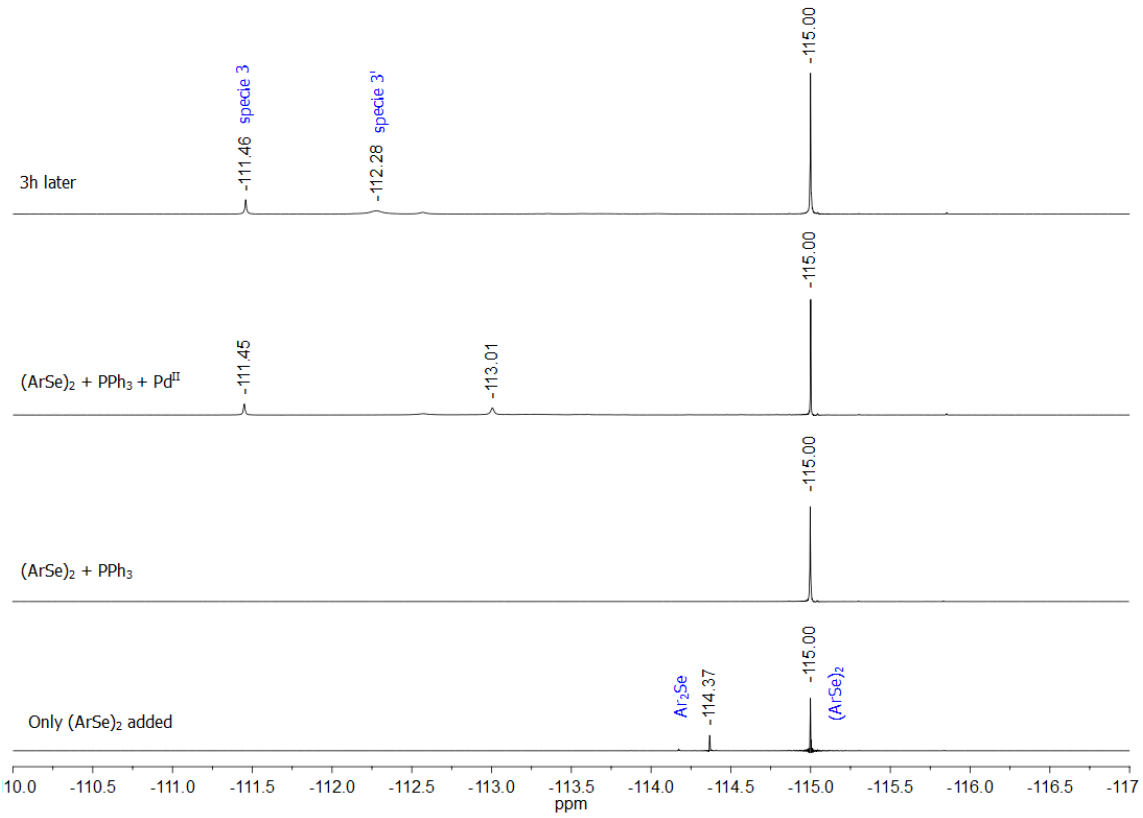

Figure S39. ^{19}F NMR spectra of the followed reaction to obtain $[Pd_2(\mu\text{-}SeC_6H_4F\text{-}p)_2(bipy)_2](PF_6)_2$ (**3**).

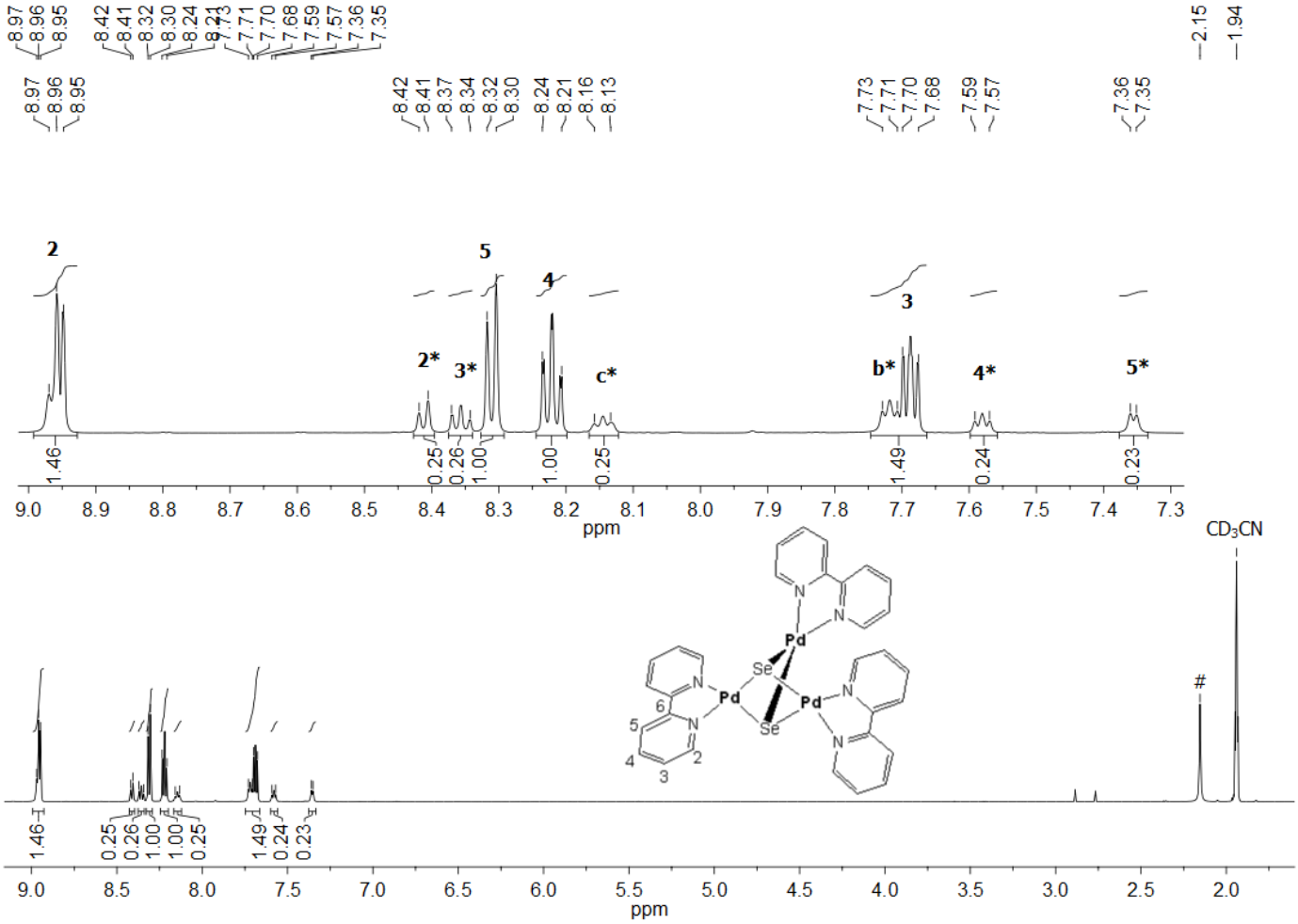

Figure S40. 600 MHz ^{1}H NMR spectrum of $[Pd_3(\mu_3\text{-}Se)_2(bipy)_3](PF_6)_2{\cdot}5THF$ (**4**) in CD_3CN at 25 ºC. # = water from the solvent; number* = residual bipy; letter* = residual py.

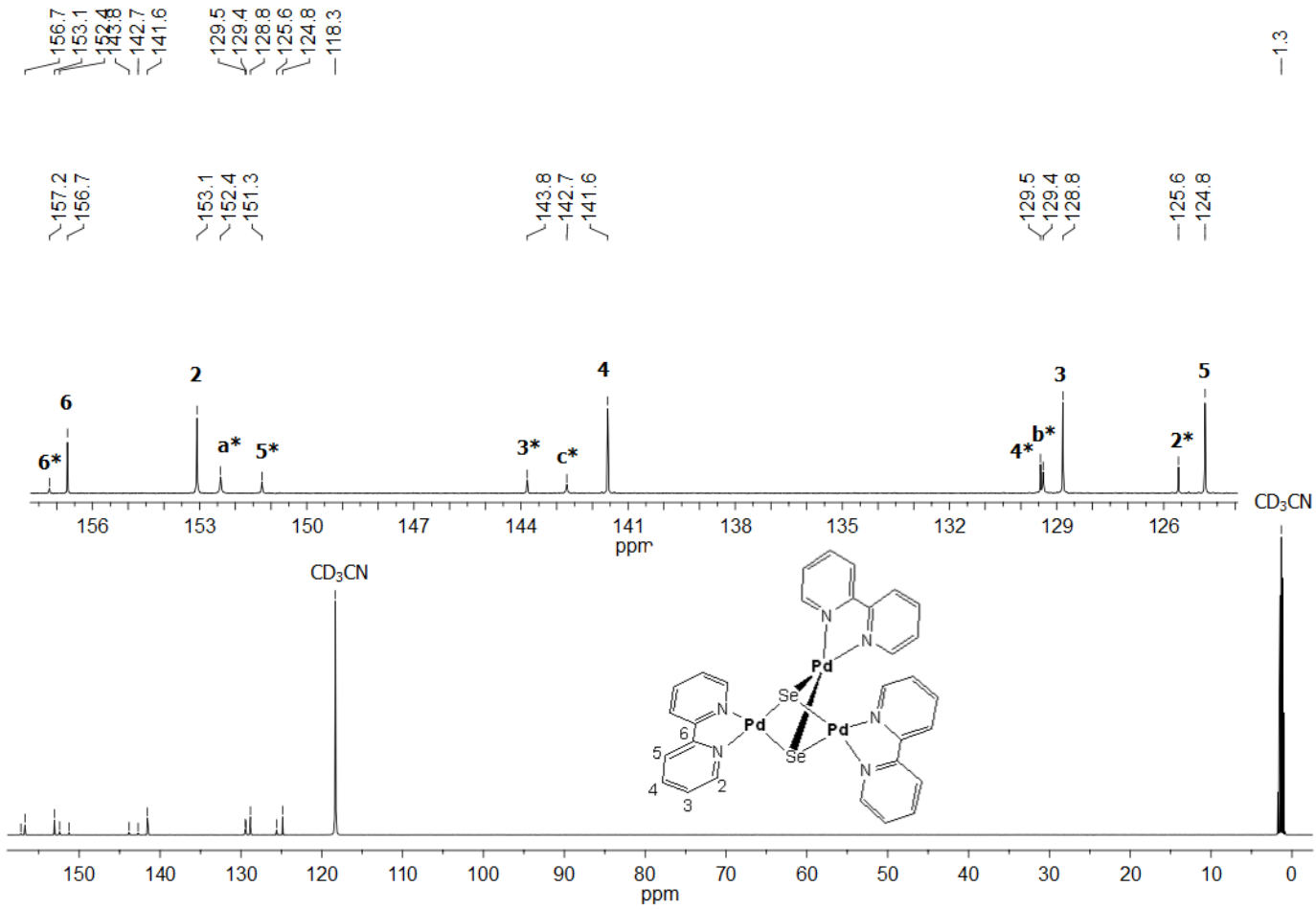

Figure S41. 151 MHz $^{13}C\{^{1}H\}$ NMR spectrum of $[Pd_3(\mu_3\text{-}Se)_2(bipy)_3](PF_6)_2\cdot 5THF$ (**4**) in CD_3CN at 25 ºC. Number* = residual bipy; letter* = residual py.

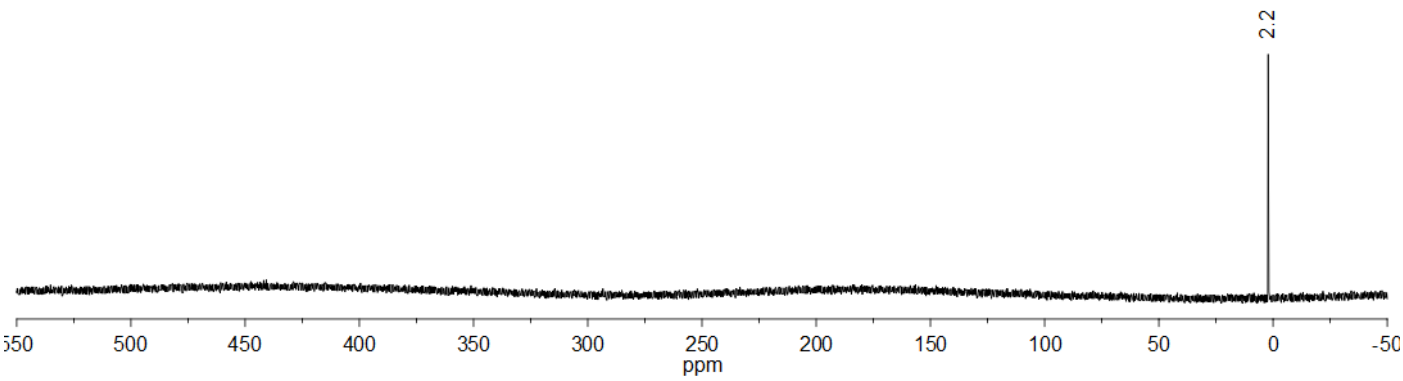

Figure S42. 114 MHz ^{77}Se NMR spectrum of $[Pd_3(\mu_3\text{-}Se)_2(bipy)_3](PF_6)_2\cdot 5THF$ (**4**) in CD_3CN at 25 ºC.

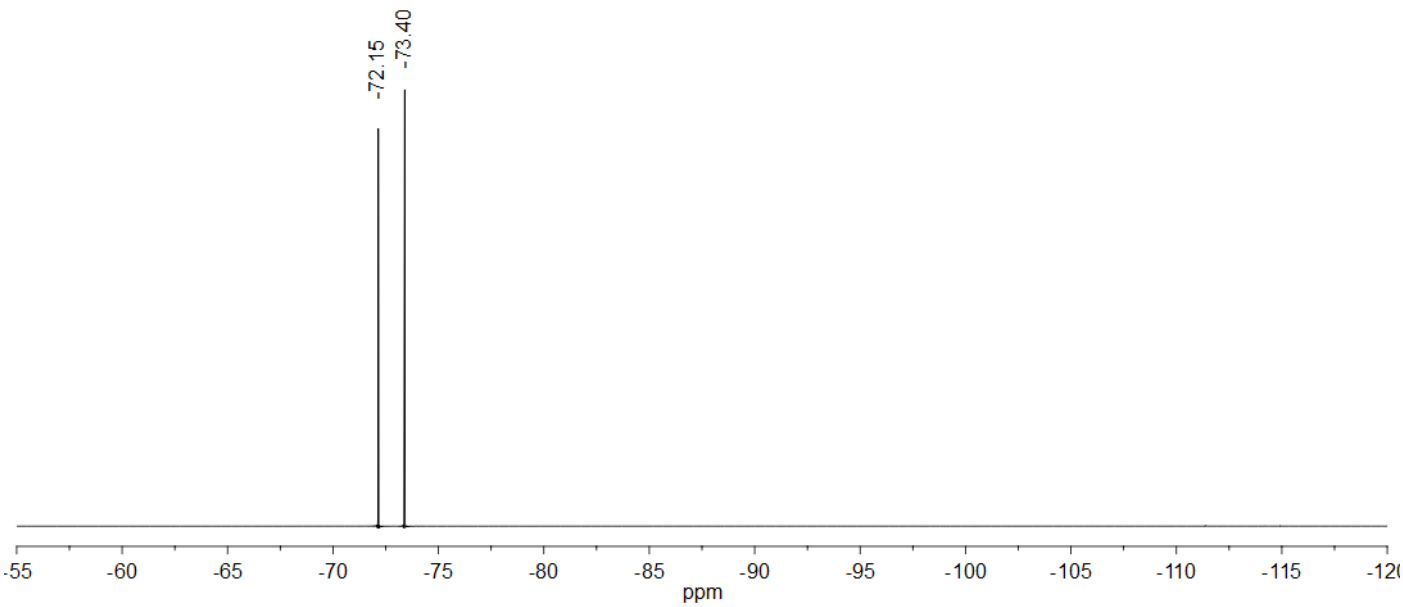

Figure S43. 565 MHz ^{19}F NMR spectrum of $[Pd_3(\mu_3\text{-}Se)_2(bipy)_3](PF_6)_2\cdot 5THF$ (**4**) in CD_3CN at 25 ºC.

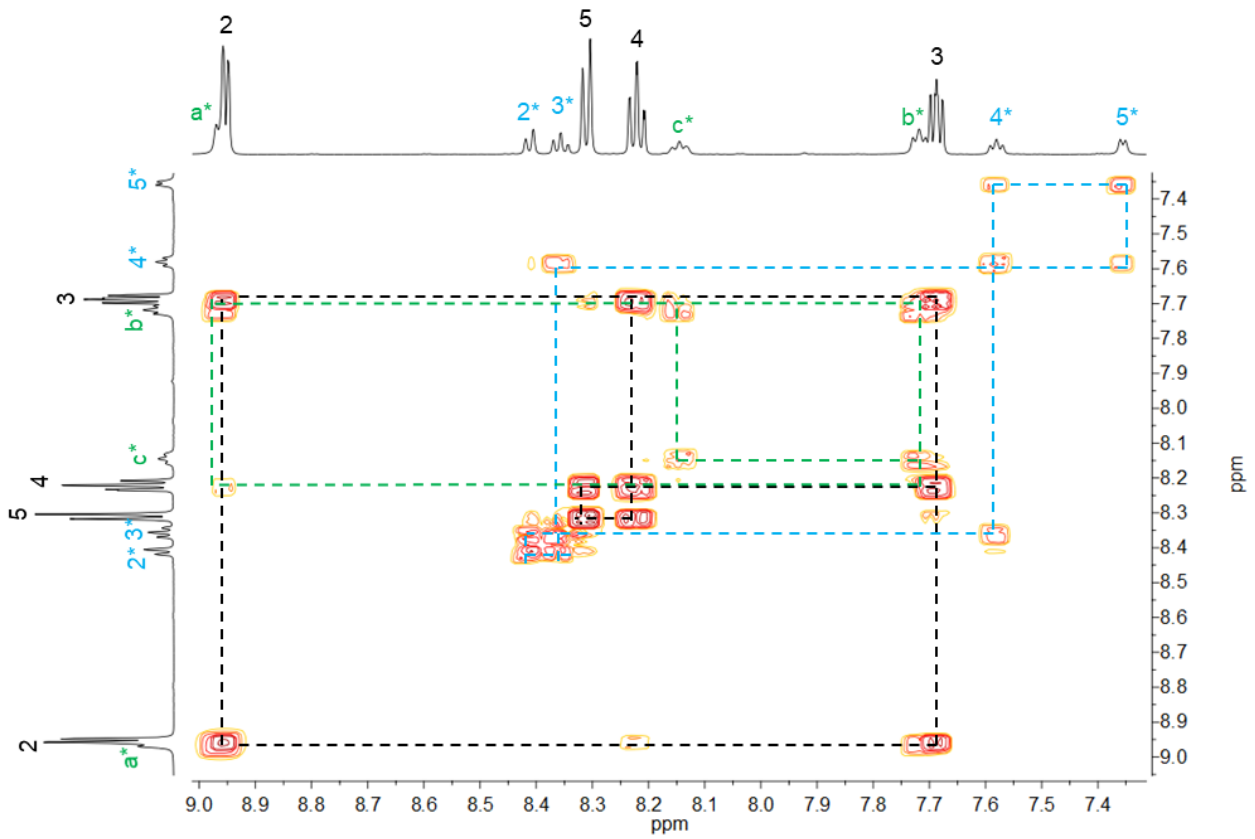

Figure S44. 2D COSY NMR spectrum of $[Pd_3(\mu_3\text{-}Se)_2(bipy)_3](PF_6)_2\cdot 5THF$ (**4**). number* = residual bipy; letter* = residual py.

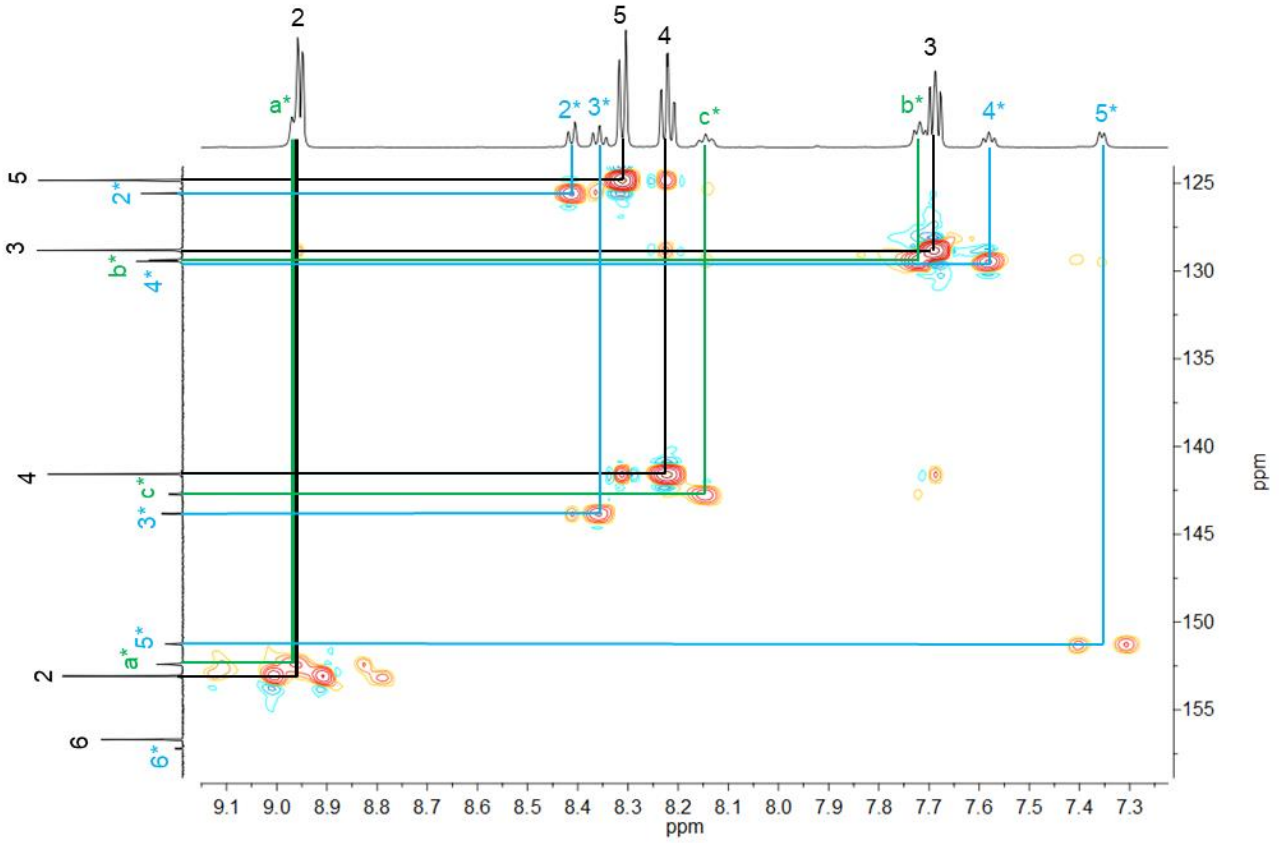

Figure S45. 2D HSQC NMR spectrum of $[Pd_3(\mu_3\text{-}Se)_2(bipy)_3](PF_6)_2\cdot 5THF$ (**4**). number* = residual bipy; letter* = residual py.

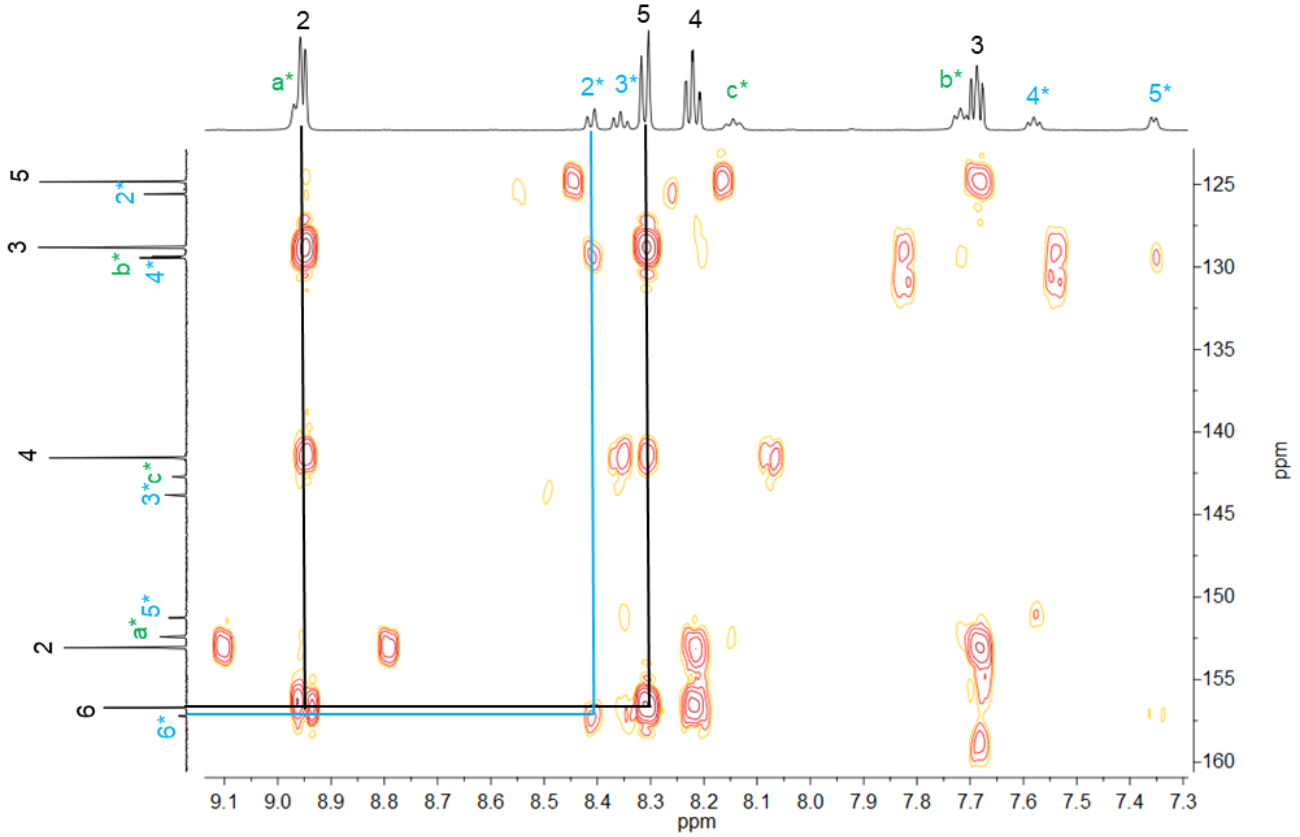

Figure S46. 2D HMBC NMR spectrum of $[Pd_3(\mu_3\text{-}Se)_2(bipy)_3](PF_6)_2\cdot 5THF$ (**4**). number* = residual bipy; letter* = residual py.

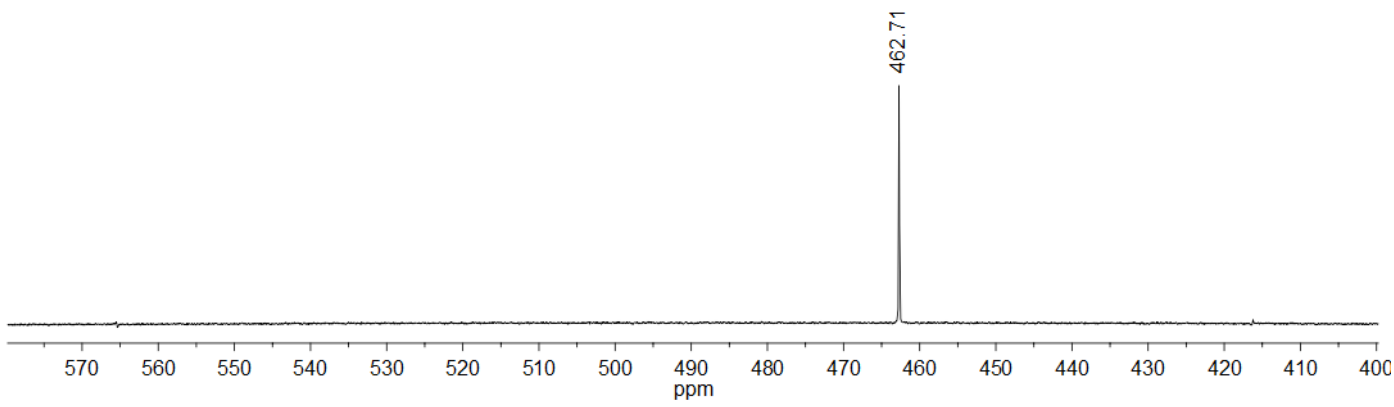

Figure S47. 114 MHz ^{77}Se NMR spectrum of $(PhSe)_2$ in $CDCl_3$.

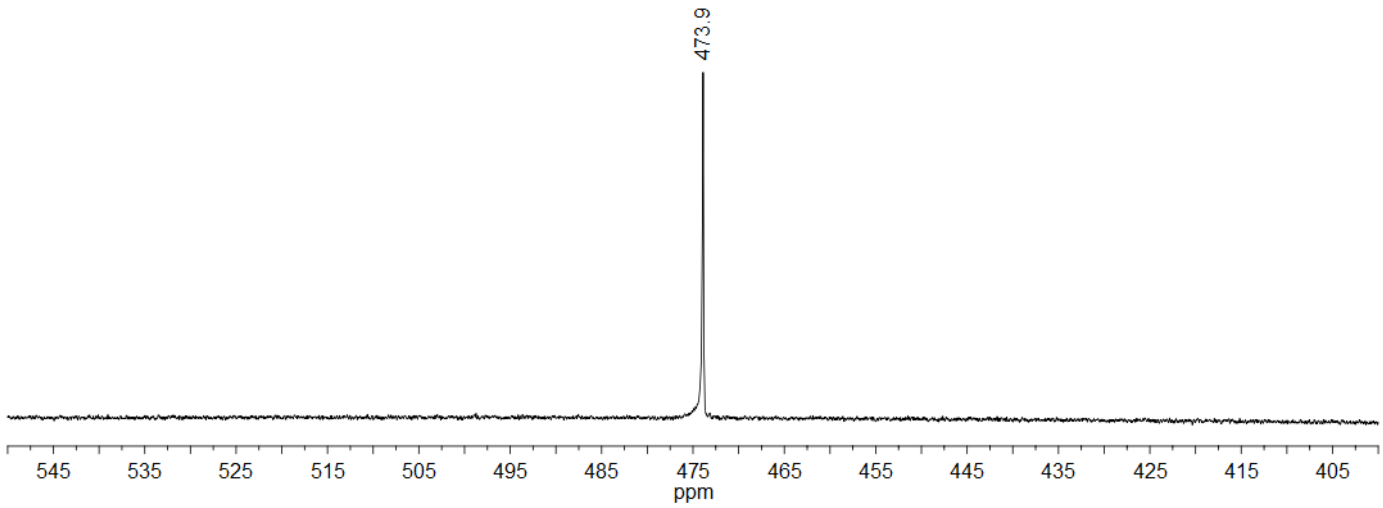

Figure S48. 114 MHz ^{77}Se NMR spectrum of $(p\text{-}ClC_6H_4Se)_2$ in $CDCl_3$.

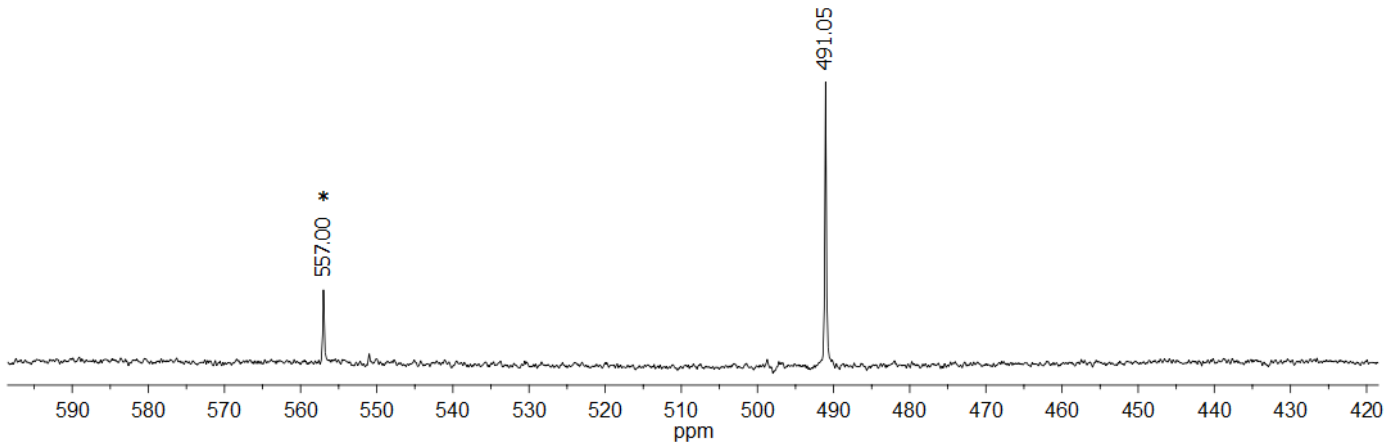

Figure S49. 114 MHz ^{77}Se NMR spectrum of $(p\text{-}FC_6H_4Se)_2$ in $CDCl_3$. * = impurity of $(p\text{-}FC_6H_4)_2Se$.

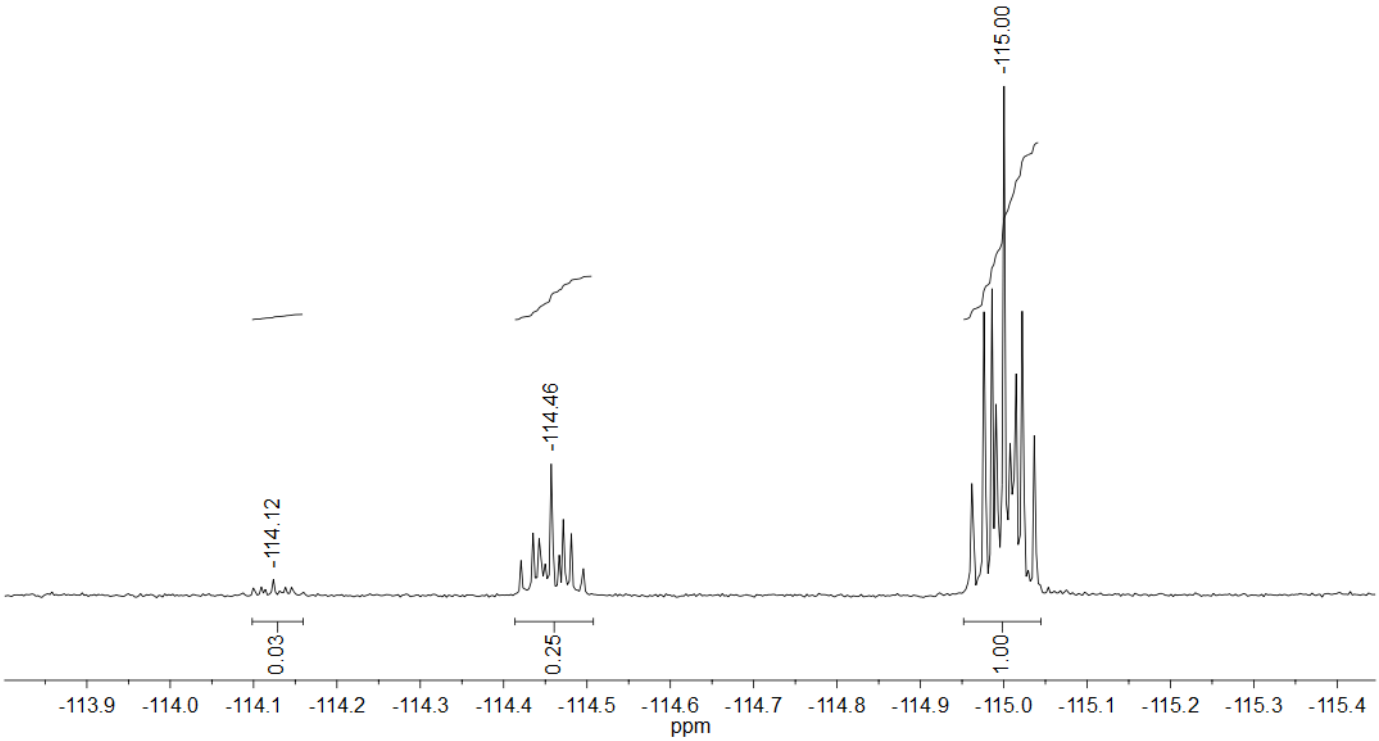

Figure S50. 565 MHz ^{19}F NMR spectrum of (p-$FC_6H_4Se)_2$ in $CDCl_3$. * = impurity of (p-$FC_6H_4)_2Se$.

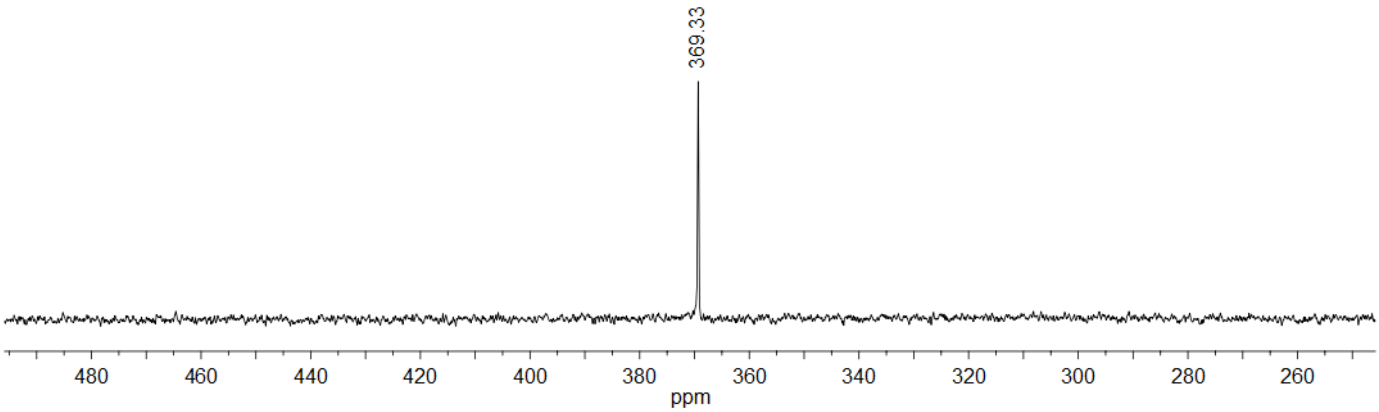

Figure S51. 114 MHz ^{77}Se NMR spectrum of $(MesSe)_2$ in $CDCl_3$.

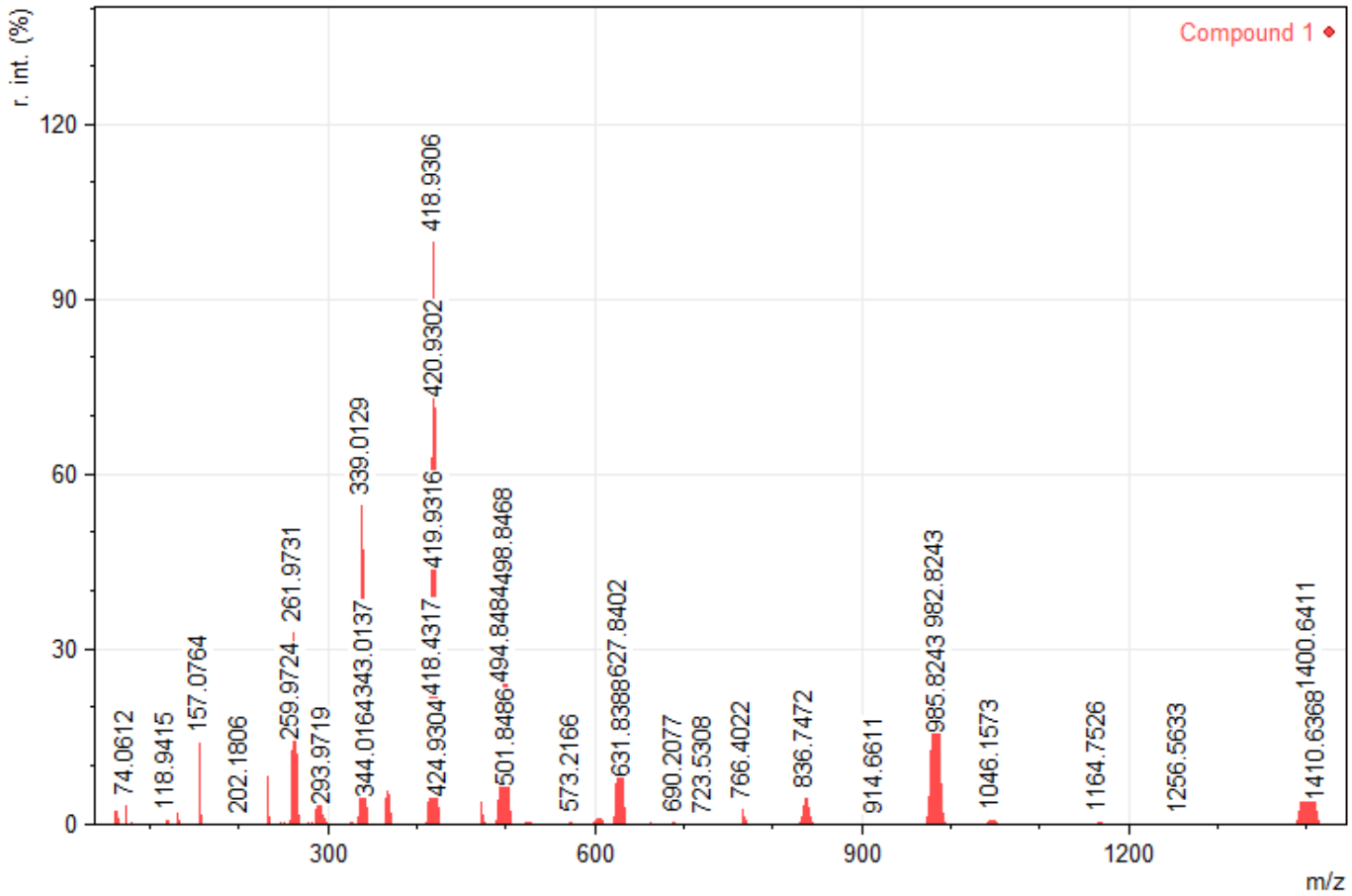

Figure S52. ESI$^+$ mass spectrum for compound $[Pd_2(\mu\text{-SePh})_2(bipy)_2](PF_6)_2$ (**1**).

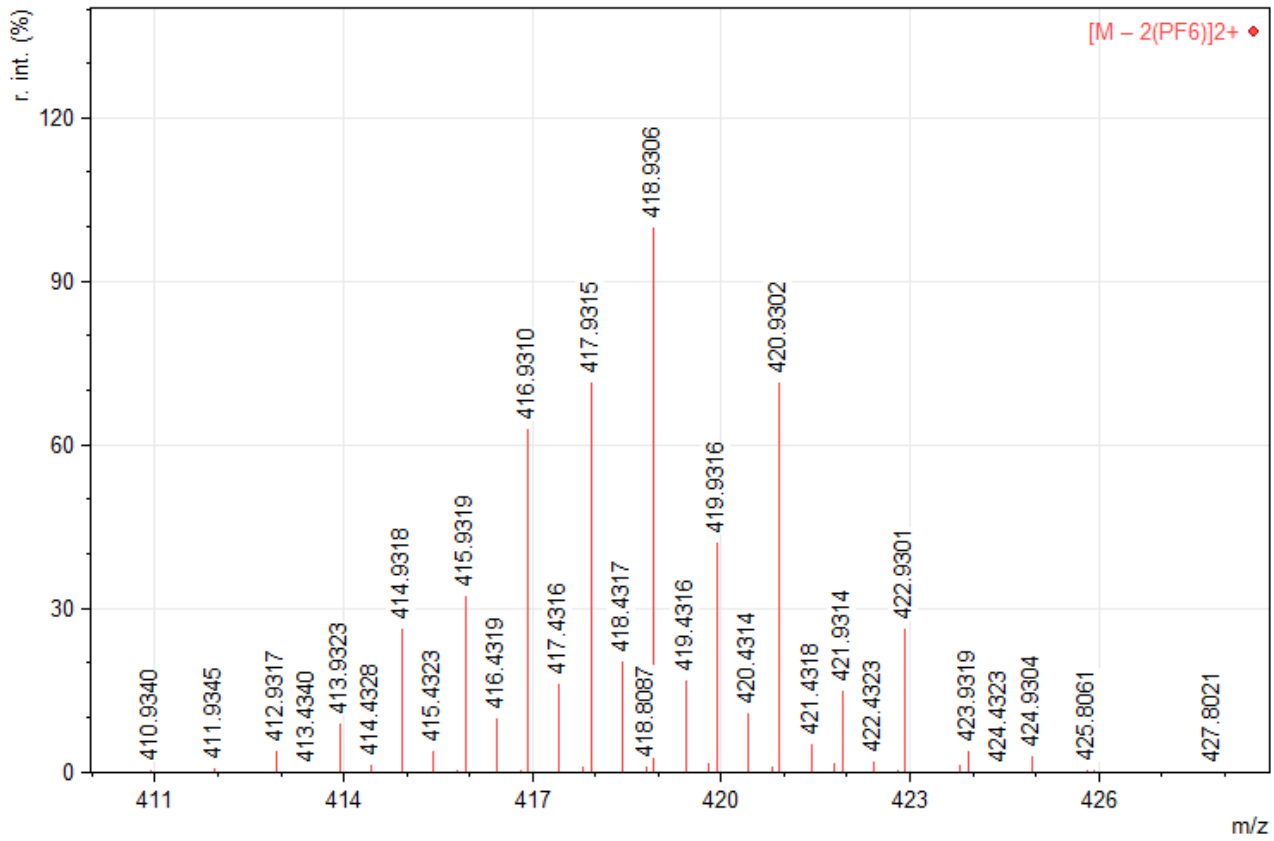

Figure S53. ESI$^+$ mass spectrum of **1** zoomed in the molecular ion fragment $[M – 2(PF_6)]^{2+}$.

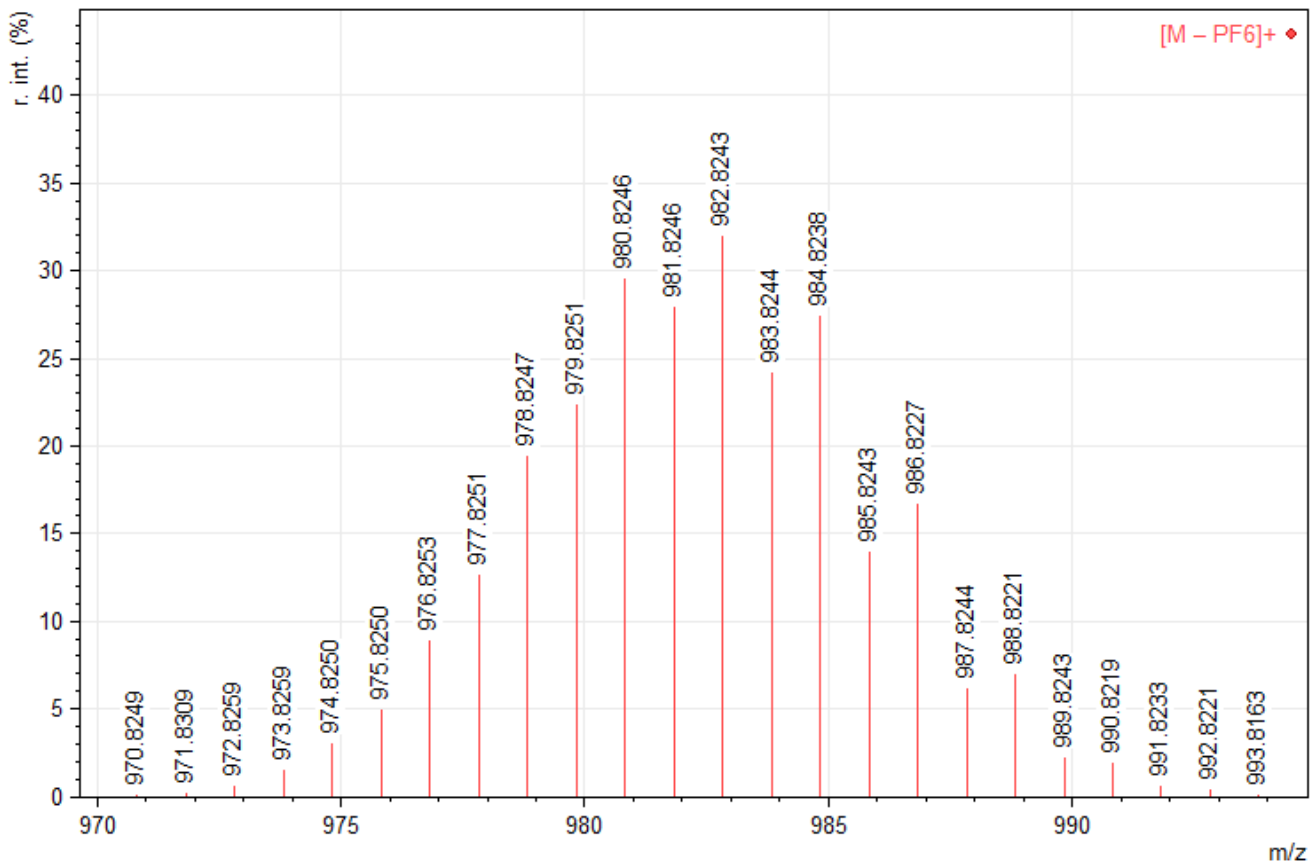

Figure S54. ESI$^+$ mass spectrum of **1** zoomed in the molecular ion fragment $[M – PF_6]^+$.

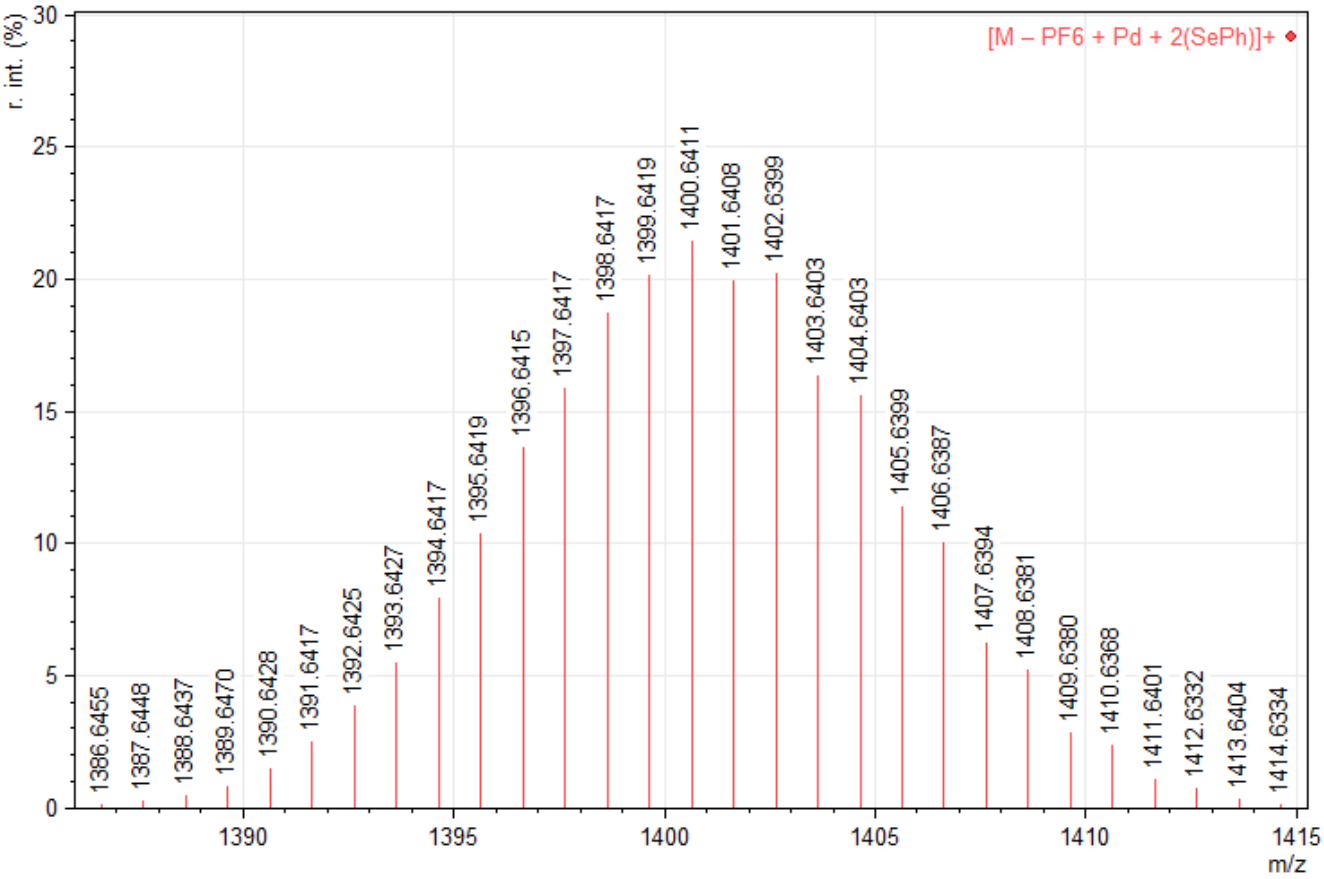

Figure S55. ESI$^+$ mass spectrum of **1** zoomed in the trinuclear fragment $[M – PF_6 + Pd + 2(SePh)]^+$.

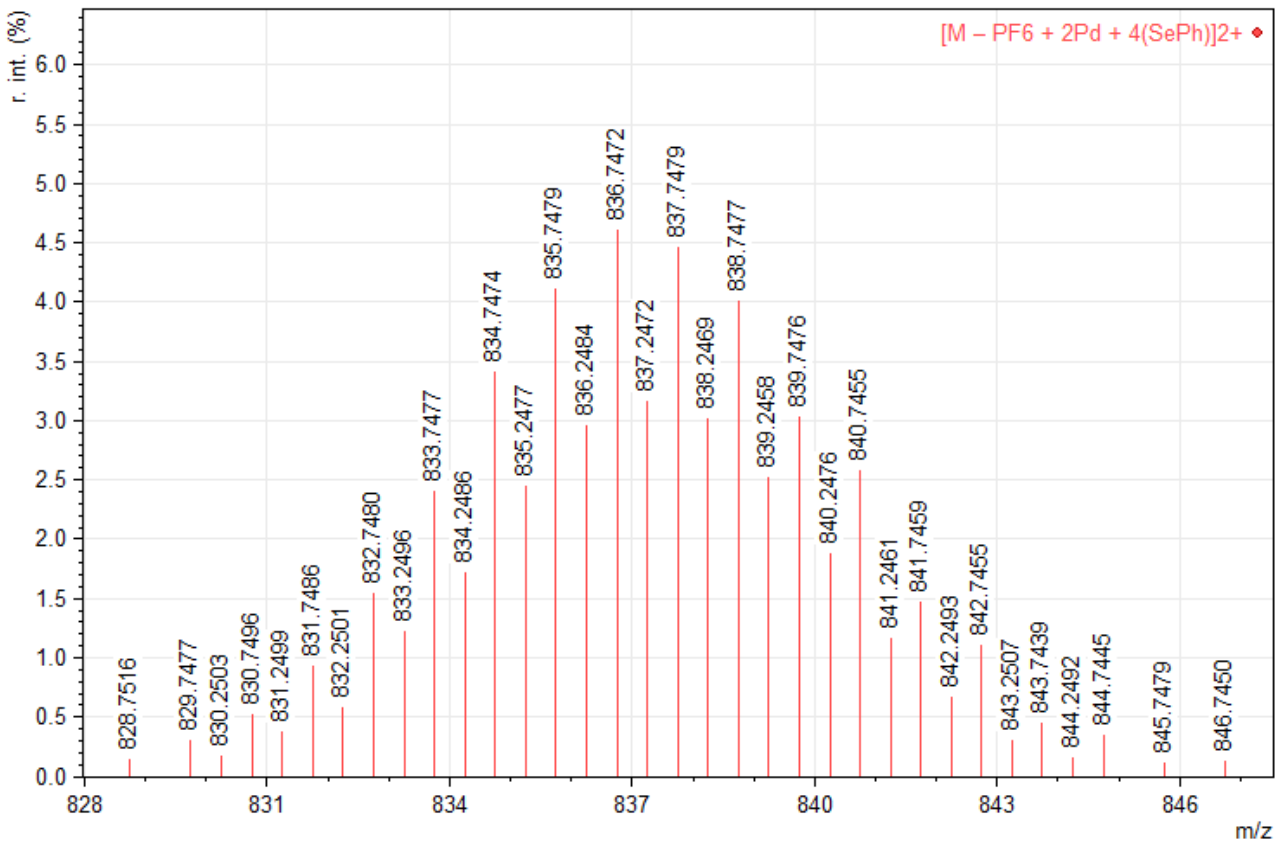

Figure S56. ESI$^+$ mass spectrum of **1** zoomed in the tetranuclear fragment $[M – 2(PF_6) + 2Pd + 4(SePh)]^{2+}$.

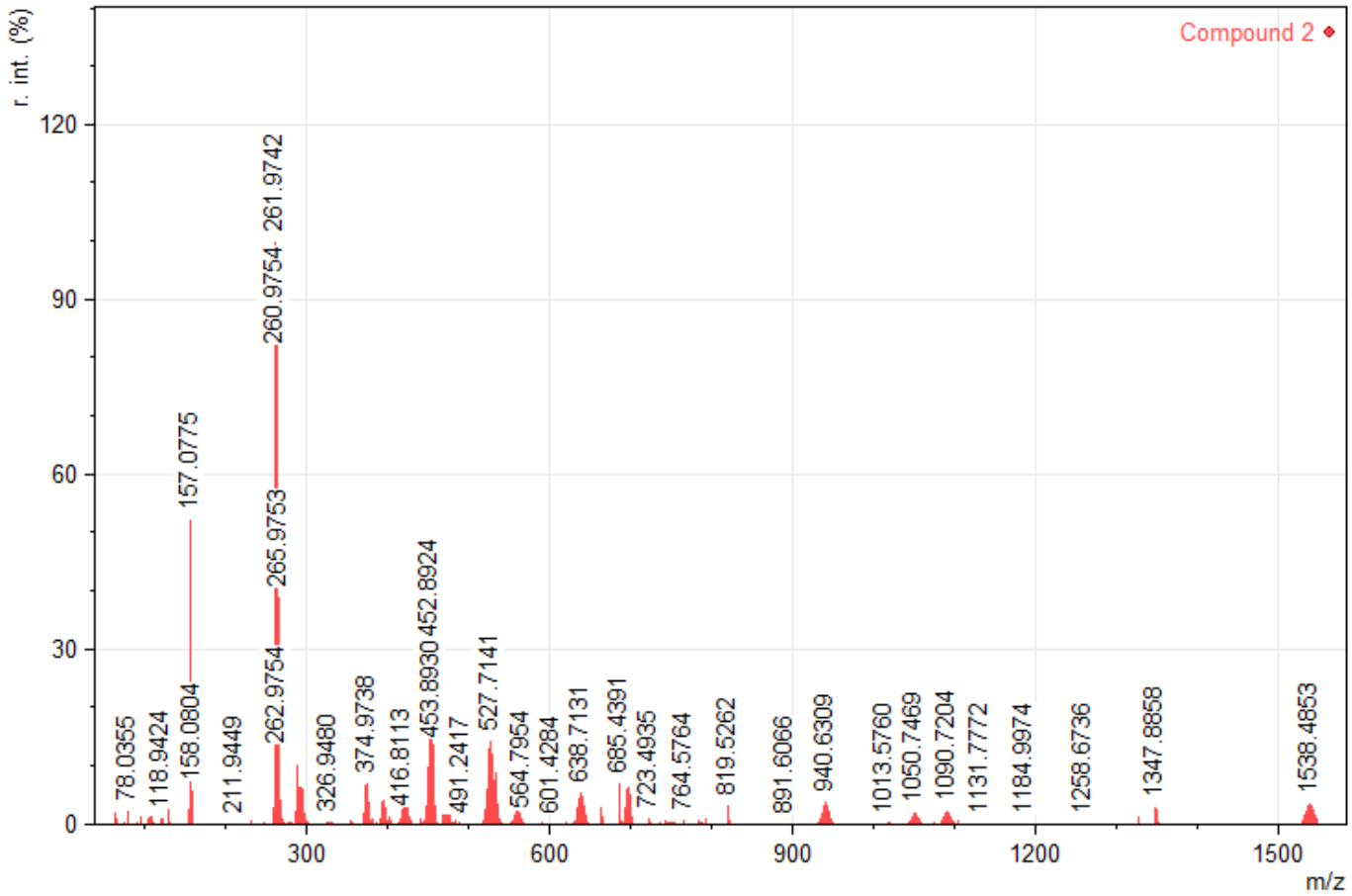

Figure S57. ESI$^+$ mass spectrum for compound $[Pd_2(\mu\text{-}SeC_6H_4Cl\text{-}p)_2(bipy)_2](PF_6)_2$ (**2**).

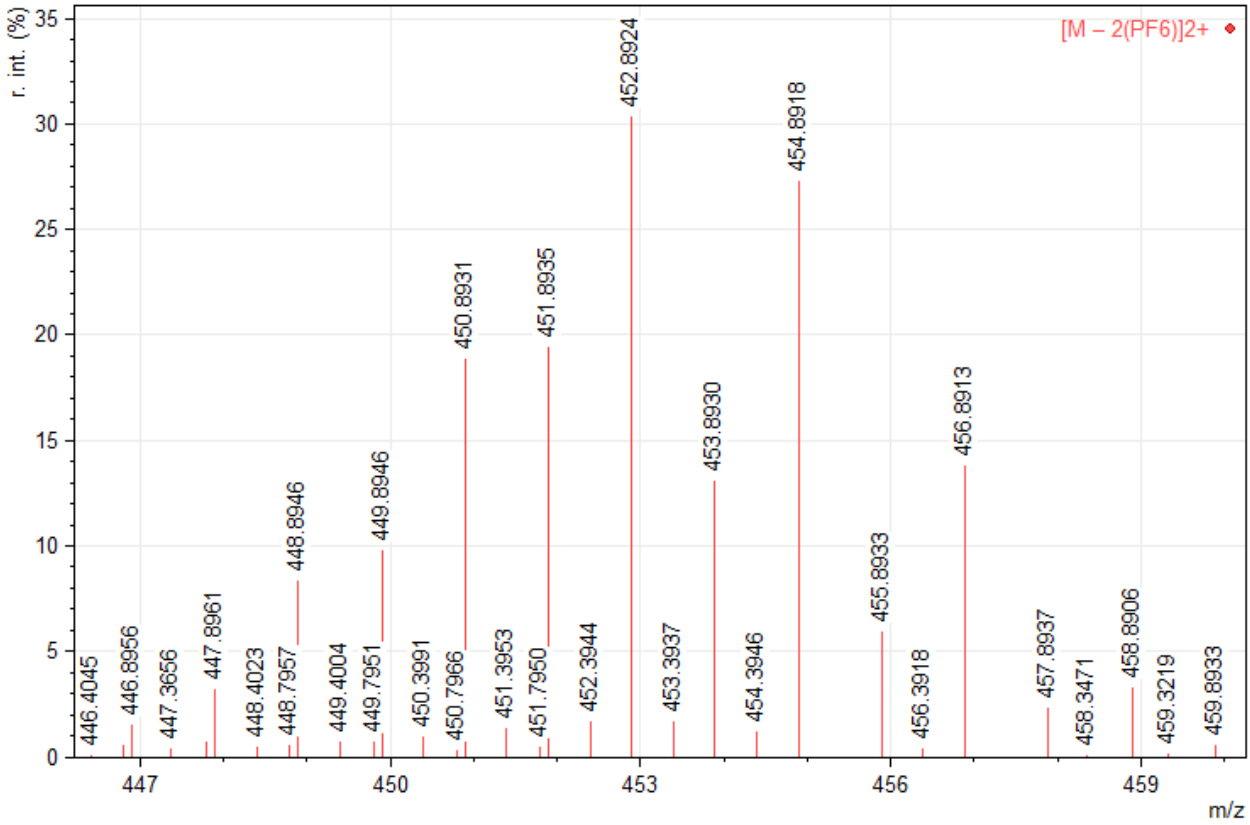

Figure S58. ESI$^+$ mass spectrum of **2** zoomed in the molecular ion fragment $[M – 2(PF_6)]^{2+}$.

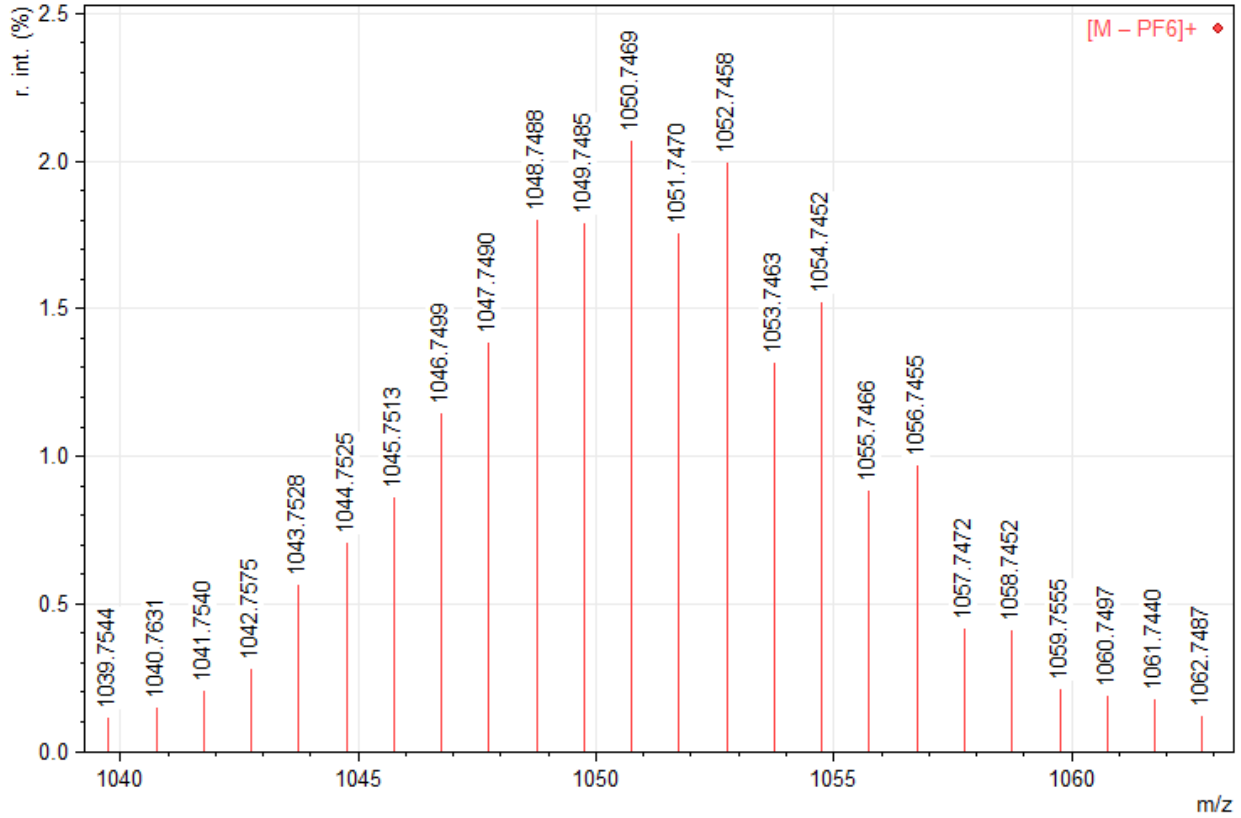

Figure S59. ESI$^+$ mass spectrum of **2** zoomed in the molecular ion fragment $[M – PF_6]^+$.

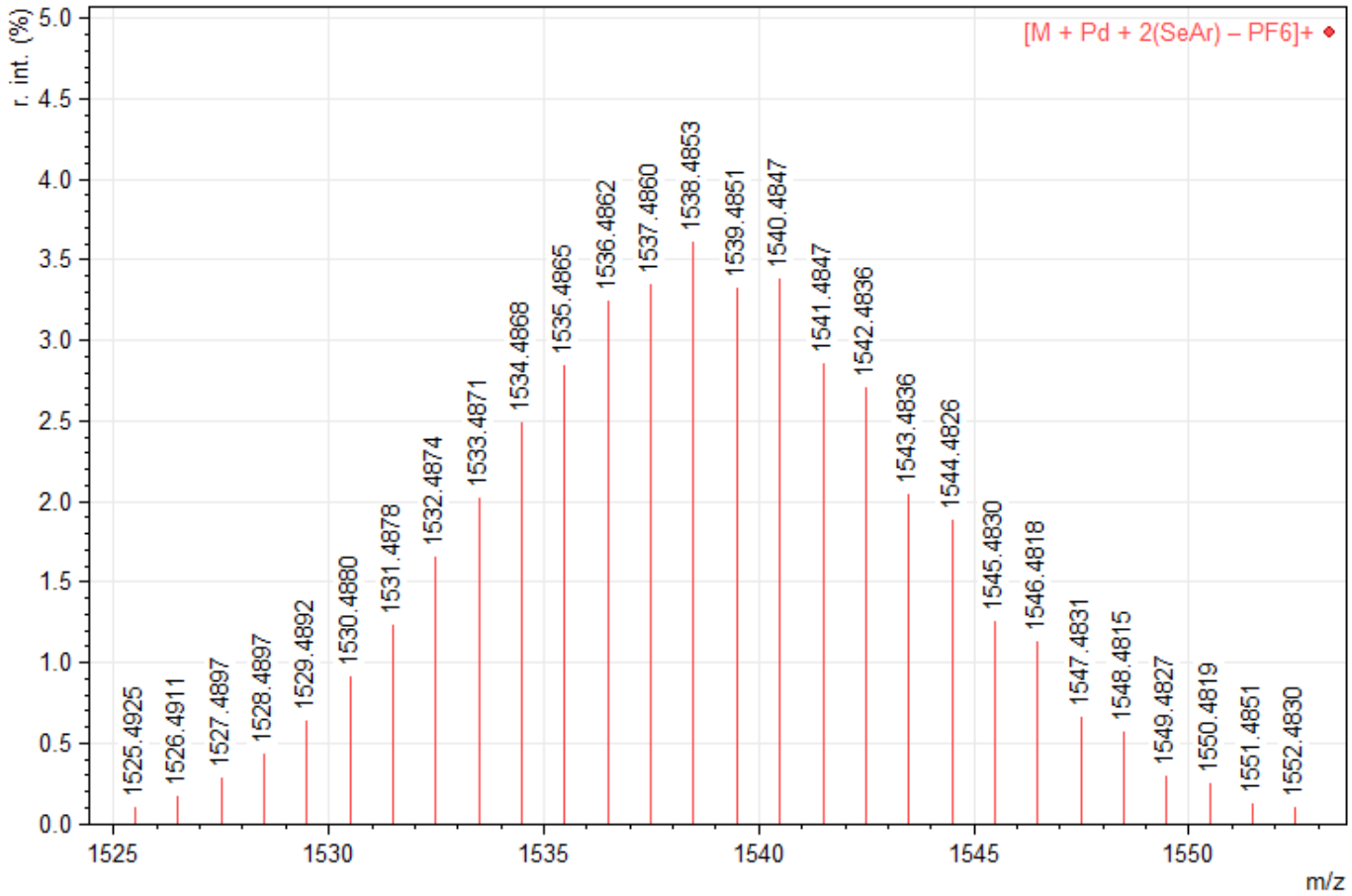

Figure S60. ESI$^+$ mass spectrum of **2** zoomed in the trimeric fragment [M + Pd + 2(SeAr) – PF_6]$^+$.

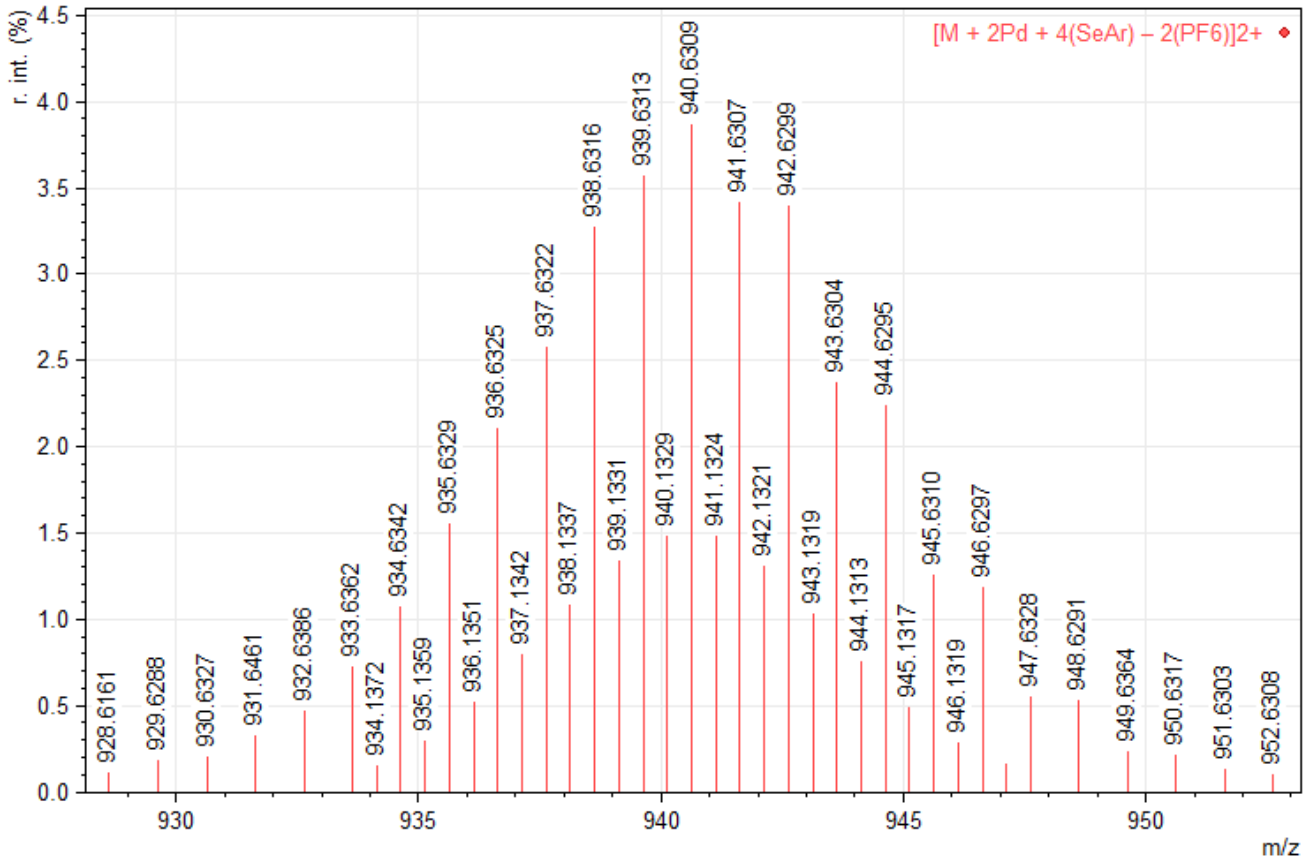

Figure S61. ESI$^+$ mass spectrum of **2** zoomed in the tetrameric fragment [M + 2Pd + 4(SeAr) – 2(PF_6)]$^{2+}$.

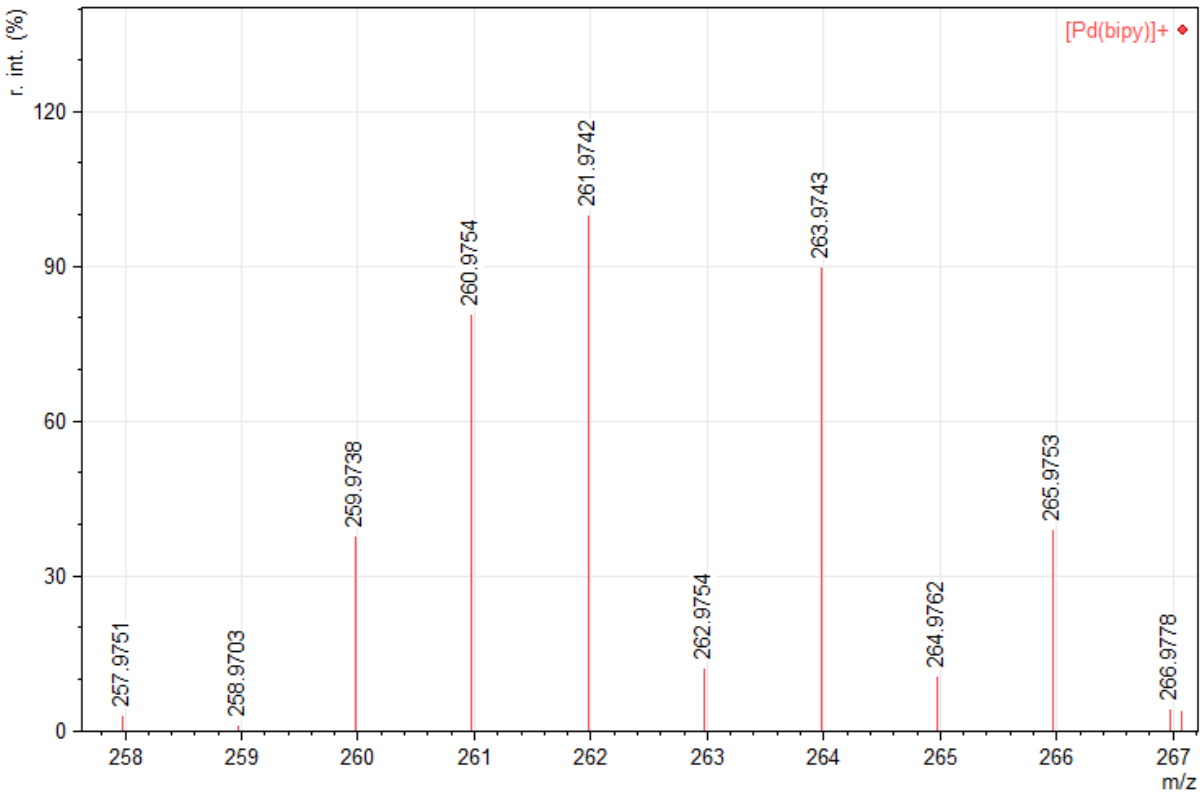

Figure S62. ESI$^+$ mass spectrum of **2** zoomed in the base peak [Pd(bipy)]$^+$.

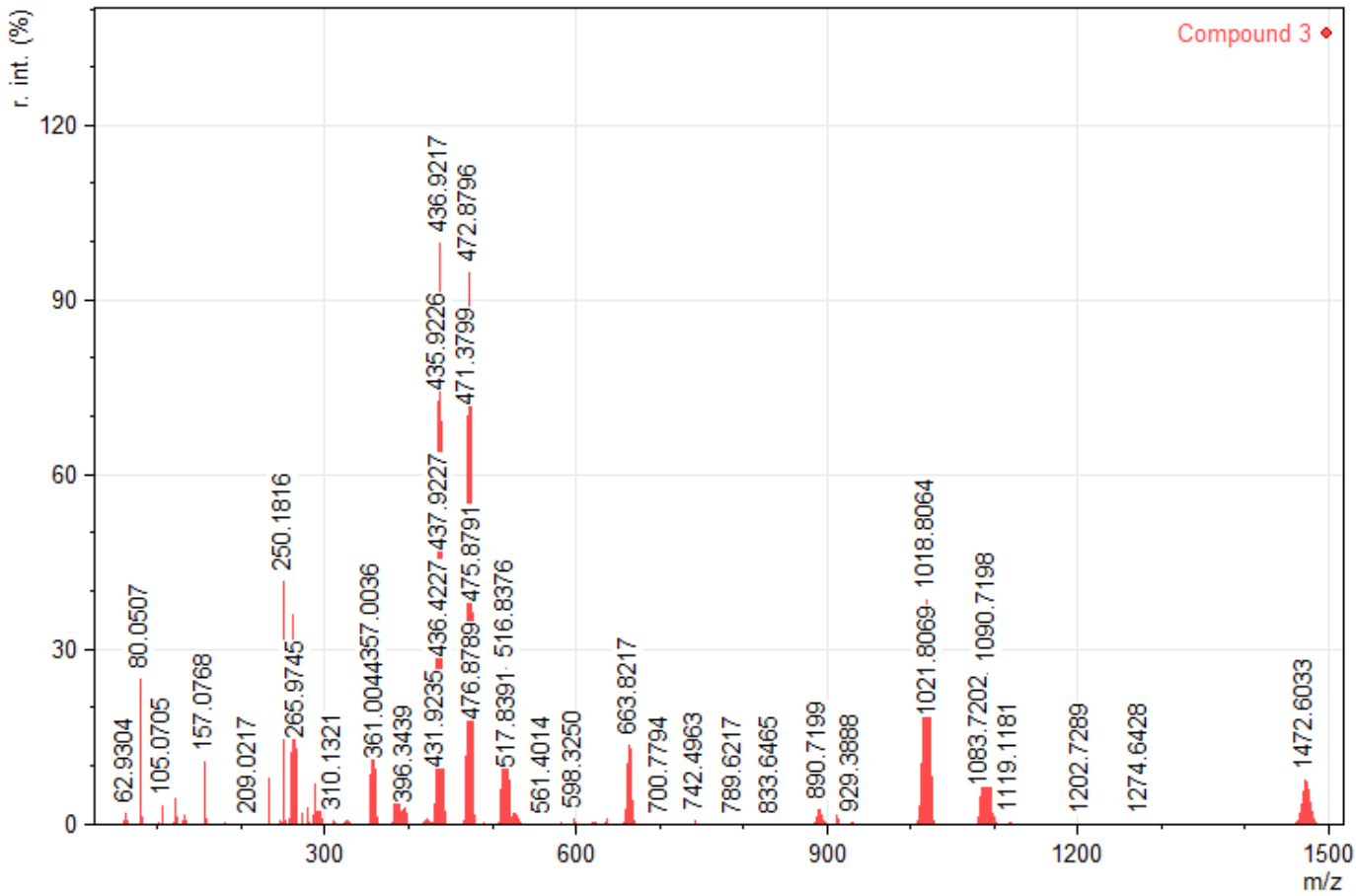

Figure S63. ESI$^+$ mass spectrum for compound $[Pd_2(\mu\text{-}SeC_6H_4F\text{-}p)_2(bipy)_2](PF_6)_2$ (**3**).

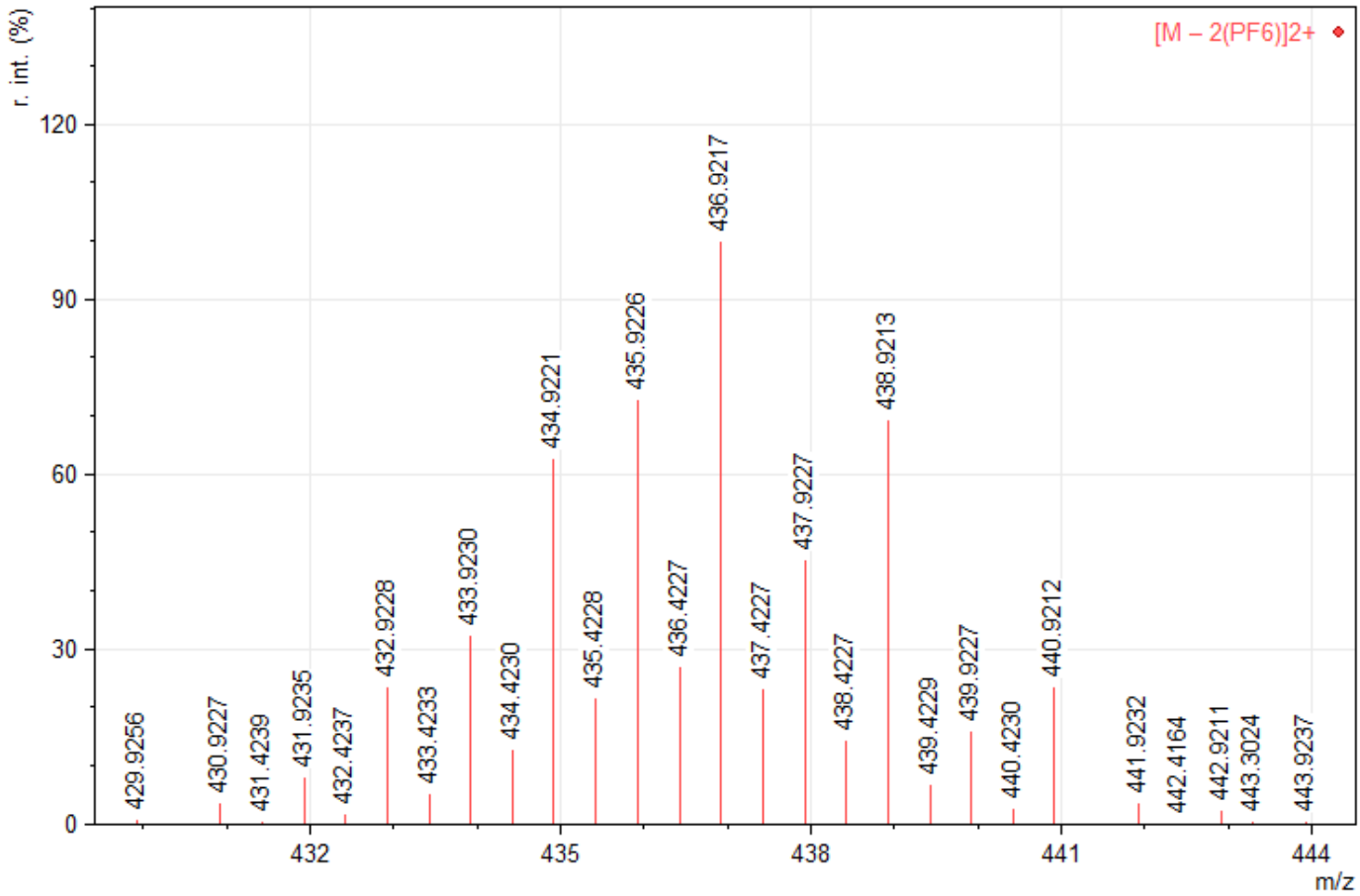

Figure S64. ESI$^+$ mass spectrum of **3** zoomed in the molecular ion fragment $[M – 2(PF_6)]^{2+}$ as the peak base.

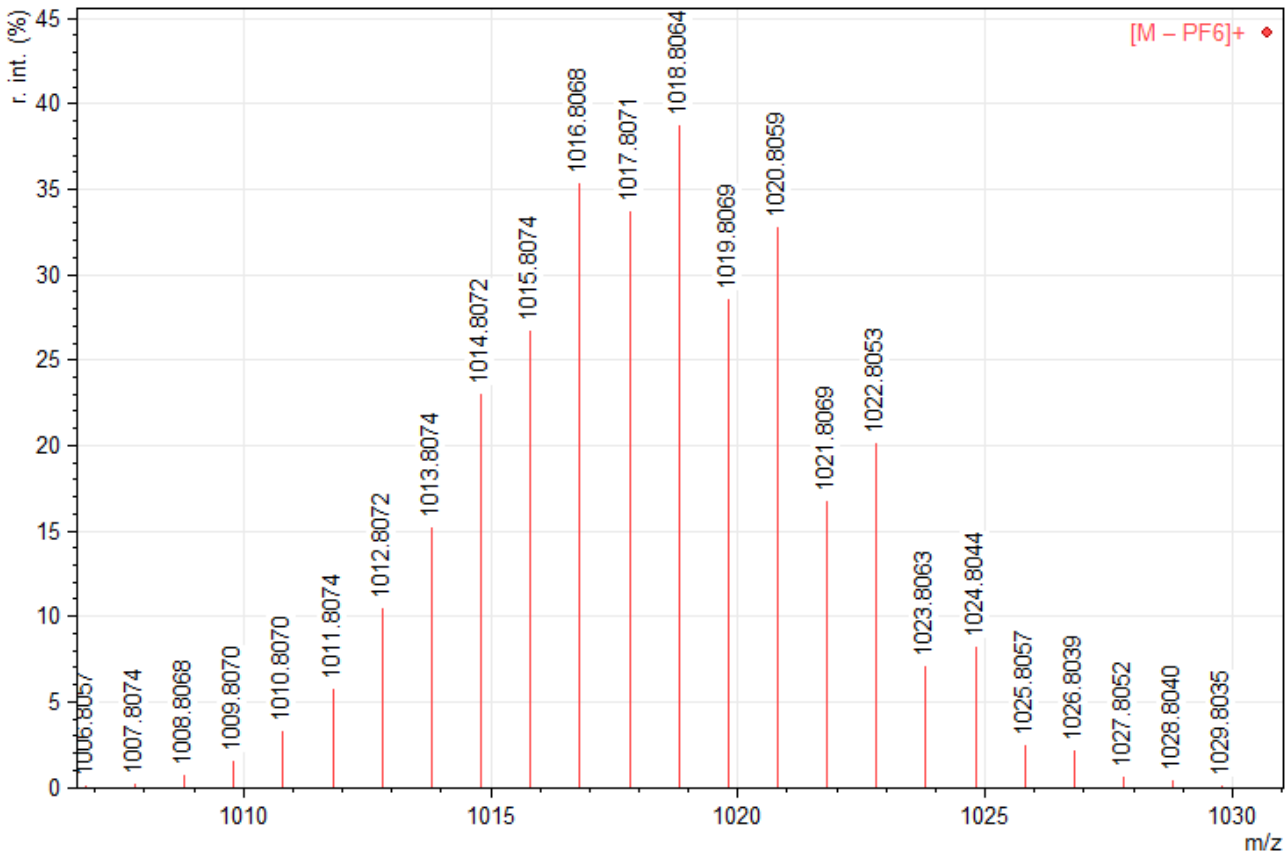

Figure S65. ESI$^+$ mass spectrum of **3** zoomed in the molecular ion fragment $[M – PF_6]^+$.

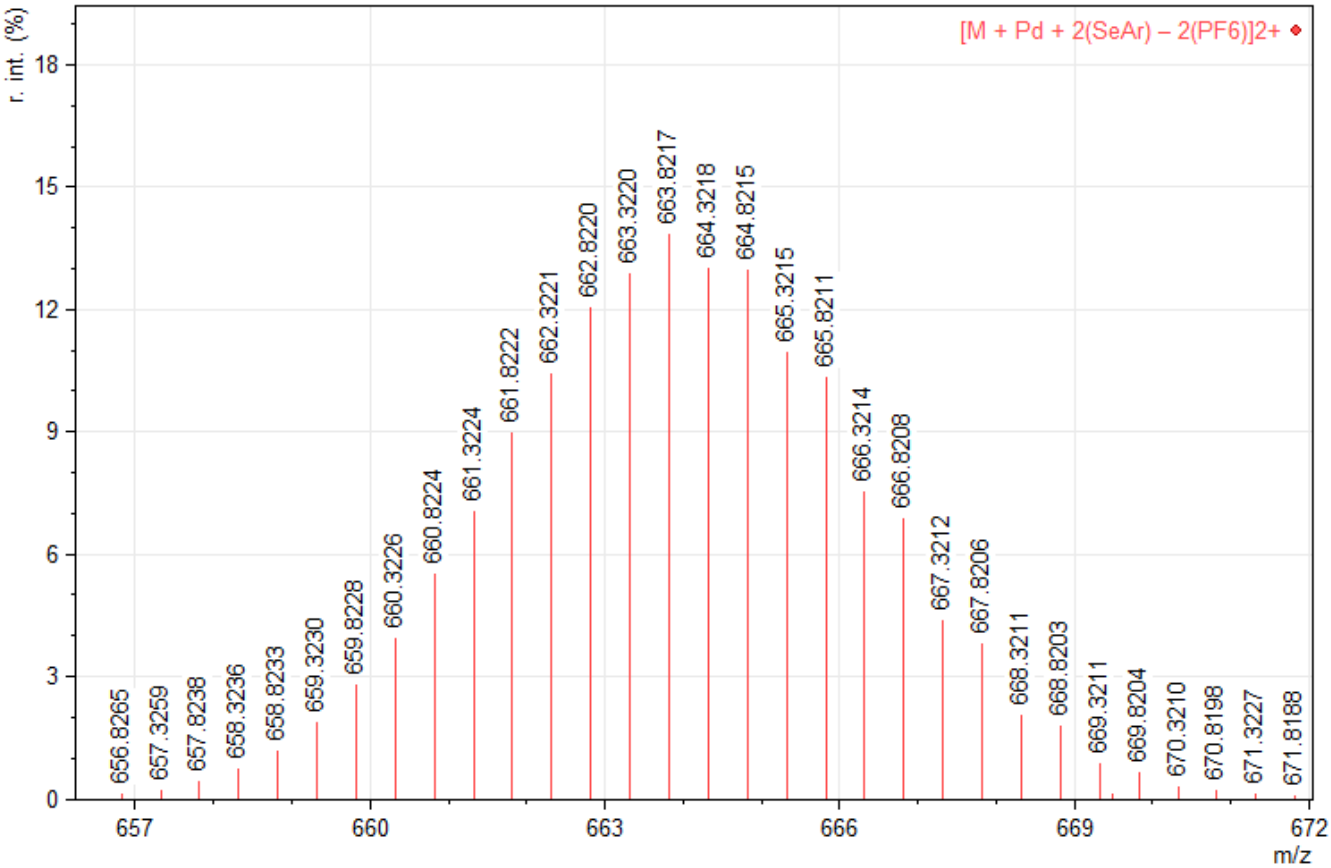

Figure S66. ESI$^+$ mass spectrum of **3** zoomed in the trimeric fragment [M + Pd + 2(SeAr) – 2(PF_6)]$^{2+}$.

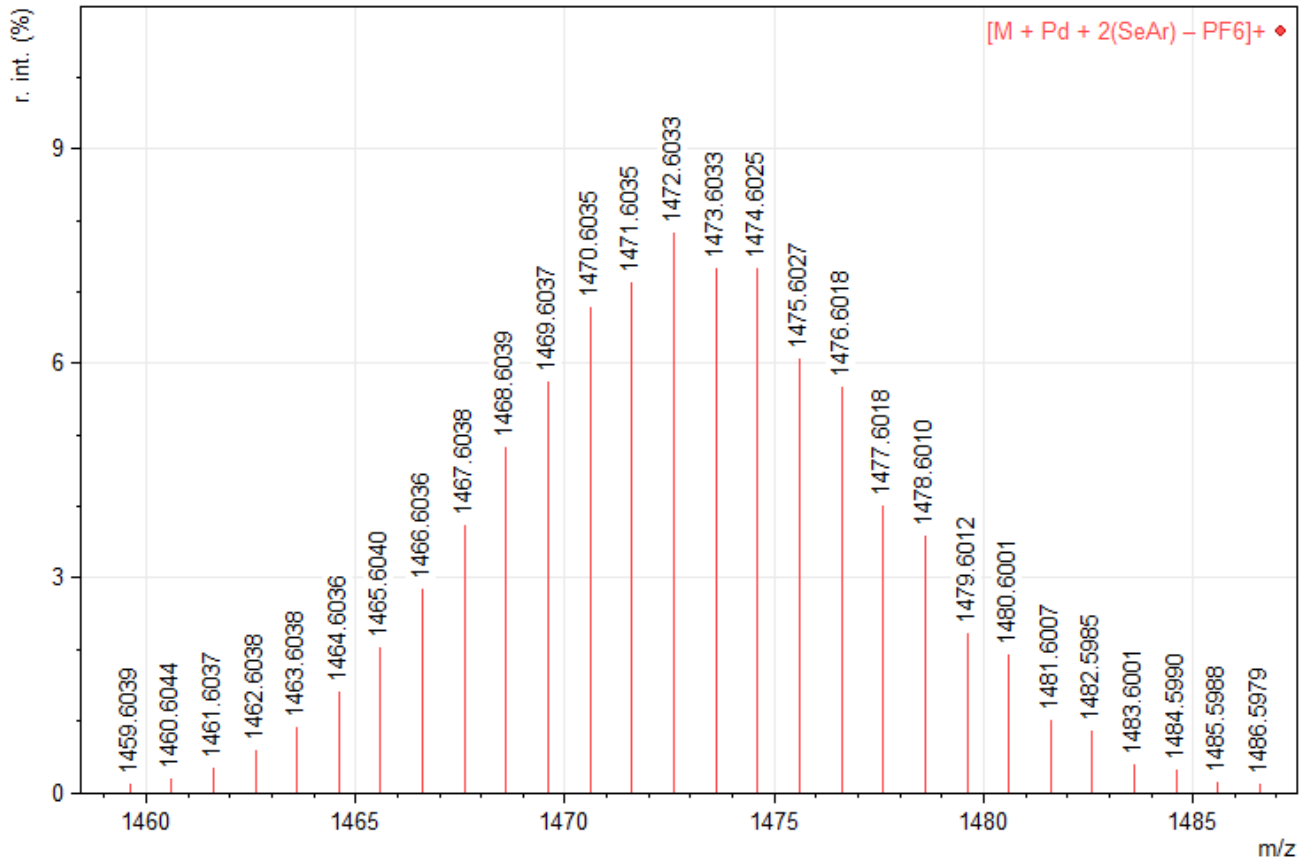

Figure S67. ESI$^+$ mass spectrum of **3** zoomed in the trimeric fragment [M + Pd + 2(SeAr) – PF_6]$^+$.

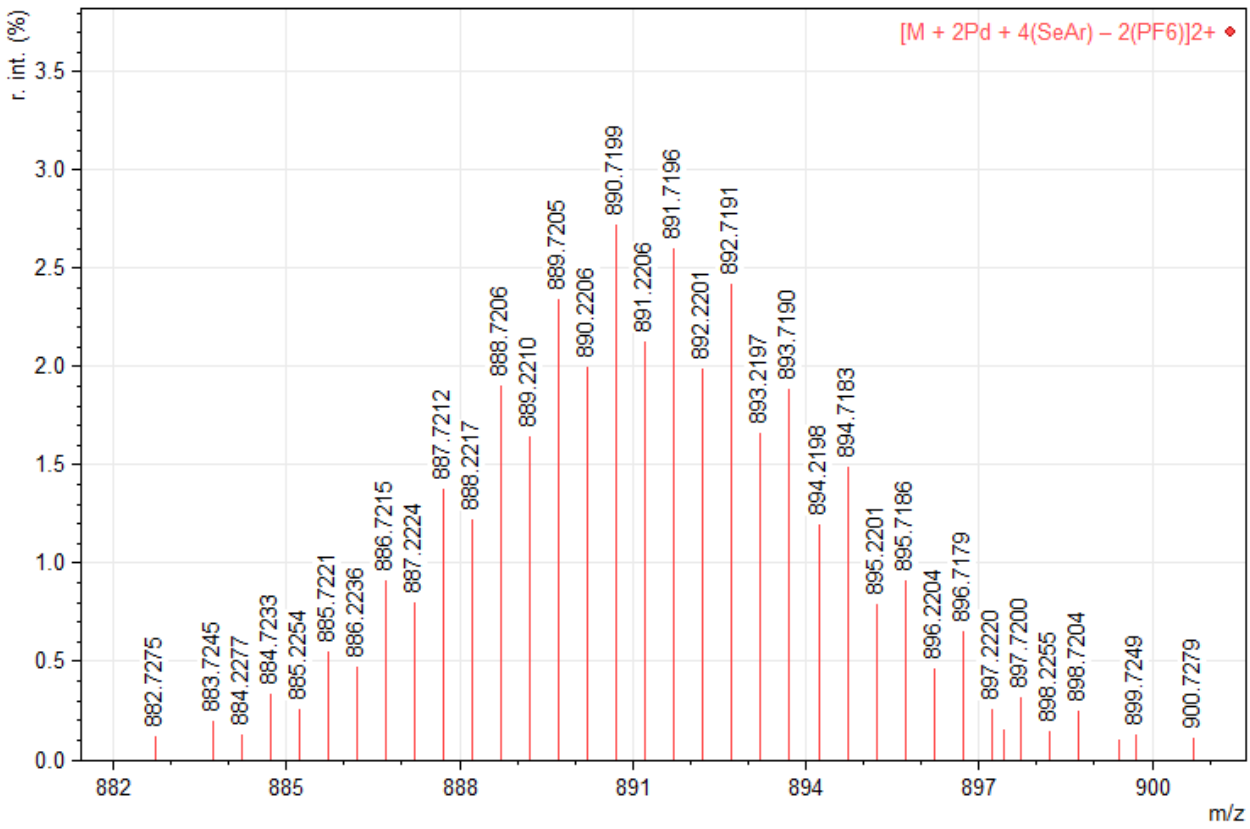

Figure S68. ESI$^+$ mass spectrum of **3** zoomed in the tetrameric fragment [M + 2Pd + 4(SeAr) – 2(PF_6)]$^{2+}$.

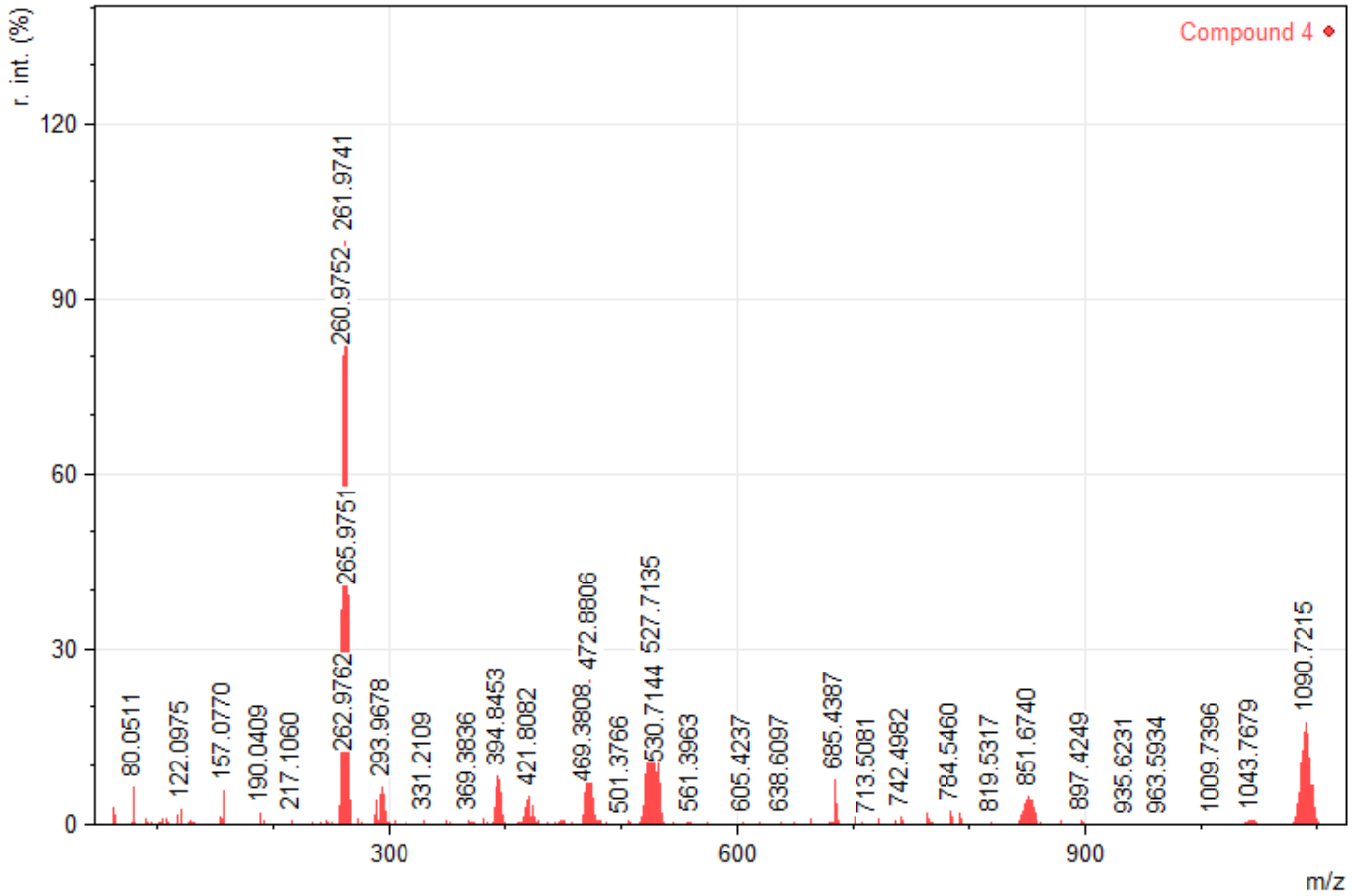

Figure S69. ESI$^+$ mass spectrum for compound [$Pd_3(\mu_3\text{-}Se)_2(bipy)_3$]($PF_6$)$_2$·5THF (**4**).

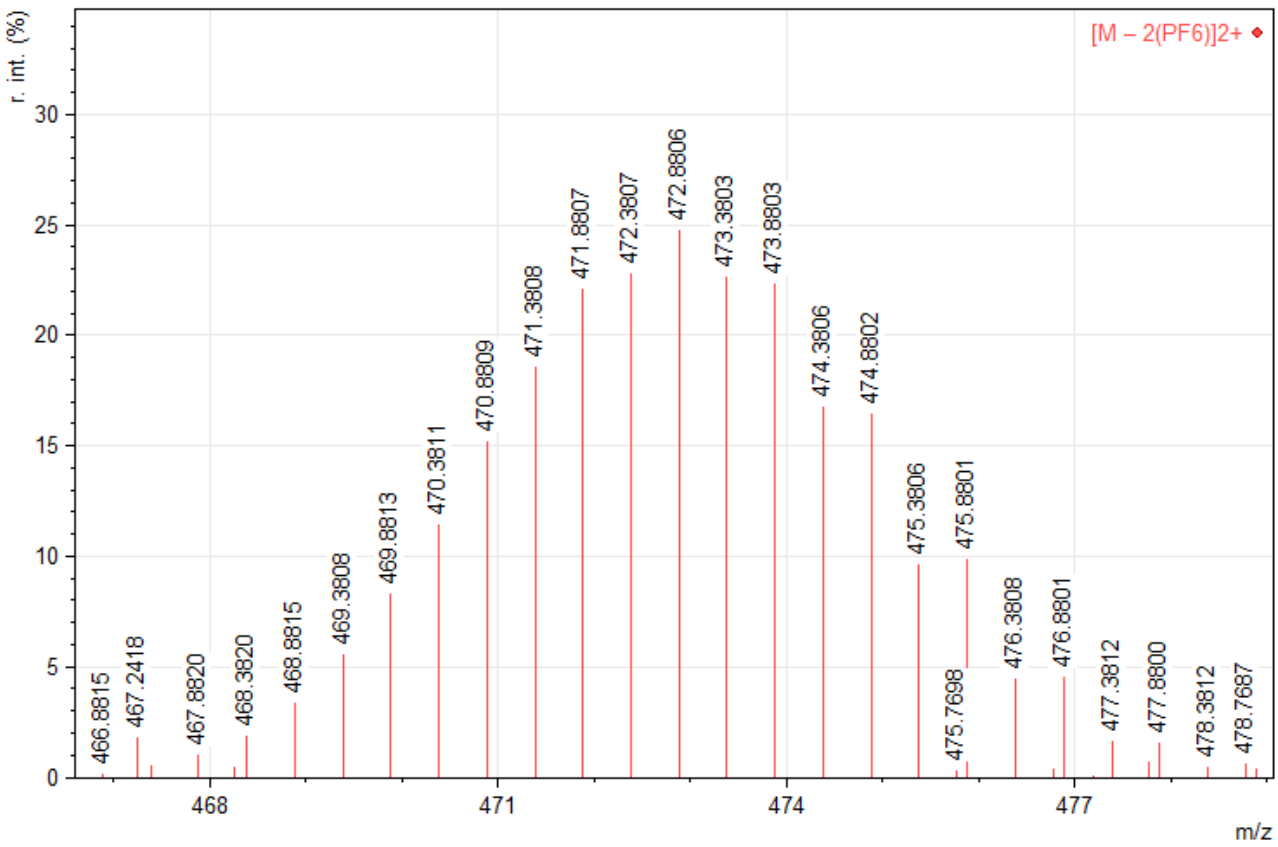

Figure S70. ESI$^+$ mass spectrum of **4** zoomed in the molecular ion fragment $[M – 2(PF_6)]^{2+}$.

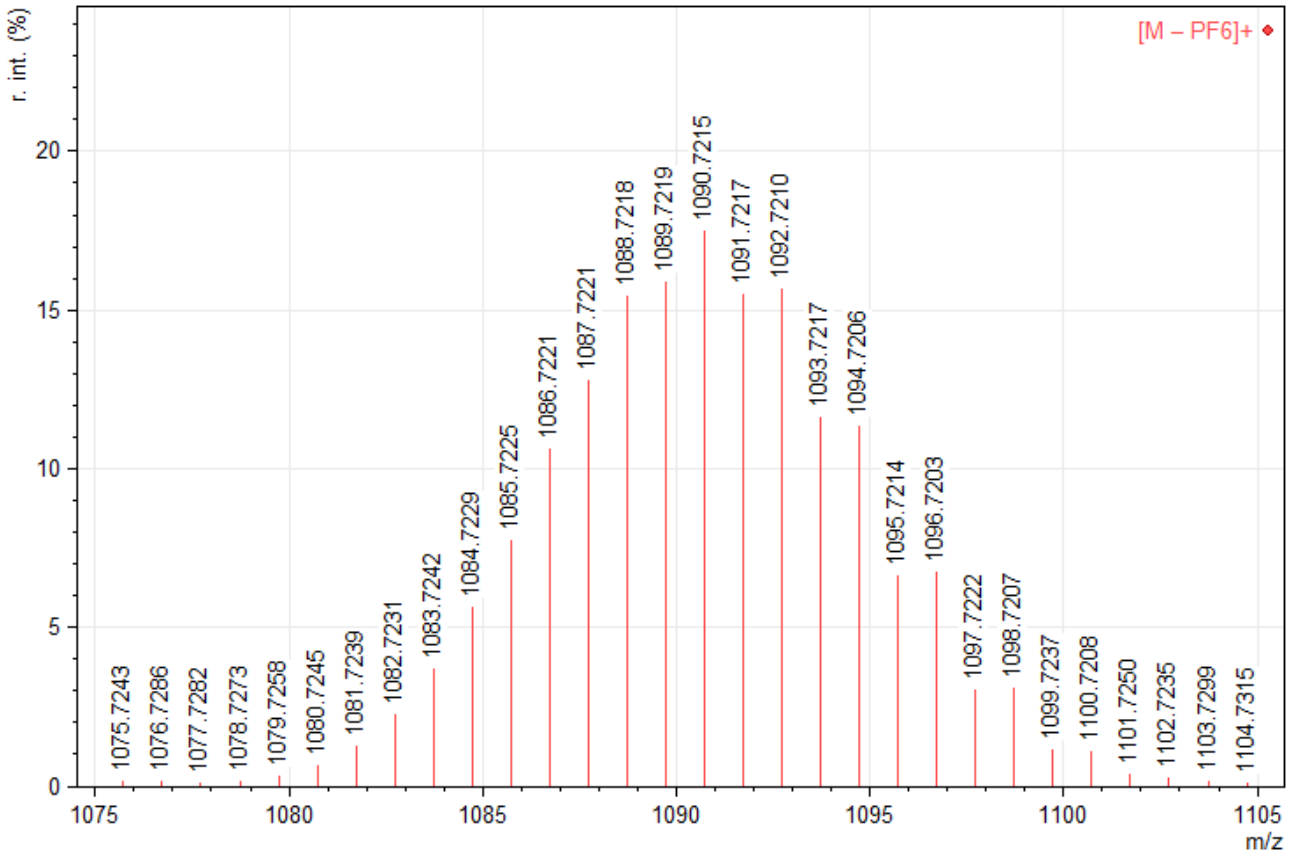

Figure S71. ESI$^+$ mass spectrum of **4** zoomed in the molecular ion fragment $[M – PF_6]^+$.

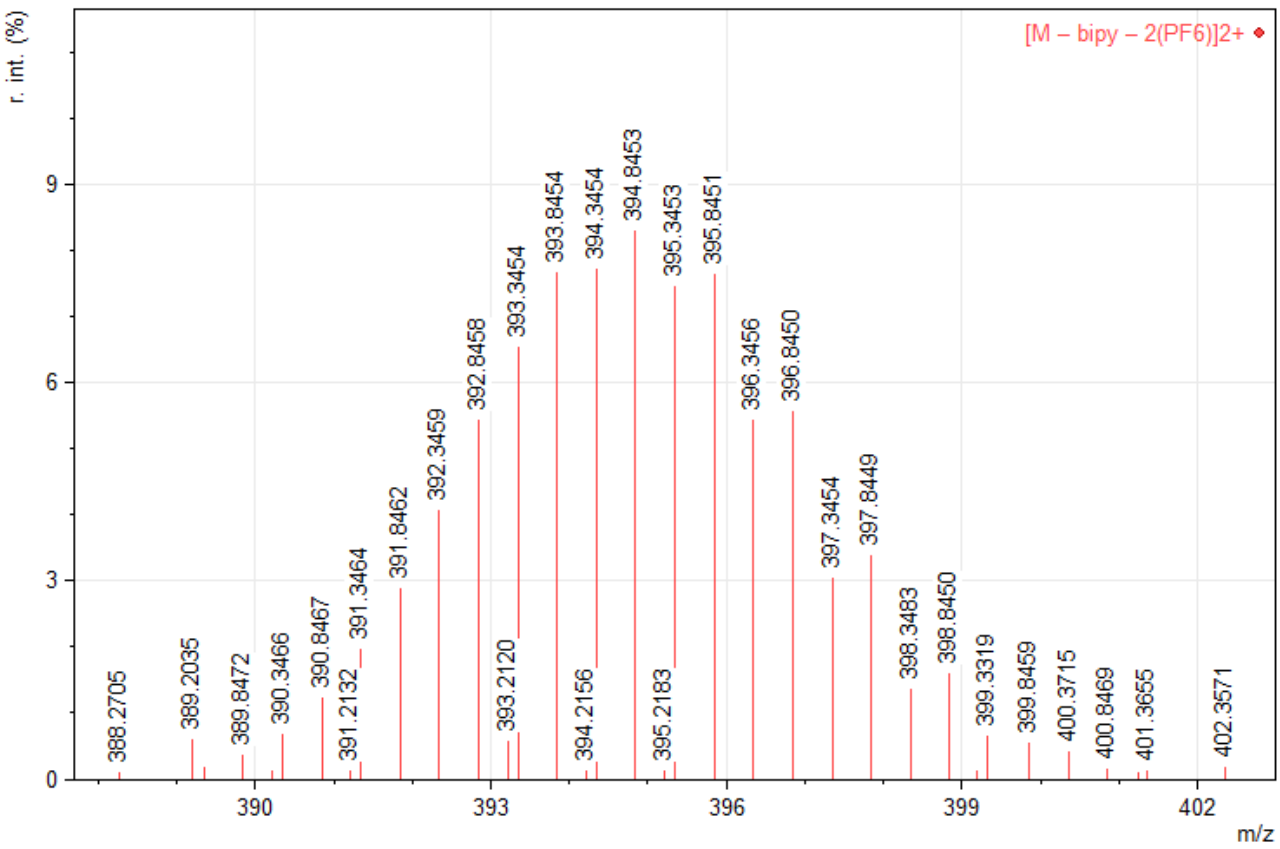

Figure S72. ESI$^+$ mass spectrum of **4** zoomed in the fragment $[M – bipy – 2(PF_6)]^{2+}$.

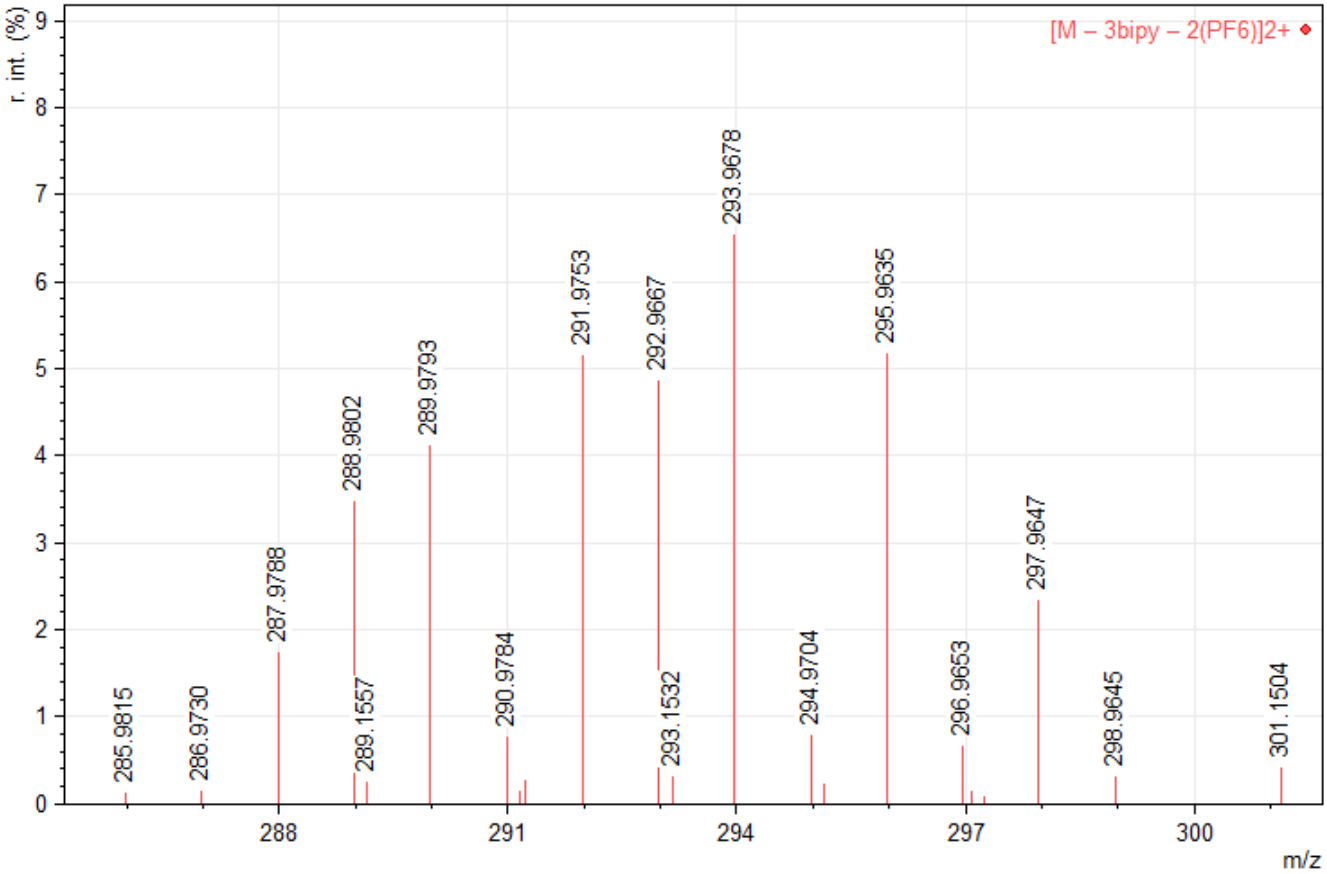

Figure S73. ESI$^+$ mass spectrum of **4** zoomed in the fragment $[M – 3bipy – 2(PF_6)]^{2+}$.

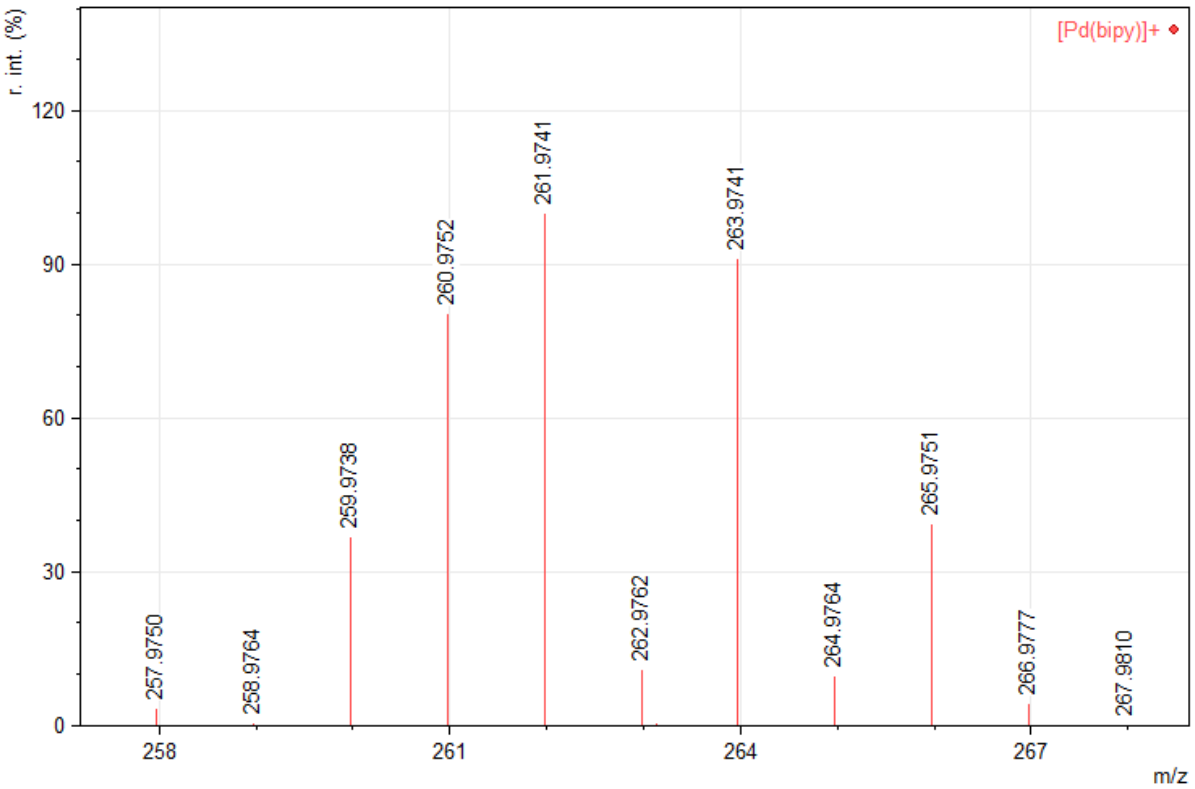

Figure S74. ESI$^+$ mass spectrum of **4** zoomed in the base peak [Pd(bipy)]$^+$.

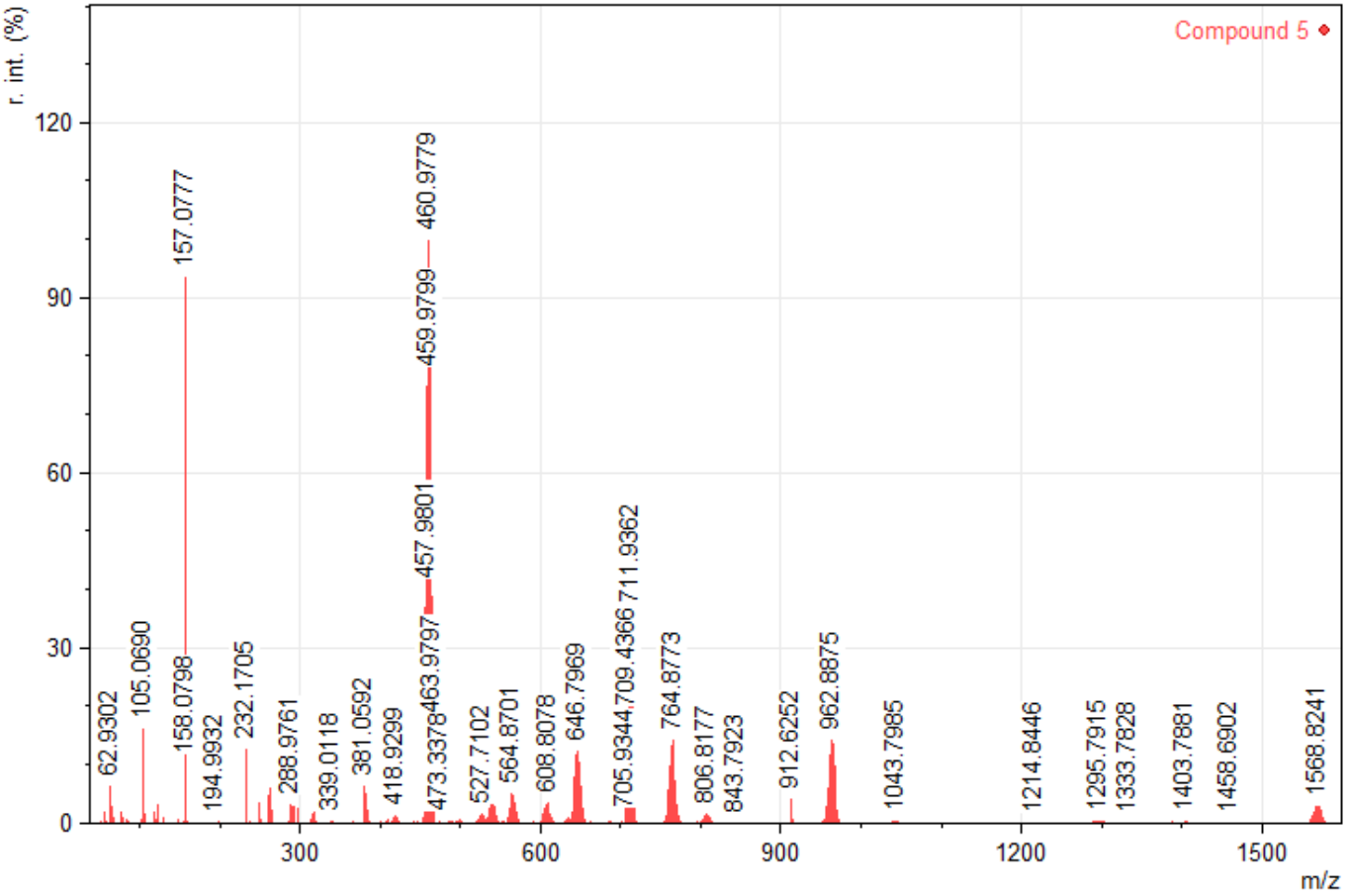

Figure S75. ESI$^+$ mass spectrum for compound $[Pd_3(\mu\text{-SeMes})_4(bipy)_2](PF_6)_2\cdot 2MeCN$ (**5**).

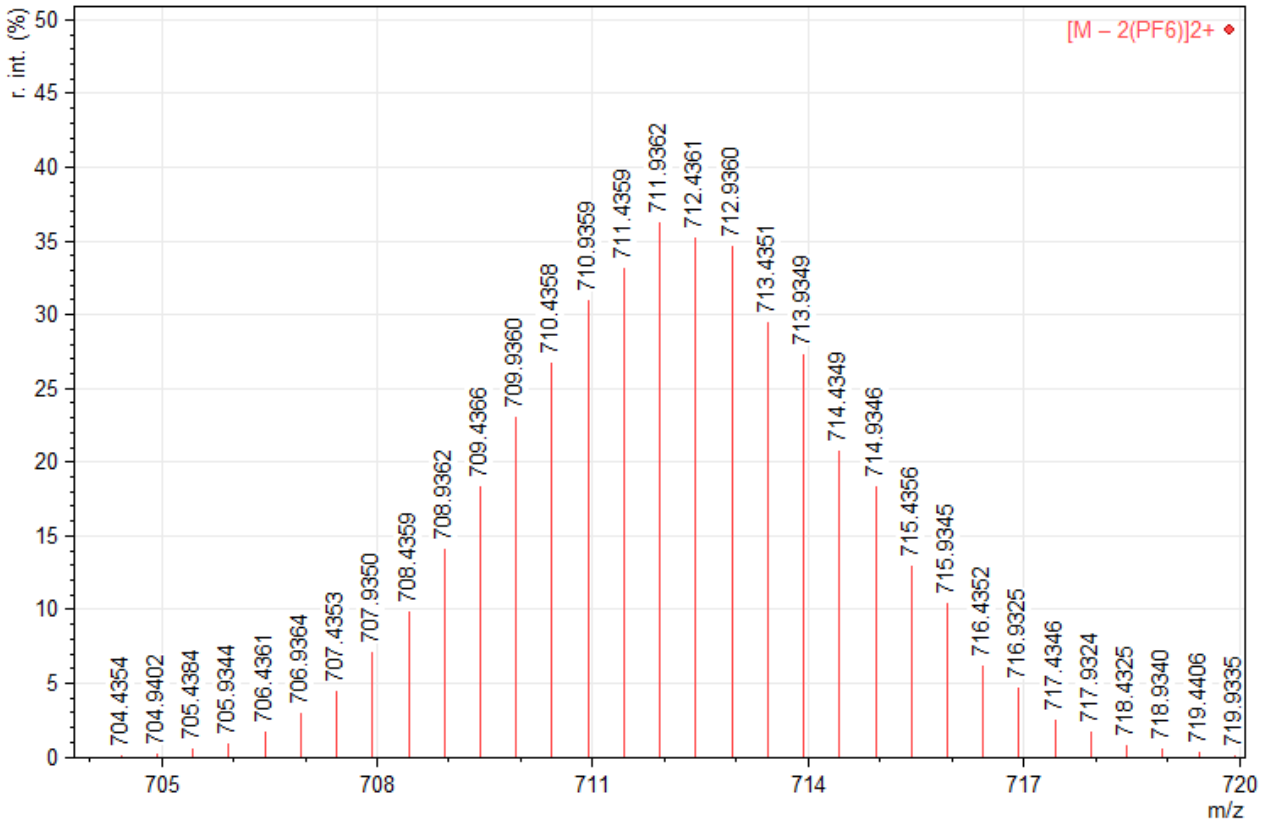

Figure S76. ESI$^+$ mass spectrum of **5** zoomed in the molecular ion fragment $[M – 2(PF_6)]^{2+}$.

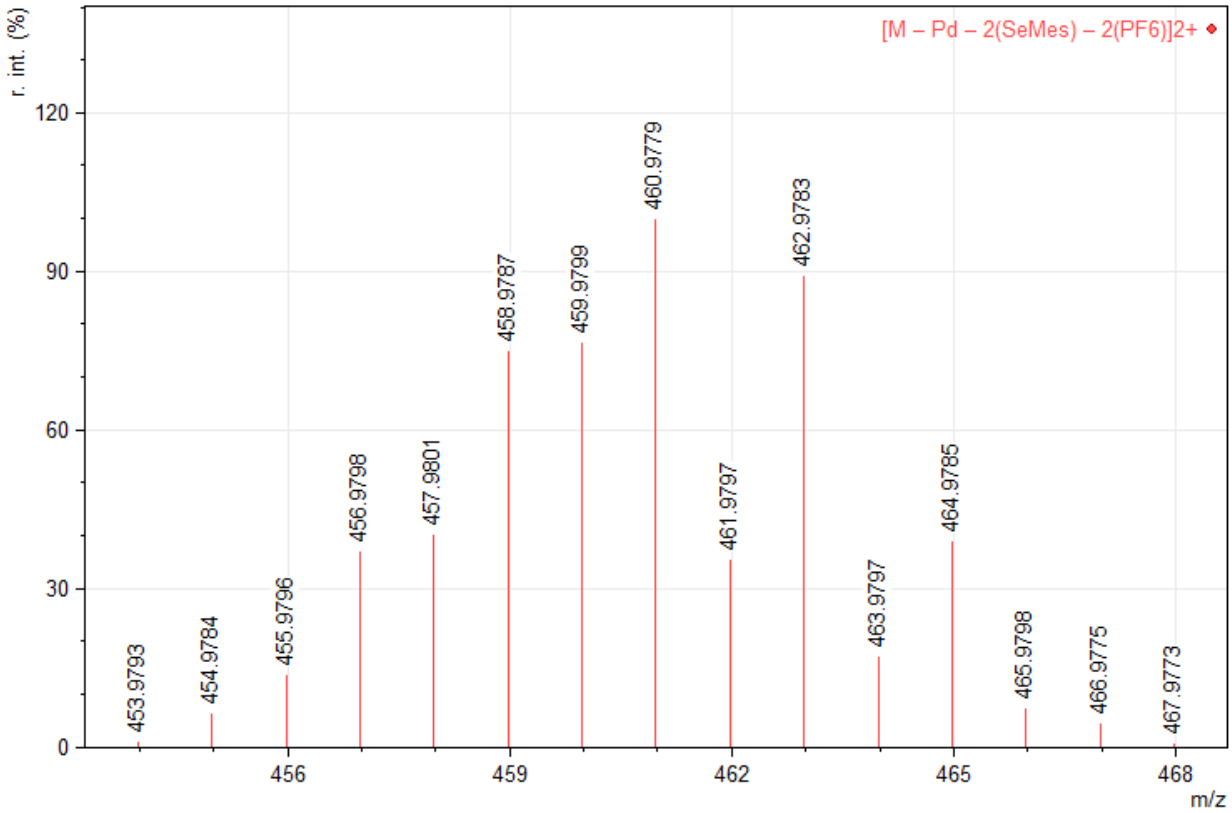

Figure S77. ESI$^+$ mass spectrum of **5** zoomed in the dinuclear fragment $[M – Pd – 2(SeMes) – 2(PF_6)]^{2+}$ as the base peak.

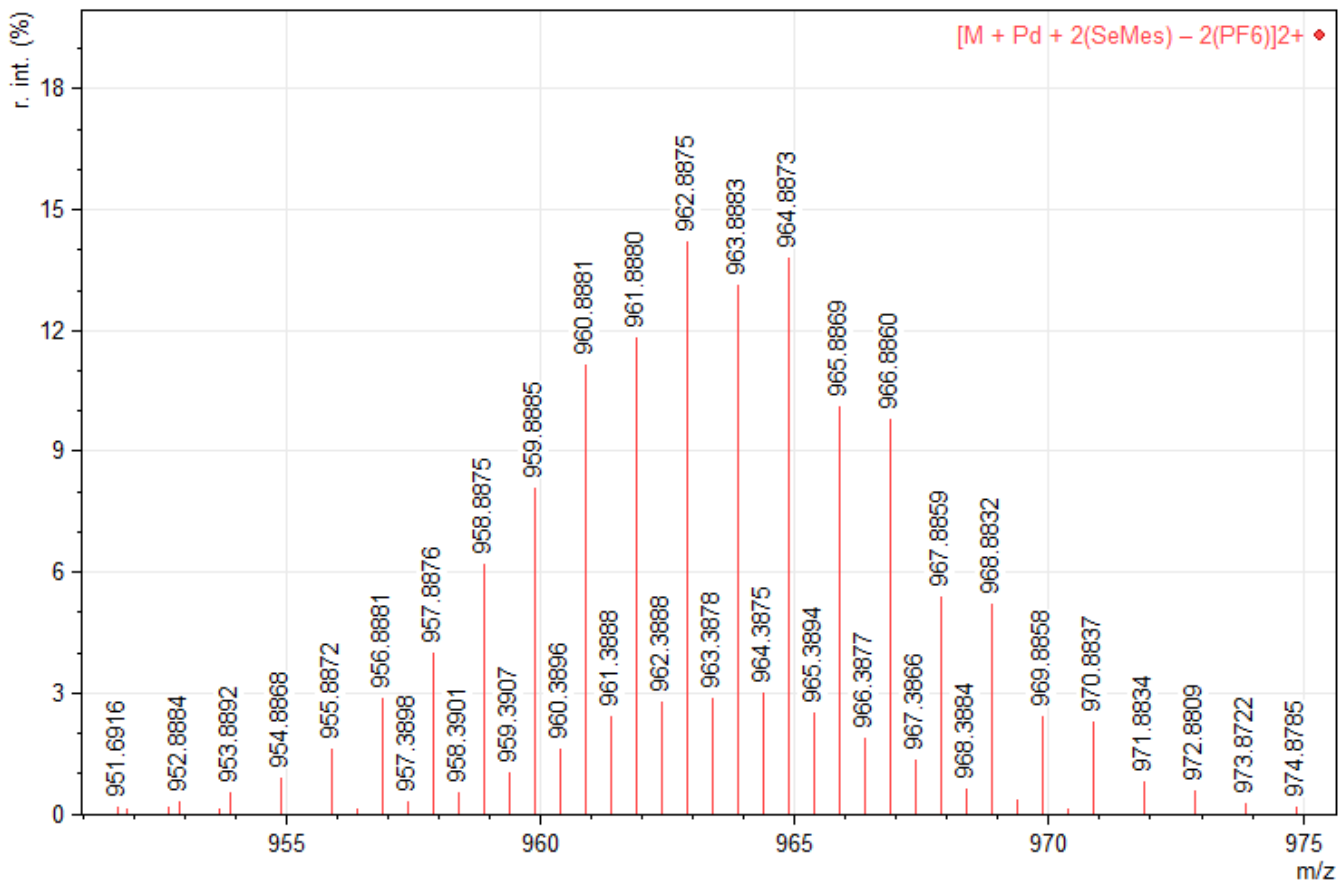

Figure S78. ESI$^+$ mass spectrum of **5** zoomed in the dinuclear fragment [M + Pd + 2(SeMes) – 2(PF_6)]$^{2+}$.

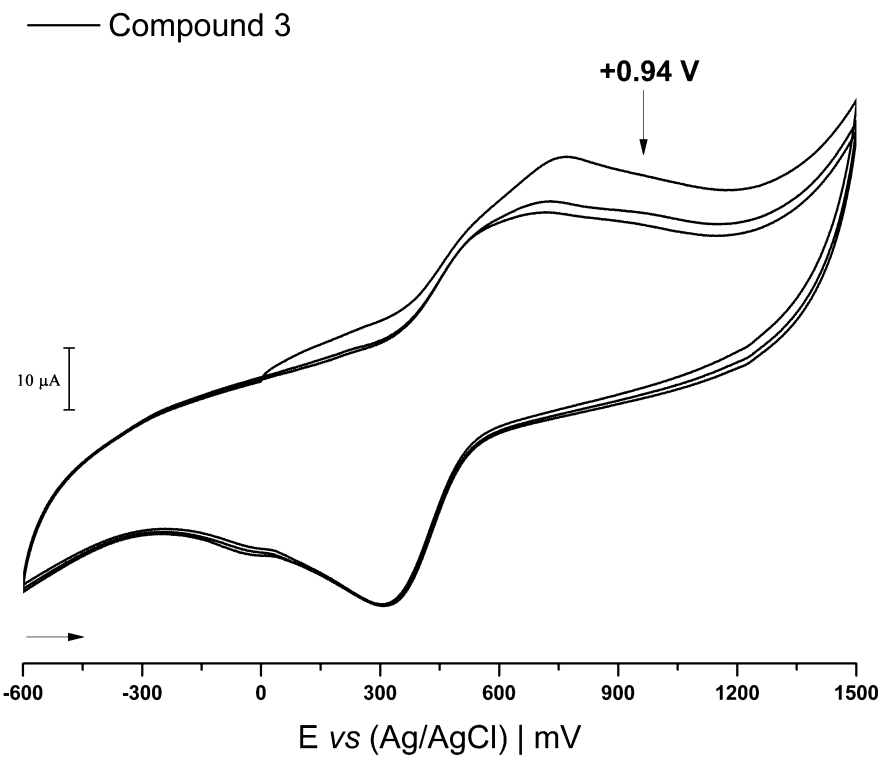

Figure S79. Cyclic voltammogram for compound **3** performed after electrolysis of 300 s at -0.6 V, immobilized onto graphite electrode in contact with 0.01 mol L^{-1} H_2SO_4. CV parameters: scan rate 50 mV s^{-1}, E_{step} 2 mV and scan range from -0.5 to +1.5 V with start potential at 0 V.

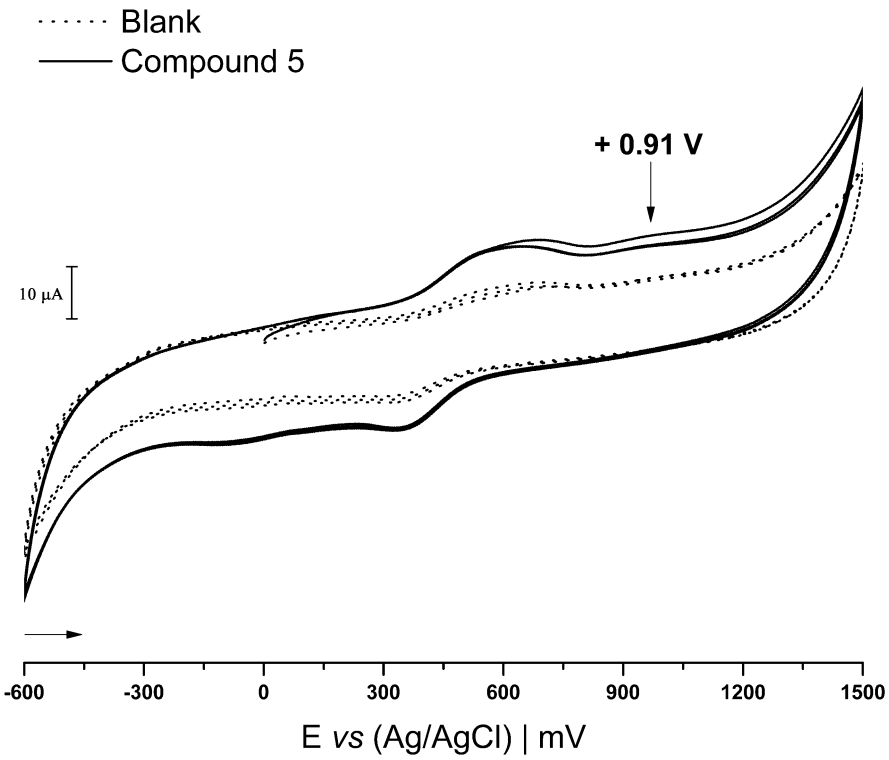

Figure S80. Cyclic voltammogram for compound **5** performed after electrolysis of 300 s at -0.6V, immobilized onto graphite electrode in contact with 0.01 mol L^{-1} H_2SO_4. CV parameters: scan rate 50 mV s^{-1}, E_{step} 2 mV and scan range from -0.5 to +1.5 V with start potential at 0 V.

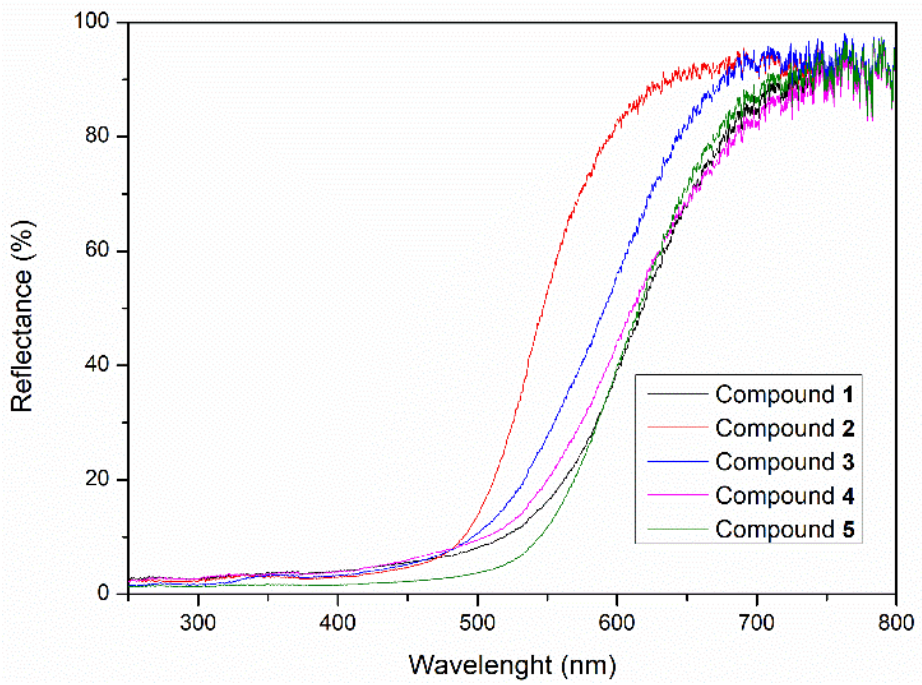

Figure S81. Diffuse reflectance spectra of compounds **1** – **5**.

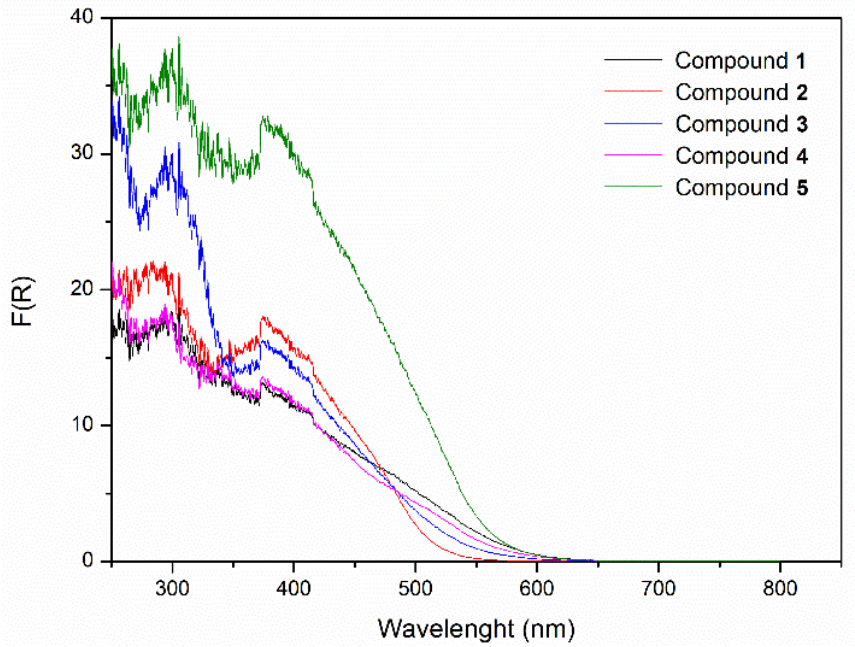

Figure S82. Kubelka-Munk absorbance spectra of compounds **1** – **5**.

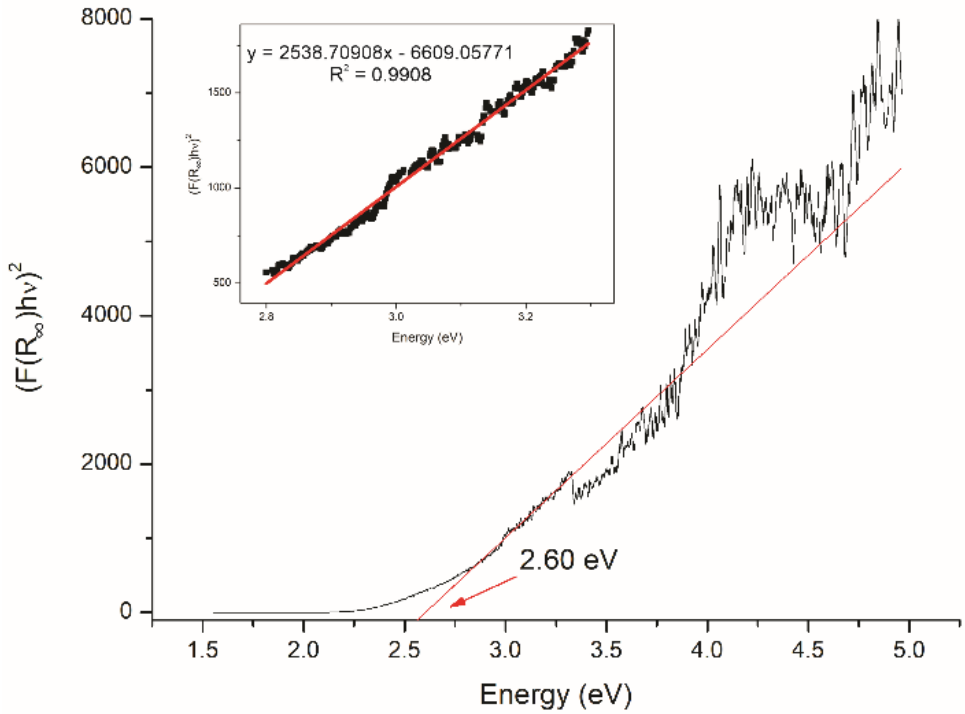

Figure S83. Optical band gap energy (E_g) from the Tauc plot for compound **1**.

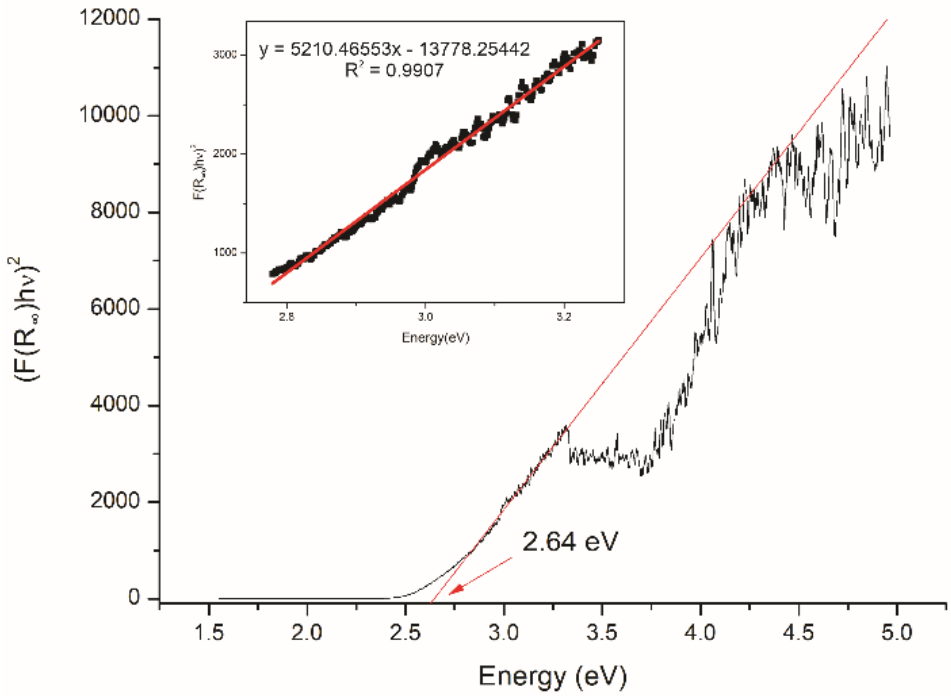

Figure S84. Optical band gap energy (E_g) from the Tauc plot for compound **2**.

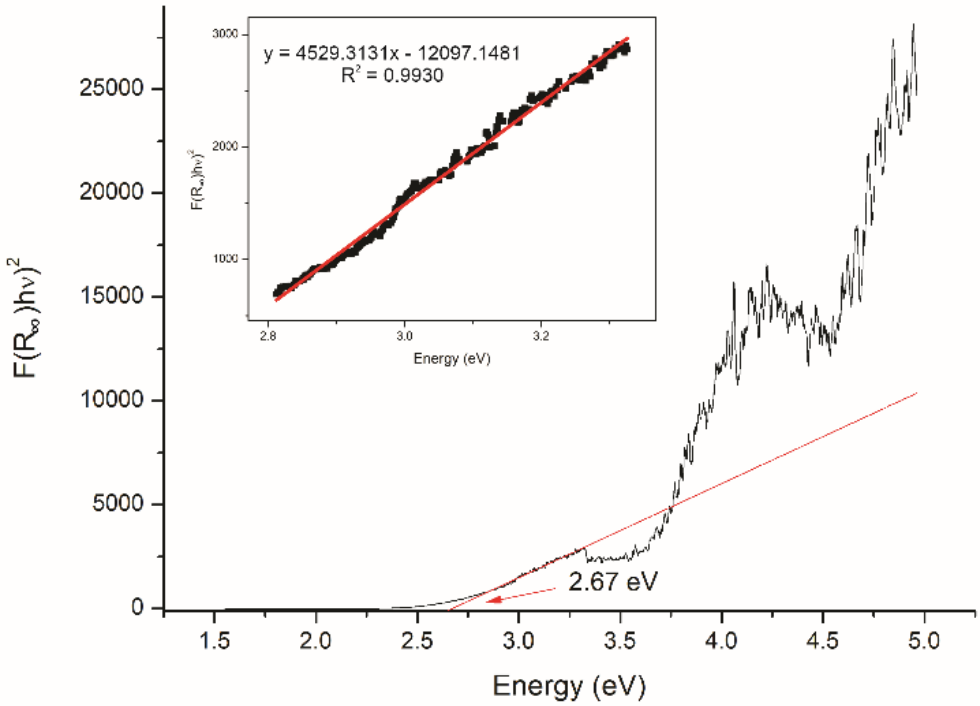

Figure S85. Optical band gap energy (E_g) from the Tauc plot for compound **3**.

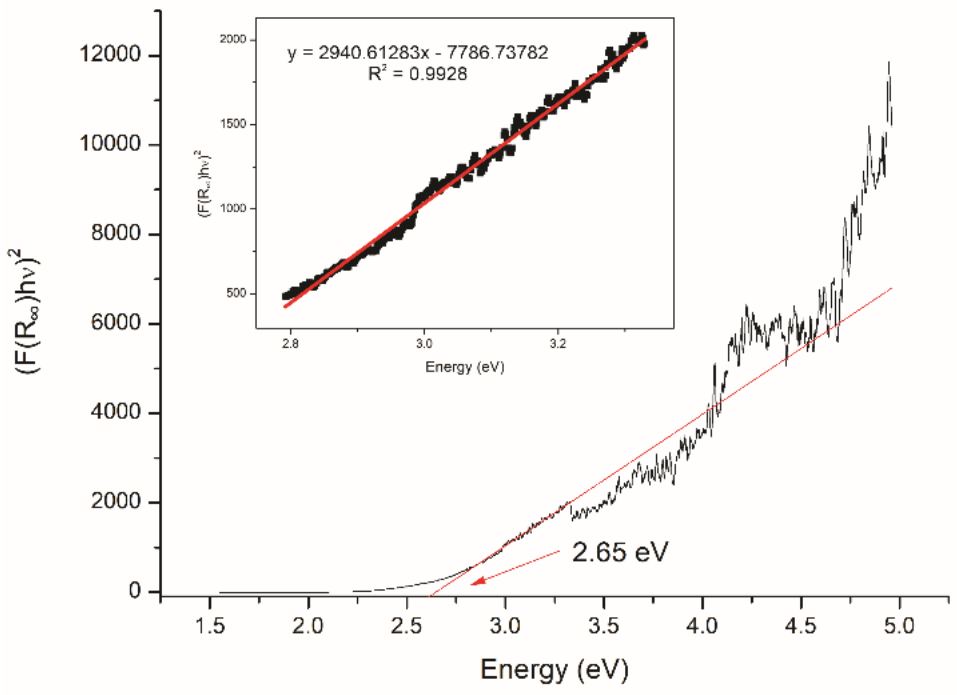

Figure S86. Optical band gap energy (E_g) from the Tauc plot for compound **4**.

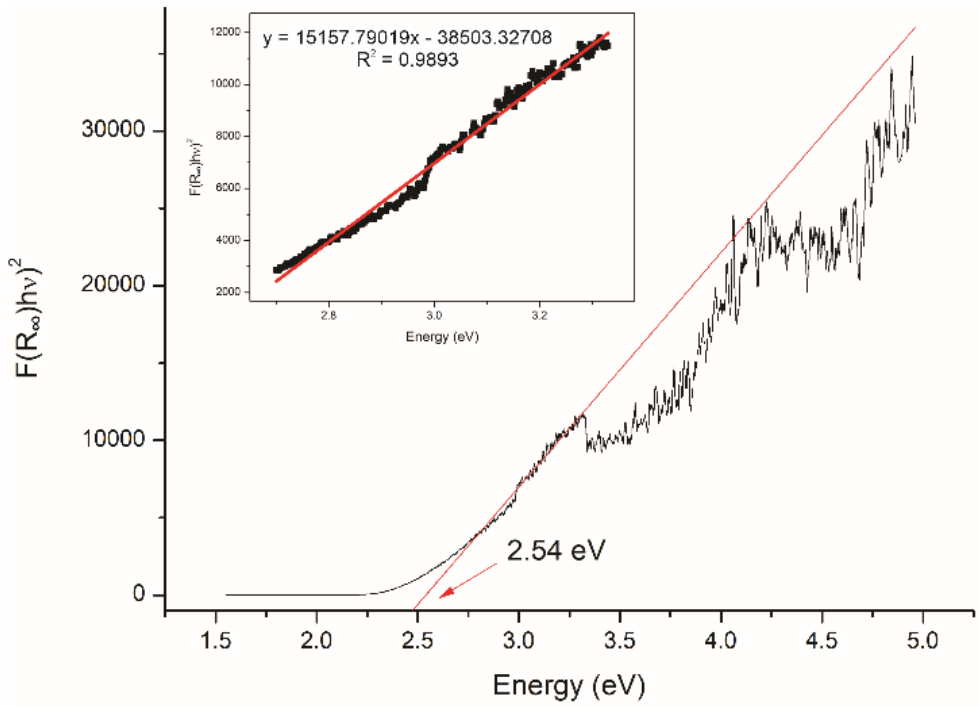

Figure S87. Optical band gap energy (E_g) from the Tauc plot for compound **5**.

References

1 W. S. Haller and K. J. Irgolic, *J. Organomet. Chem.*, 1972, **38**, 97.

2 S. S. Y. Chui, K. H. Low, J. Lu, V. A. L. Roy, S. L. F. Chan and C. M. Che, *Chem. Asian J.*, 2010, **5**, 2062.

3 S. V. Jagtap and R. M. Deshpande, *Kinet. Catal.*, 2013, **54**, 314.

4 A. Rotondo, G. Bruno, M. Cusumano and E. Rotondo, *Inorganica Chim. Acta*, 2009, **362**, 4767.

5 G. M. Sheldrick, *Acta Cryst. A*, 2015, **71**, 3.

6 G. M. Sheldrick, *Acta Cryst. C*, 2015, **71**, 3.

7 W. T. Pennington, *J. Appl. Cryst.*, 1999, **32**, 1028.

8 P. R. Jubu, F. K. Yam, V. M. Igba and K. P. Beh, *J. Solid State Chem.*, 2020, **290**, 121576.

9 A. B. Murphy, 2007, **91**, 1326.

10 P. Makula, M. Pacia and W. Macyk, *J. Phys. Chem. Lett.*, 2018, **9**, 6814.